March 2015

EXPERIMENTAL AND MODELING STUDIES ON THE FORMULATION OF STABLE LIPID NANOPARTICLE DISPERSIONS

Yihui Yang

EXPERIMENTAL AND MODELING STUDIES ON THE FORMULATION OF STABLE LIPID NANOPARTICLE DISPERSIONS

A Dissertation Presented

by

YIHUI YANG

Submitted to the Graduate School of the
University of Massachusetts Amherst in partial fulfillment
of the requirements for the degree of

DOCTOR OF PHILOSOPHY

February 2015

Chemical Engineering

EXPERIMENTAL AND MODELING STUDIES ON THE FORMULATION OF STABLE LIPID NANOPARTICLE DISPERSIONS

A Dissertation Presented

by

YIHUI YANG

Approved as to style and content by:

_____
Michael A. Henson, Chair

_____
Surita R. Bhatia, Member

_____
D. Julian McClements, Member

_____
John Collura, Interim Department Chair
Chemical Engineering

I would like to dedicate my thesis to my beloved grandparents and parents for making me who I am, and friends for all the help and support

ACKNOWLEDGMENTS

I would like to express my gratitude to my advisor Prof. Michael A. Henson for giving me the opportunity to work on this project. I would like to thank you for encouraging my research and for allowing me to grow as a research scientist. Your advice on both research as well as on my career have been priceless. I would like to thank Alessandro Corona from P&G for the financial support granted through my Ph. D career as well as the advice and help on the experiments. I would like to thank Prof. Surita R. Bhatia and Prof. D. Julian McClement for serving as my committee members. I would like to express my gratitude to Prof. Surita R. Bhatia for the help on the rheology work. I am grateful to Prof. D. Julian McClements for his help and also for allowing me to use equipments in his laboratory.

A special thanks to my family. Words cannot express how grateful I am to my grandparents and my parents for all of the sacrifices that you've made on my behalf. I am also grateful to all my friends in Amherst who make these five years really unforgettable, especially the class of 2009 and all the Chinese graduate students in my department. I would also like to thank all my group members for all the help on my research.

ABSTRACT

EXPERIMENTAL AND MODELING STUDIES ON THE FORMULATION OF STABLE LIPID NANOPARTICLE DISPERSIONS

FEBRUARY 2015

YIHUI YANG

B.A., DALIAN UNIVERSITY OF TECHNOLOGY

Ph.D., UNIVERSITY OF MASSACHUSETTS AMHERST

Directed by: Professor Michael A. Henson

Solid lipid nanoparticles (SLNs) have applications in drug delivery and the encapsulation of bioactive, lipophilic compounds such as those required for functional foods. A major obstruction to the industrial use of SLNs is their tendency to aggregate and form large particles and eventually gels when stored at room temperature. Aggregation is driven by the lipid crystals undergoing a polymorphic transformation from the thermodynamically unstable α-form through the β'-form to the stable β-form. A large increase in surface area occurs as spherical α particles are transformed into platelet-like β particles, causing a substantial decrease in surfactant coverage on the hydrophobic surfaces and inducing particle aggregation. Second generation encapsulation systems have been developed by incorporating a liquid carrier oil into the solid lipid matrix to form so-called nanostructured lipid carriers (NLCs). NLCs have been shown to have improved bioactive compound encapsulation and delivery properties compared to SLNs, but the enhanced stability of NLC dispersions to aggregation is not well understood.

This thesis presents both experimental and modeling studies on the formulation of stable lipid nanoparticle dispersions. A population balance equation (PBE) model was developed for prediction of the average polymorph content and aggregate size distribution to better understand the undesirable SLN aggregation behavior. Experimental and modeling studies showed that the polymorphic

transformation was the rate determining step for my system, SLNs with smaller initial size distributions aggregated more rapidly, and aggregates contained particles with both α and β crystals. Next the effect of different liquid carrier oils on the crystallization and aggregation behavior of tristearin NLC dispersions was investigated. I found that NLC dispersion stability was strongly affected by the type and amount of the oil. The results suggested that oil trapped within the growing crystal matrix accelerated the polymorphic transformation but retarded the large shape change normally associated with the transformation. Based on PBE simulation results, I hypothesized that improved NLC dispersion stability was attributable to both reduced particle shape change, which created less new surface area to be covered by surfactant, and increased mobility of surfactant molecules, which resulted in available surfactant being more efficient at covering created surface area. Finally I also studied the effect of formulation variables on the aggregation behavior and rheology of NLC dispersions. I found that NLC dispersion viscosity was strongly affected by particle aggregation. The viscosity of the dispersion could be modified by at least an order of magnitude by controlling particle aggregation using different surfactant and oil concentrations. Oscillatory sweep tests showed typical behaviors of a viscoelastic liquid and a viscoelastic solid for non-aggregated and aggregated NLC dispersions, respectively. Modeling results suggested a stronger bonding force and a higher aggregation efficiency with decreasing surfactant and/or oil concentrations. Both oscillatory sweep experiments and modeling results indicated an interconnected network structure in the aggregated dispersions, while no indication of network formation was observed for non-aggregated dispersions. These results suggested that controlled aggregation represents a promising approach for modifying the viscosity of NLC dispersions without adding viscosity enhancers and could reduce the time and cost for NLC production.

TABLE OF CONTENTS

Page

LIST OF TABLES

LIST OF FIGURES

Figure Page

CHAPTER 1

INTRODUCTION

1.1 Colloidal Delivery System

The encapsulation, protection, and release of active lipophilic compounds (*e.g.,* pharmaceuticals, nutraceuticals, antimicrobials, antioxidants, and vitamins) have wide applications in the pharmaceutical, food, and personal care industries [1, 2]. Nevertheless, the effective utilization of these bioactive components is often limited because of their low bioavailability and poor storage stability. The poor bioavailability of these compounds is often associated with their high melting points, slow dissolution rates, and limited water-solubility [3, 4], whereas their poor storage stability is associated with their tendency to undergo chemical degradation or phase transitions [5]. Various emulsion-based colloidal delivery systems have been developed to overcome these problems, including microemulsions, nanoemulsions, multilayer emulsions, multiple emulsions, filled hydrogel microspheres, nanostructured lipid carriers, and solid lipid nanoparticles [5-7]. Each delivery system has advantages and disadvantages for particular applications, depending on the nature of the bioactive compound (*e.g.,* physical state, rheology, solubility, chemical stability), the nature of the delivery vehicle (*e.g.,* tablet, capsule, syrup, spray, cream, food, beverage), and the desired delivery route (*e.g.,* intravenous, oral, nasal, topical). Two of the most promising emulsion-based delivery systems for oral applications in the pharmaceutical and functional food industries are solid lipid nanoparticles (SLNs) and nanostructured lipid carriers (NLCs), both of which consist of crystalline lipid particles dispersed within an aqueous medium.

1.2 Solid Lipid Nanoparticles

Solid lipid nanoparticles consist of a core of solid lipid with the active ingredients (e.g., drugs, nutritional agents) being a part of the lipid matrix [8]. The particle is stabilized by a surfactant layer, which may consist of a single surfactant, but typically is composed of a mixture of surfactants [8]. Solid lipid nanoparticles have attracted increasing attention during recent years. SLNs have application in many areas such as the food industry, drug delivery and consumer products. In food science, SLNs can be used as carriers for strongly lipophilic compounds that possess virtually no water solubility and functional foods [9]. SLNs also have advantages in targeted delivery and controlled release of drugs [7, 10, 11]. It is has been agreed that SLNs combine the advantages and avoid the disadvantages of other colloidal carriers. The advantages of SLNs include [12]:

1. Controlled release and drug targeting.
2. Increased drug and nutritional agent stability.
3. High bioactive compound loading.
4. Incorporation of lipophilic and hydrophilic ingredients.
5. No biotoxicity of the carrier.
6. No use of organic solvents.
7. Easy for large scale production and sterilization.

1.2.1 SLN Preparation

The hot high pressure homogenization method has been developed as the most common technique for the preparation of SLNs [12]. Hot homogenization is carried out at a temperature above the melting point of the lipid; therefore it can be regarded as homogenization of the lipid emulsion. The drugs or bioactive ingredients are dissolved in the melted lipid. A coarse

emulsion premix is made by mixing the lipid phase with an aqueous surfactant solution using a high speed blender. High pressure homogenization of the premix is carried out at a temperature above the melting point of lipid. Usually, high temperatures will result in smaller particle size because of the decrease of viscosity of the lipid phase [13]. However, high temperature can increase the degradation of active ingredients inside the lipid phase. In most cases, 3-5 homogenization passes at 500-1500 bar are sufficient to obtain the desired particle size. . SLNs are formed by cooling down the hot emulsion obtained after high pressure homogenization at ambient or subambient conditions. Due to the small particle size and the presence of surfactant, the crystallization process may be retarded and the sample may remain as a supercooled melt for several months [14]. The choice of ingredient composition will also influence the product quality. It has been found that the average particle size of SLNs increases with higher melting lipids [15]. Broader particle size distributions were observed in most cases when increasing the lipid content over 5-10% [15, 16]. The selection of the surfactants and their concentrations has a great impact on the quality of the SLN products [15, 17]. Different surfactants may need different homogenization parameters [18].

There are other methods for production of SLNs, such as cold homogenization, solvent emulsification/evaporation and microemulsion based preparation [19-21]. Compared to hot homogenization, larger particle sizes and broader size distributions are observed in cold homogenization [15]. The main disadvantage of the solvent emulsification evaporation method is the use of organic solvents. For microemulsion based SLN preparation, the achievable lipid contents are considerably lower compared with hot high pressure homogenization because of the dilution step.

1.2.2 Crystal Polymorphs and Aggregation Phenomena

The crystallization of lipids cannot be described only as crystallized or non-crystallized, since the crystallized lipid can form several different polymorphs. Triacylglycerides (TAGs) are commonly used as SLN lipids [8, 12]. Typically, TAGs exhibit three different crystal polymorphs, the α, β' and β forms that have hexagonal, orthorhombic, and triclinic unit structures, respectively [22]. The α polymorph is the thermodynamically least stable form and has the lowest melting point. Lipid crystals in a thermodynamically unstable state generally have higher mobility and lower density than stable crystals [12]. Therefore, α-form crystals have the largest capacity to incorporate other molecules and offer the highest loading of the three TAG polymorphs. While the β polymorph is thermodynamically most stable and has the highest melting point, this crystal form offers the lowest loading of the three polymorphs. The shape of an α crystal is approximately spherical, while β crystals have shapes that are needle or platelet like [23, 24]. The properties of the β' polymorph are between those of the α and β forms.

SLN aggregation is driven by polymorphic transformation of the crystalline SLNs [8, 12, 23, 25]. An increase in particle surface area occurs as spherical α particles are transformed into needle- and platelet-shaped β particles [24], causing a decrease in surfactant coverage on the hydrophobic surfaces of the particles. Attractive forces cause the partially covered particles to adhere together when they collide, resulting in the formation of large aggregates and eventually gels [23]. The lipid material has been identified as an important parameter for affecting the structure and stability of SLNs. Polymorphic transformation kinetics were slowed when SLNs were made from lipids with long carbon chains such as tripalmitin and tristearin [26, 27]. High lipid concentrations and high ionic strengths increase the aggregation rate [28, 29]. Co-surfactants also influence SLN formation and stabilization; *e.g.,* studies have shown that the polymorphic transformation can be retarded by using certain types of co-surfactants such as sodium

glycocholate, saturated phospholipids, and poly(vinyl alcohol) [26, 27, 30, 31]. SLNs with higher fractions of the α polymorph have been obtained with high melting surfactants [32]. The effect of surfactant surface coverage on SLN stability has also been studied experimentally [33]. The results suggested that high surface coverage favored the α-polymorph and reduced the polymorphic transformation rate. Several studies have shown that faster cooling rates retard the polymorphic transformation and increase SLN stability [34]. Other factors such as high lipid concentrations, high storage temperatures, and exposure to light and mechanical stress have been shown to increase aggregation rates [28, 35].

1.3 Nanostructured Lipid Carriers

The second generation of lipid nanoparticles, commonly termed nanostructured lipid carriers (NLCs), was developed by mixing a liquid lipid (carrier oil) with the solid lipid prior to particle formation [11, 36-42]. Many studies have been performed to investigate the effects of the lipid/carrier oil system on NLC drug loading and release properties [43-53]. These studies suggest that incorporation of the carrier oil into the solid lipid matrix improves loading capacity, physical and chemical stability and triggered release by disrupting the crystal packing structure [38]. Moreover, NLC crystallization and melting temperatures and polymorphic content have been shown to be strongly dependent on the amount of oil added [11, 37]. However, the effect of oil type on NLC polymorphic behavior and shape change remains poorly understood [36, 38].

While the use of NLCs to enhance bioactive compound encapsulation and delivery has received considerable attention, the impact of the carrier oil on NLC dispersion stability has not been extensively investigated. In one study in which NLCs were prepared with tripalmitin as the lipid and fish oil as the carrier oil, the oil was shown to inhibit the large shape change normally associated with the polymorphic transformation, putatively reducing hydrophobic attraction

between particles [37]. The NLC lipid crystals appeared to be less ordered than SLN crystals as lower melting and crystallization temperatures were observed in the presence of oil. In another study with glyceryl behenate (Compritol 888 ATO) used as the lipid and caprylic/capric triglycerides (Miglyol 812) used as the oil, NLC dispersions were shown to be most stable in the absence of oil and at high oil concentrations [11]. The large fraction of monoglycerides and diglycerides in Compritol was argued to be responsible for the long-term stability of SLN dispersions in the absence of oil. The highly disordered state of Compritol NLCs with high concentrations of Miglyol was believed to delay recrystallisation and improve physical stability. However, another series of studies on Compritol/Miglyol NLCs showed that the lipid crystals were not disturbed in their structure as expected by oil addition [54-56]. Instead, these studies indicated that the NLCs consisted of an external liquid compartment on the particle surface that strongly interacted with the solid lipid. Therefore, NLCs may not be solid lipid nanoparticles with embedded liquid droplets as reported in the literature [36, 38], but rather they may consist of an oil layer between the solid lipid and the surfactant layer [54-56].

1.4 Rheology of Lipid Nanoparticle Dispersions

Rheological properties such as viscosity are critical parameters of lipid nanoparticle dispersions for typical applications such as pharmaceutical and cosmetic products [57-63]. A common method to produce lipid nanoparticle systems with the desired rheological properties involves incorporating the SLN or NLC dispersion into topical vehicles such as creams or hydrogels [64-67]. This approach has several disadvantages, including limited SLN/NLC loading, possible incompatibilities with the added viscosity enhancer and more complex manufacturing steps [60, 68]. Consequently, the creation of NLC dispersions with rheological properties that can be tailored without the use of additional ingredients is highly desirable.

A few previous studies have focused on the influence of key SLN properties (particle size, physical state of the lipid, emulsifier amount) on the rheological properties of the dispersion as well as understanding how the formulation can be modified to produce dispersions with the desired rheological properties without adding further ingredients [58-60]. I hypothesized that the rheological properties of NLC dispersions could be tuned by controlling the degree of aggregation since properties such as viscosity should depend on the aggregated particle network structure [60, 69, 70]. To the best of my knowledge, the rheological properties of NLC dispersions with controlled aggregation have not been investigated.

1.5 Particle Aggregation and Polymorphic Transformation Modeling

Mathematical modeling is a powerful complementary tool to experimentation for understanding and manipulating SLN aggregation behavior. Starting from the classic work of Smoluchowski [71], the population balance equation (PBE) has been widely used to model the aggregation dynamics of particle suspensions [72-77]. The PBE is a mass balance on particles and requires specification of the aggregation rate $\beta_{i,k}$ between two particles of size i and *k* [78]. The aggregation rate is the product of the particle collision frequency and the aggregation efficiency, which is typically specified in terms of the stability ratio. Most PBE models of particle aggregation are based on the assumption that the particle collision frequency is determined by Brownian diffusion. Calculation of the stability ratio requires specification of the interaction potential between particles[79, 80]. In DLVO theory for charged particles [72, 74, 75, 77, 81], the interaction potential includes van der Waals attraction and electrostatic repulsion forces[80]. While the literature on PBE modeling of nanoparticle aggregation is extensive, the use of PBE models to describe solid-state polymorphic transformations has received little attention. One exception is a PBE model for the solid-state polymorphic transformation of TiO_2 that involves a first-order rate

expression for transformation combined with Smoluchowski coalescence for coarsening of anatase and rutile particles [82].

The characterization of solid-state kinetics typically involves modeling the fraction transformed as a function of time on the basis of some topological mechanism. This form of characterization has been dominated by the kinetic model proposed (independently) by Avrami [83-85] and Erofeyev [86] which has found wide applicability. The Avrami-Erofeyev relationship assumes that the transformation proceeds by a nucleation-and-growth mechanism and takes into account the coalescence and ingestion of other nuclei as the new phase grows. Nucleation is assumed to be random, that is, if the entire sample was divided into small equal volumes, then the probability of a nucleus forming in each element in unit time is the same. The theory also assumes isotropic growth and that the number of potential nucleation sites are limited. An important exception where the Avrami-Erofeyev model is inappropriate is the situation where the sample consists of a fine powder. Here the transformation resulting from any nucleation event is constrained to the individual crystallite by the crystallite's boundaries [87].

Prior to my research, there was no published applications of PBE modeling to the aggregation of lipid nanoparticles dispersions.

CHAPTER 2

EXPERIMENTAL INVESTIGATION AND POPULATION BALANCE EQUATION MODELING OF SOLID LIPID NANOPARTICLE AGGREGATION DYNAMICS

2.1 Introduction

In this chapter, a PBE model was formulated to predict SLN aggregation and the particle volume percent distribution under the assumption that particles collide due to Brownian motion and that only β particles could aggregate. The polymorphic transformation was assumed to occur in the solid state and the rate was modeled to be first-order in the concentration of α particles, which is consistent with a nucleation controlled transformation [88]. The effect of temperature was not considered in this study. The PBE model explicitly accounted for the effects of surfactant coverage on the polymorphic transformation rate and the aggregation efficiency as well as the surface area increase caused by the creation of β primary particles. This effort represents a first step towards model-based design of SLN formulation and processing strategies that maximize particle stability and minimize aggregation.

2.2 Materials and Methods

2.2.1 Materials

The lipid tristrearin was purchased from Fisher Scientific. The surfactants Tween 60 and Span 60 were supplied by Procter and Gamble. All materials were used as received.

2.2.2 SLN Preparation

An aqueous phase was prepared by mixing nanopure water with 1 weight percent surfactant followed by heating to 85°C. The surfactant was a mixture of Tween 60 and Span 60

with a molar ratio of 1.61. This ratio was determined by matching the hydrophilic-lipophilic balance (HLB) value of the surfactant mixture with the tristrearin HLB value of 11. Coarse oil-in-water emulsions with 5 weight percent lipid and 1 weight percent surfactant were prepared by blending the lipid and aqueous phases at 85°C using a high speed blender (Ultra-Turrax Model T25, Rose Scientific Ltd.) for 5 minutes at 16,000 rpm. Fine emulsions were obtained by passing the coarse emulsion through a high pressure homogenizer (Emulsiflex C-3, Avestin Inc.) 1-5 times at 500 bar. The coarse and fine emulsions were cooled in an ice bath for 8 hours to obtain SLNs, and the resulting dispersions were stored at 20°C.

2.2.3 SLN Characterization

Particle size distributions of SLN suspensions was measured daily at room temperature by static light scattering (Mastersizer 2000, Malvern Instruments). A refractive index of 1.47 for the particles and 1.33 for water was used to calculate particle size distributions.

The relative amount of α and β crystal polymorphs in the solid lipid phase was determined daily by differential scanning calorimetry (DSC; Q100-0416, TA Instruments). Approximately 7-10 mg of an SLN dispersion was placed in a hermetic aluminum pan and sealed. An empty pan was used as a reference. The SLN dispersions were scanned in the temperature range of 40°C to 65°C at a heating rate of 2°C/min. The melting points of the two polymorphs corresponded to peaks in the heating curve at approximately 48.7°C for the α polymorph and 56.8°C for the β polymorph. These values are lower than those reported elsewhere in the literature (54.0°C for the α polymorph and 72.5°C for the β polymorph [89]), presumably due to melting point reduction for the small particle sizes considered in my study [90]. The relative amount of each polymorph on a weight basis was determined by integrating the area of each peak and dividing the area by the

melting enthalpy of the associated polymorph. The melting enthalpies used were 145.08 kJ/mole and 203.26 kJ/mole for α-form and β-form crystals, respectively [89].

2.2.4 Mathematical Model

Two versions of the PBE model were developed for predicting SLN aggregation dynamics. The basic model consisted of a standard discretized PBE for pure aggregation processes [76]. The second model was an enhanced version of the basic model which accounted for the polymorphic transformation and surfactant surface coverage.

2.2.4.1 Basic PBE Model

The discretized population balance equation for pure aggregation processes is [76]:

$$\frac{dN_i(t)}{dt} = \frac{1}{2}\sum_{k=1}^{i-1} \beta_{i-k,k} N_{i-k}(t) N_k(t) - N_i(t) \sum_{k=1}^{M} \beta_{i,k} N_k(t) \tag{2.1}$$

where N_i is the number concentration of the particles at volume x_i and $\beta_{j,k}$ is the aggregation rate between particles of volume x_j and x_k. The two terms on the right hand side of Eq. (2.1) correspond to the rate of particle creation and loss at volume x_i due to aggregation. Since the SLN dispersions were simply stored, the particles were assumed to collide due to Brownian motion and the following aggregation rate function was used:

$$\beta_{\mathrm{b}} = \frac{\beta_0}{W}(x_j^{1/3} + x_k^{1/3})\left(\frac{1}{x_j^{1/3}} + \frac{1}{x_k^{1/3}}\right) \tag{2.2}$$

$$\beta_0 = \frac{2k_{\mathrm{B}}T}{3\mu} \tag{2.3}$$

where T is the absolute temperature, μ is the dynamic viscosity of the dispersion, and k_{B} is the Boltzmann constant. The stability ratio W represents the reciprocal of the collision efficiency and is calculated as the ratio of the aggregation rates without and with colloidal interactions. For

dispersed systems with only van der Waals attraction and electrical repulsion, the stability ratio can be calculated by the well known DLVO theory [72, 74, 75, 77]. In SLN dispersions, additional forces such as hydrophobic attraction between uncovered lipid surfaces and interactions between surfactant molecules can be important. Because these forces were difficult to include in the PBE model, the stability ratio *W* was used as an adjustable parameter to match the experimentally observed time scale.

2.2.4.2 Enhanced PBE Model

An enhanced PBE model was developed from the basic model by incorporating the effects of the polymorphic transformation and surfactant surface coverage on aggregation dynamics. The enhanced model was formulated under the simplifying assumptions that primary particles comprised entirely of α crystals were transformed into primary particles comprised entirely of β crystals and that only β-form particles could aggregate. The PBE was written as:

$$\frac{dN_{\alpha,i}(t)}{dt} = -kN_{\alpha,i} \tag{2.4}$$

$$\frac{dN_{\beta,i}(t)}{dt} = kN_{\alpha,i} + \frac{1}{2}\sum_{k=1}^{i-1}\beta_{i-k,k}N_{\beta,i-k}(t)N_{\beta,k}(t) - N_{\beta,i}(t)\sum_{k=1}^{M}\beta_{i,k}N_{\beta,k}(t) \tag{2.5}$$

where $N_{\alpha,i}$ is the number concentration of α-form particles at volume x_i, $N_{\beta,i}$ is the number concentration of β-form particles at volume x_i, and k is the polymorphic transformation rate. As shown in Eq. (2.4), the transformation rate was assumed to be first order in the concentration of α-form particles.

Experimental studies have shown that increased surfactant surface coverage will alter crystallization behavior, reduce shape change, and slow polymorphic transformation and particle aggregation (Fig.2.1 (a) and (b)) [33]. To partially incorporate this effect, the polymorphic transformation rate k was modeled to be first order in the particle surface coverage:

$$k = k(\Gamma) = \left(1 - \frac{\Gamma}{\Gamma_c}\right) k_0 \tag{2.6}$$

where Γ is the surface coverage of the particle (mole/cm^2), and Γ_c is the critical surface coverage at which the transformation rate will be zero. To account for the effect of surface coverage on the aggregation rate, the aggregation function was modified as follows:

$$\beta(x_j, x_k) = \left(1 - \frac{\Gamma_j}{S\Gamma_\infty}\right)\left(1 - \frac{\Gamma_k}{S\Gamma_\infty}\right)\beta_b \tag{2.7}$$

where Γ_∞ is the maximum surface coverage at which the aggregation rate will be zero. The first two terms account for the effects of surface coverage and shape change on the collision efficiency, while the last term is the aggregation rate function used in the basic model (Eq. (2.2)).

The surface area increase *S* due to polymorphic transformation was calculated by assuming β-form particles have a cylindrical shape with height much less than the diameter (Fig. 2.1(c)):

$$S = \frac{1 + p}{2(0.75p)^{2/3}} \tag{2.8}$$

where l_1 and l_2 are the height and diameter of the cylinder, respectively, and the aspect ratio $p = l_1/l_2$. The relationship between *p* and *S* is shown in Fig. 2.1(d). From electron micrographs of tristearin nanoparticles[24], the aspect ratio *p* was estimated to be 0.2. The corresponding surface area increase was calculated to be $S = 2.12$, which was consistent with a value reported in the literature [30]. Because the effect of surface coverage on shape variability was not considered in this model, all β-form particles were assumed to have same aspect ratio *p*. For the *i*-th particle, the shape change was assumed to cause a decrease in the surface coverage from Γ_i for the α-form particle to Γ_i/S for the β-form particle. The effect of reduced surface coverage of β-form particles was included in the collision efficiency (Eq. (2.7)) through multiplicative terms for the *i*-

th and *j*-th particles such that the efficiency was increased if both particles had relatively low coverage.

2.2.4.3 Numerical Solution

The basic and extended PBE models were solved numerically using the fixed pivot technique [91] with 64 node points for discretizing particle size. This method was chosen due to its relatively low computational cost and ability to calculate the particle size distribution with great precision [76]. The PBE models were discretized at every node point, yielding 64 nonlinear ordinary differential equations (ODEs) in time for the basic model and 128 nonlinear ODEs for the extended model owing to the use of two particle types. The ODE systems were integrated in time with the Matlab code ode15s to calculate the volume percent distribution at each node point.

2.3 Results and Discussion

2.3.1 Experimental Results

Emulsions prepared with 5 weight percent lipid and 1 weight percent surfactant by subjecting the lipid/surfactant/water mixture to high speed mixing (premix emulsion) followed by one homogenizer pass (1^{st} pass emulsion) or five homogenizer passes (5^{th} pass emulsion) were cooled and stored to investigate aggregation dynamics. The evolution of the particle size distribution of SLNs prepared from the premix, 1^{st} pass, and 5^{th} pass emulsions is shown in Fig. 2.2(a)-(c). Smaller initial size distributions were obtained as the number of homogenization passes increased, and the initial distribution was unimodal for each sample. Aggregation was first apparent in the 5^{th} pass sample on day 2 of storage as a second peak centered at a much larger size emerged and the distribution became bimodal. The second peak was indicative of large aggregates being formed. Biomodal distributions for the 1^{st} pass sample and premix sample were

not observed until days 3 and 7, respectively. The first peak in the size distribution of the 5th pass sample disappeared after 6 days, suggesting the incorporation of all primary particles into much larger aggregates. Disappearance of the first peak for the 1st pass sample and premix sample was not observed until days 11 and 15, respectively. The evolution of the average diameter d_{32} of the premix, 1st pass, and 5th pass samples is shown in Fig. 2.2(d). The d_{32} value of 5th pass sample increased most rapidly and jumped to 65 μm after 5 days. Similar abrupt changes in the d_{32} value of the 1st pass and premix samples were not observed until days 9 and 13, respectively. These results show that SLNs with smaller initial size distributions, and therefore less surfactant surface coverage, exhibited faster aggregation dynamics. I incorporated this effect into the PBE model by making the collision efficiency a function of surfactant coverage as shown in Eq. (2.7).

Differential scanning calorimetry (DSC) was used to examine the evolution of the crystal polymorph content of SLNs prepared from the premix, 1st pass, and 5th pass emulsions. Fig. 2.2(e) shows a representative DSC scan for the stored 5th pass sample. The melting points of the α and β polymorphs corresponded to the two peaks in the heating curves, as the β' polymorph was not identified due to rapid transformation of β' crystals to β crystals [23]. Initially only a single peak was observed at about 48.7°C, corresponding to the α-form crystal melting temperature. On day 2 of storage, another melting peak emerged at about 56.8°C, corresponding to the melting of β-form crystals. Over time, the first peak became smaller and the second peak became larger as α-form crystals were transformed into β-form crystals. The relative amount of the two polymorphs was obtained by integrating the area of each peak and dividing by the melting enthalpy of the associated polymorph. The evolution of the α polymorph content (C_α) in the premix, 1st pass, and 5th pass samples is shown in Fig. 2.2(f). The α content decreased most rapidly in the 5th pass sample and most slowly in the premix sample. Moreover, the largest total change in α content was observed in the 5th pass sample even through this sample was only stored 6 days while the

1st pass and premix sample were stored 11 and 15 days, respectively. These results demonstrate that SLNs with smaller initial size distributions and less surfactant surface coverage exhibited faster and more complete polymorphic transformation. I incorporated this effect into the PBE model by making the polymorphic transformation rate a function of surfactant coverage as shown in Eq. (2.6).

A comparison of the average particle sizes in Fig. 2.2(d) and the polymorph contents in Fig. 2.2(f) show that particle aggregation and polymorphic transformation occurred at approximately the same rate. This observation suggests that polymorphic transformation was the rate limiting step of the aggregation process, and that primary particles quickly aggregated once they had sufficient β content. I incorporated this effect into the PBE model by allowing only β-form particles to aggregate as shown in Eq. (2.5). However, the DSC results clearly demonstrate that aggregating particles had substantial α content, which contradicts my modeling assumptions that dispersions were comprised of purely α-form and β-form particles and that only β-form particles could aggregate. Because the removal of these simplifying assumptions would require the development of a considerably more sophisticated PBE model, I pursued the simpler PBE models described earlier.

2.3.2 Comparison of the Basic and Enhanced PBE Models

To evaluate the importance of explicitly modeling the polymorphic transformation, the basic and enhanced PBE models were compared to the experimental data in Fig. 2.2. The basic model required specification of the constant $\beta_0 = 2k_BT/3\mu$ and the stability ratio W in Eq. (2.2). I used T = 293K and μ = 10.02 Po by approximating the dynamic viscosity of the dispersion by the value for pure water, yielding $\beta_0 = 2.3\times10^{-13}$ m^{3}day^{-1}. The stability ratio was chosen to be W = 100 because this value yielded the correct timescale for the aggregation dynamics as reflected by the

evolution of the particle size distribution. The initial particle size distribution used for simulation corresponded to the initial particle size distribution of the 5th pass sample.

The predicted evolution of the particle size distribution obtained with the basic PBE model is presented in Fig. 2.3(a). Unlike experimental data, the particle size distribution remained unimodal throughout the aggregation process. Rather than a second peak at large particle sizes growing as aggregation proceeded, the single peak moved gradually toward large particle sizes with a fast initial rate and a slower rate as the particle number concentration decreased. A similar result has been reported for PBE modeling of aggregation dynamics in dense silica suspensions [76]. These results demonstrate that the basic PBE model is insufficient to qualitatively describe aggregation behavior in SLN dispersions.

The extended PBE model required specification of the polymorphic transformation rate constant k_0, the critical surface coverage Γ_c, and the aspect ratio γ, as well as the constant β_0 and W. The critical surface coverage was chosen to be Γ_c = 1.19×10^{-9} mole/cm^2 based on the assumption of complete surface adsorption for the premix sample, while the aspect ratio was estimated as p= 0.2 from electron micrographs of tristearin nanoparticles [24]. The maximum surface coverage Γ_∞ is assumed to have the same value with Γ_c. The constants β_0 and W and the initial particle size distribution remained unchanged from the basic model. For this comparison, the polymorphic transformation rate k was specified directly. If the transformation rate was assumed to be fast by selecting k = 20 day^{-1}, the extended and basic models produced almost identical predictions characterized by unimodal particle size distributions (not shown). Conversely, bimodal distributions in agreement with experiments were obtained when the transformation rate was assumed to be slow by selecting k = 0.2 day^{-1} as shown in Fig. 2.3(b). The predicted evolution of the average particle α content (C_α) obtained with the enhanced PBE model

in Fig. 2.3(c) also agreed qualitatively with data. These results suggest that explicit modeling of the polymorphic transformation was critical for capturing the aggregation dynamics.

2.3.3 Parameter Estimation for the Enhanced PBE Model

The stability ratio value W = 30 was obtained by approximately matching the experimentally observed growth rate of the second peak at large particle sizes. The polymorphic transformation rate constant k_0 and the critical surface coverage Γ_c were estimated from my experimental data to further demonstrate that polymorphic transformation is the rate determining step and to obtain improved model predictions. The analytical solution of the first-order ODE for the polymorphic transformation (Eq. (2.4)) is:

$$\frac{N_{\alpha,i}(t)}{N_{\alpha,i,0}} = -e^{kt} \tag{2.9}$$

where $N_{\alpha,i,0} = N_{\alpha,i}(0)$. The ratio on the left-hand side of Eq. (9) can be shown to equal the α-form crystal mass content C_α:

$$C_\alpha = -e^{kt} \tag{2.10}$$

$$\ln(C_\alpha) = -kt \tag{2.11}$$

Therefore, k was obtained by linear regression of the average α content versus time data obtained from DSC (Fig. 2.2(f)) as shown in Fig. 2.4(a)-(c) for the three SLN samples. The large correlation coefficient (R) values obtained supported the hypothesis that the polymorphic transformation rate was first order in the concentration of α-form particles. The estimated k values ranged from 0.04 to 0.26 day^{-1}, which further supported the conclusion that polymorphic transformation was the rate determining step in the aggregation process.

Eq. (2.6) can be rewritten as:

$$k(\Gamma) = k_0 - \left(\frac{k_0}{\Gamma_c} \right) \Gamma \tag{2.12}$$

Therefore, the model parameters k_0 and Γ_c were estimated by linear regression of the polymorphic transformation rate k versus the surface coverage Γ. Because the surface coverage was not measured in my study, approximate values were obtained as follows. For each sample, the surface coverage was calculated by dividing the total moles of surfactant by the total surface area calculated from the particle size distribution at day 0 assuming that all surfactant was equally adsorbed on particle surfaces. The linear regression results in Fig. 2.4(d) supported the hypothesis that the polymorphic transformation rate was a linear function of surface coverage and yielded the following parameter values: k_0 = 0.57 day^{-1} and Γ_c = 0.13×10^{-10} mole/cm^2.

2.3.4 Simulation Results for the Enhanced PBE Model

The enhanced PBE model was simulated with the estimated parameters k_0 and Γ_c to generate particle size distribution predictions for the three SLN samples as shown in Fig. 2.5(a)-(c). The model was able to capture the bimodal nature of the distributions as well as the approximate size of formed aggregates observed experimentally. The model predicted the second peak would be centered at 65μm, 85μm, and 80μm for the premix, 1st pass, and 5th pass samples, while the corresponding values determined experimentally were 60μm, 80μm, and 90μm (Fig 2.2(a)-(c)). Moreover, the model reproduced the trend between initial particle size and aggregation rate as the 5th pass sample was predicted to aggregate most rapidly and the premix sample was predicted to aggregate most slowly.

As expected, due to simplicity of the enhanced PBE model, discrepancies between the experimental and predicted distributions were apparent. The model predicted that the second peak of the particle size distribution would be narrower then observed experimentally. This

discrepancy may have been partially attributable to the Brownian kernel being inadequate for describing collision events between larger particles. Other possible causes of this modeling error included that the effect of surface coverage on particle shape variability was not taken into account and that the stability ratio *W* was used as a fitting parameter independent of particle size rather than being calculated from interparticle forces [72, 74, 75, 77]. Furthermore, the model predicted that the first peak would disappear more slowly than observed experimentally. As discussed below, I believe that this discrepancy was attributable to my assumption that only β-form particles could aggregate.

Experimental and predicted average diameter d_{32} values are compared in Fig. 2.6(a)-(b). The model captured the trend that the 5th pass sample would exhibit the largest d_{32} increase while the premix sample would exhibit the smallest d_{32} increase. However, the predicted d_{32} values were consistently smaller than the corresponding experimental values. Furthermore, the model did not capture the sudden increase in d_{32} values observed experimentally (Fig. 2.2(d)) but not plotted in Fig. 2.6(a) to facilitate the comparison. These discrepancies were attributable to the slow disappearance of the first peak in the simulated particle size distributions. Experimental and predicted values of the α-form crystal mass content C_α are compared in Fig. 2.6(c)-(d). The model produced quantitatively accurate C_α predictions for the three samples.

These comparisons suggest that the enhanced PBE model provided a satisfactory description of polymorphic transformation but an incomplete description of particle aggregation. The DSC results clearly show that that aggregates had substantial α content (Fig. 2.2), contradicting my assumption that only primary particles with 100% β-polymorph content could aggregate. A more plausible hypothesis is that a particle must have a critical amount of β content to aggregate and that the aggregation rate increases with increasing β content of the colliding particles. This hypothesis would explain the slow disappearance of the first peak in the predicted

particle size distribution, as primary particles could aggregate and disappear more quickly. However, testing of this hypothesis would require the development of a considerably more sophisticated PBE model in which both particle size and polymorph content were treated as internal variables. This effort was deemed beyond the scope of the current study.

2.3.5 Experimental Validation of the Enhanced PBE Model

To investigate extensibility of the enhanced PBE model to different formulations, 1st pass and 5th pass emulsions, prepared with 5 weight percent lipid and 0.5 weight percent surfactant, were cooled to make SLN dispersions. PBE model predictions were generated with the same parameters as used for 1 weight percent surfactant. The reduced surfactant concentration was incorporated in the model through the surface coverage Γ. Experimental particle size distributions shown in Figure 2.7(a)-(b) demonstrated that the 5th pass sample aggregated more rapidly than the 1st pass sample. As compared to the 1 weight percent surfactant case (Fig. 2.2), faster aggregation dynamics were observed in the 0.5 weight percent surfactant samples because less surfactant was available for particle stabilization. Predicted particle size distributions in Figure 2.7(c)-(d) showed qualitative agreement with the experimental results, as the 5th pass sample was predicted to aggregated most rapidly and the second peaks of the predicted bimodal distributions were centered near the experimentally observed sizes. However, the model predicted that the first peak would disappear more slowly and that the second peak would be sharper than observed in experiment.

Experimental and predicted average particle diameter d_{32} values are compared in Figure 2.7(e)-(f). The model correctly predicted that the 5th pass sample would aggregate most rapidly due to smaller initial particle sizes and reduced surfactant coverage. However, the model produced slower increases in d_{32} values than observed experimentally and failed to capture the

large d_{32} increase that accompanied the disappearance of the first peak in the 5th pass sample. Experimental and predicted average particle α content C_α values are compared in Figure 2.7(g)-(h). The model produced quantitatively accurate predictions of the α content for the 1st pass sample, while predicted C_α values trailed the experimental values for the 5th pass sample. As discussed for the 1 weight percent surfactant case, the more accurate predictions obtained for the α content compared to particle size distributions suggest model deficiencies such as the use of the Brownian collision kernel for large particles, the assumption that primary particles are comprised completely of α-form or β-form crystals, and the assumption that only β-form particles can aggregate.

2.4. Conclusions

I developed a population balance equation (PBE) model to describe aggregation dynamics in stored dispersions of solid lipid nanoparticles (SLNs). The model was based on the hypothesis that particle aggregation was driven by lipid crystals undergoing a polymorphic transformation from the thermodynamically unstable α form the stable β form, which created an increase in particle surface area, a decrease in surfactant surface coverage, and an increase hydrophobic attraction between particles. Experiments with my model system of 5 weight percent tristearin and 1 weight percent surfactant (mixture of Tween 60 and Span 60) showed that the polymorphic transformation was the rate determining step in the aggregation process, SLNs with smaller initial size distributions underwent polymorphic transformation and aggregation more rapidly, and aggregates contained particles with both α and β crystals. The PBE model generated predictions of the average polymorph content and the aggregate size distribution under the simplifying assumptions that primary particles comprised entirely of α crystals were transformed into primary particles comprised entirely of β crystals, the polymorphic transformation rate was first

order in the α-form particle concentration and surfactant coverage, only β-form particles could aggregate, and particles collided due to Brownian motion.

PBE model parameters were estimated from average polymorph content and aggregate size distribution measurements for three SLN samples with different initial size distributions. I found that the model was able to capture the bimodal nature of aggregate size distributions, the α-to-β polymorph ratio, and the faster aggregation dynamics of SLNs with smaller initial size distributions. Without re-estimation of parameters, the model was able to capture the faster aggregation dynamics of SLNs prepared with 5 weight percent lipid and 0.5 weight percent surfactant. Collectively these results provide support for the hypothesis that aggregation was driven by the creation of new particle surface area and reduced surfactant coverage due to the polymorphic transformation. However, the PBE model was unable to adequately capture the fast disappearance rates of primary particles, the broad size distributions of formed aggregates, and the significant α contents of aggregating particles. These model discrepancies suggest more complex system behavior in which a particle must have a critical amount of β content to aggregate and the aggregation rate increases with increasing β content of the colliding particles. This would require the development of a more sophisticated PBE model that accounts for polymorph content as an internal variable along with aggregate size to better reproduce my experimental observations.

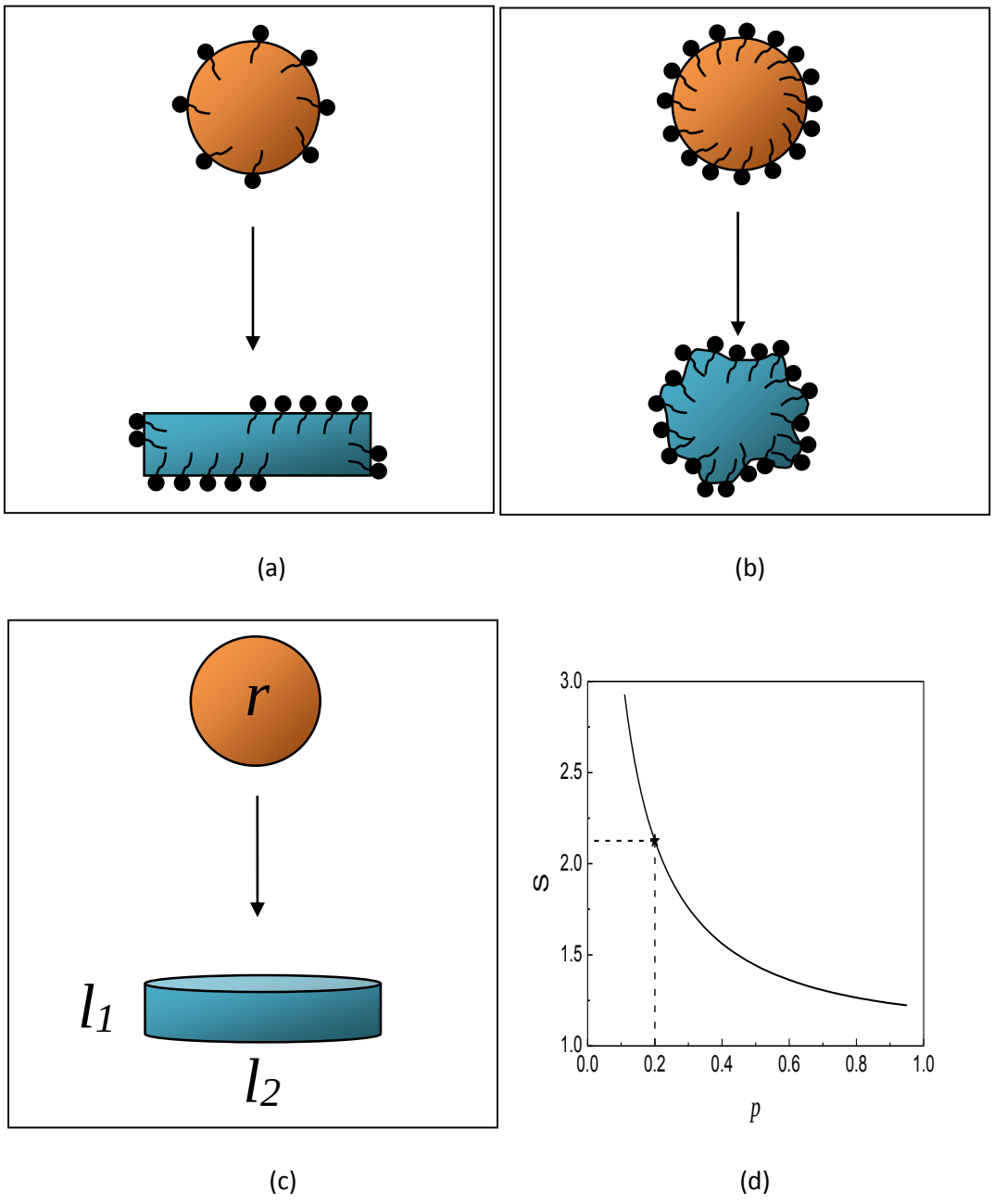

Figure 2.1. Polymorphic transformation of SLNs with (a) relatively low surfactant surface coverage and (b) relatively high surfactant surface coverage. (c) Assumed shape change due to polymorphic transformation of α-form particles to β-form particles. (d) Relationship between the aspect ratio *p* of β-form particles and the surface area increase *S* caused by polymorphic transformation. The dashed lines represent values used in simulations.

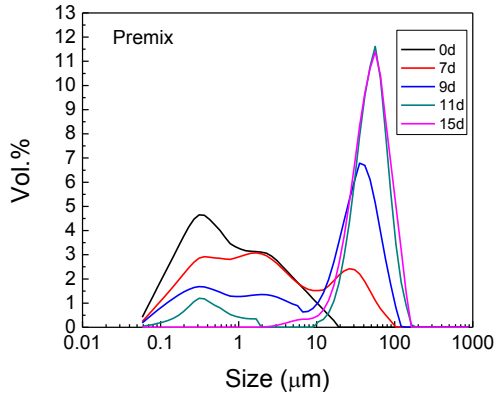
Premix
0d
7d
9d
11d
15d
Vol.%
Size (μm)

(a)

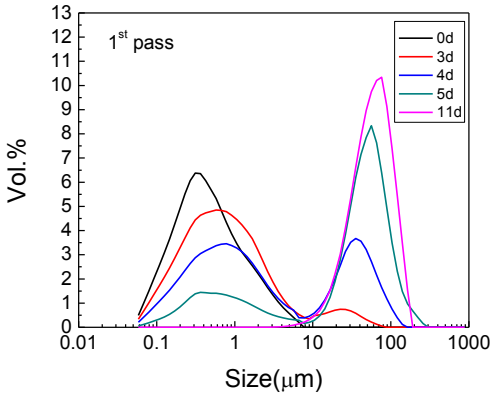
1st pass
0d
3d
4d
5d
11d
Vol.%
Size(μm)

(b)

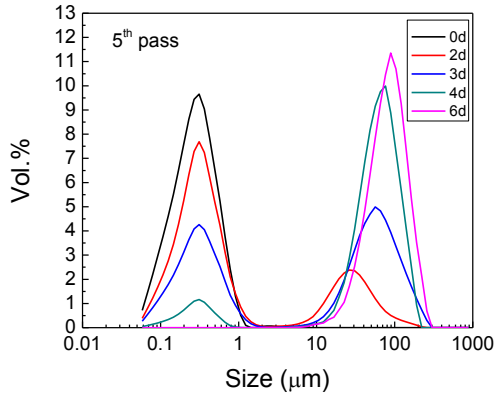
5th pass
0d
2d
3d
4d
6d
Vol.%
Size (μm)

(c)

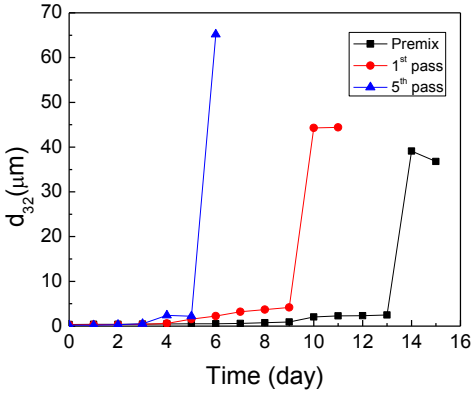
Premix
1st pass
5th pass
d32(μm)
Time (day)

(d)

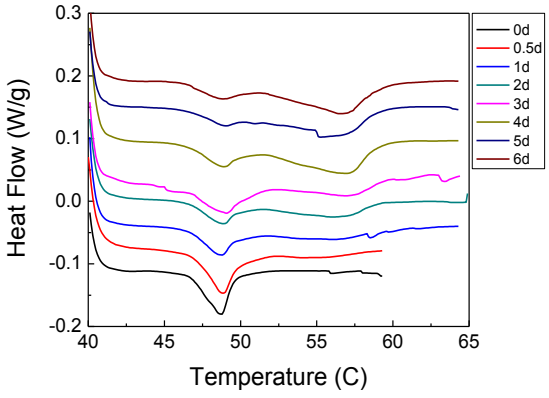
0d
0.5d
1d
2d
3d
4d
5d
6d
Heat Flow (W/g)
Temperature (C)

(e)

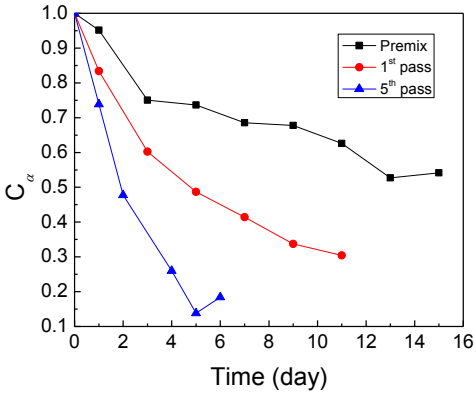
Premix
1st pass
5th pass
Cα
Time (day)

(f)

Figure 2.2. Experimental results for SLNs prepared with 5 wt% tristearin and 1 wt% surfactant. Evolution of the particle size distribution for the (a) premix sample, (b) 1st pass sample and (c) 5th pass sample on different days. (d) Evolution of the average particle size d_{32} for the three samples. (e) DSC scans for the 5th pass sample. (f) Evolution of the average α content for the three samples.

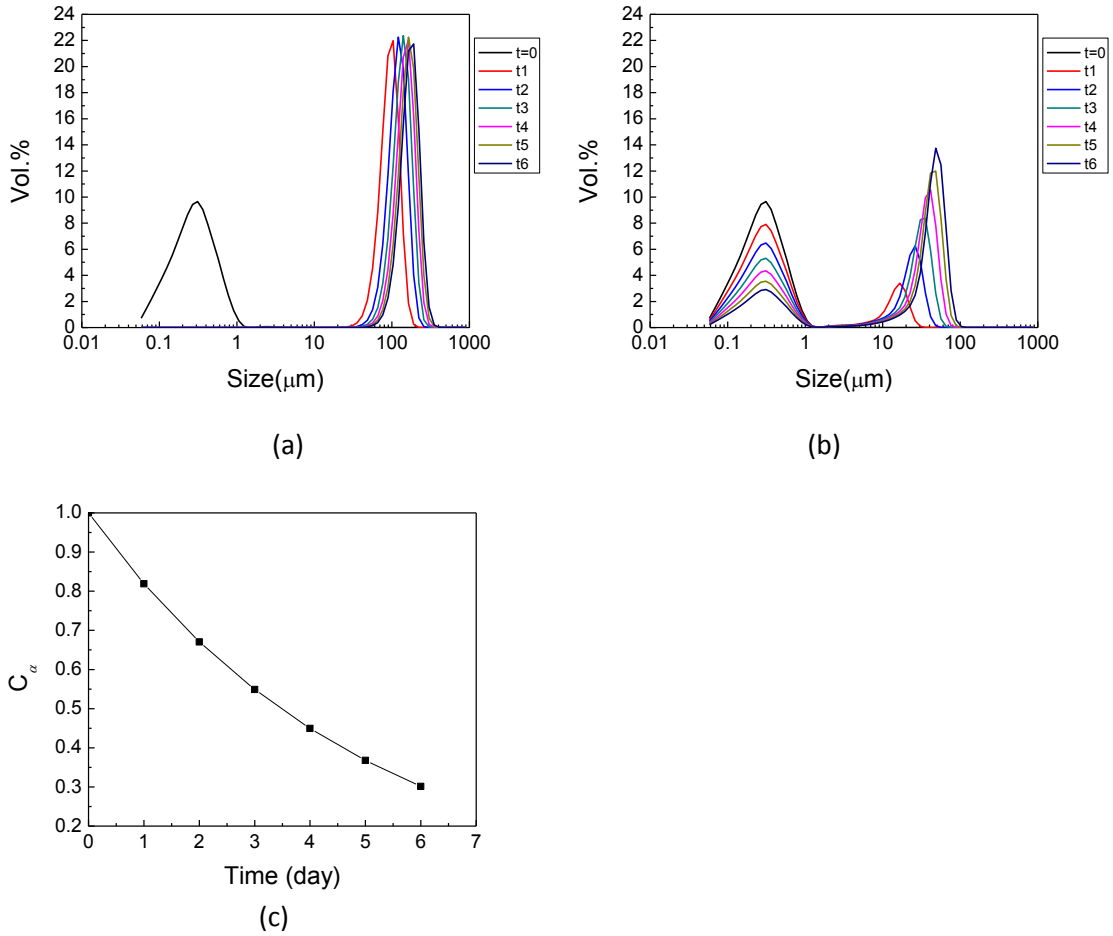

Figure 2.3. Comparison of the basic and enhanced PBE models at different scaled times. (a) Particle size distributions predicted by the basic model. (b) Particle size distribution predicted by enhanced model. (c) Average α content predicted by the enhanced model.

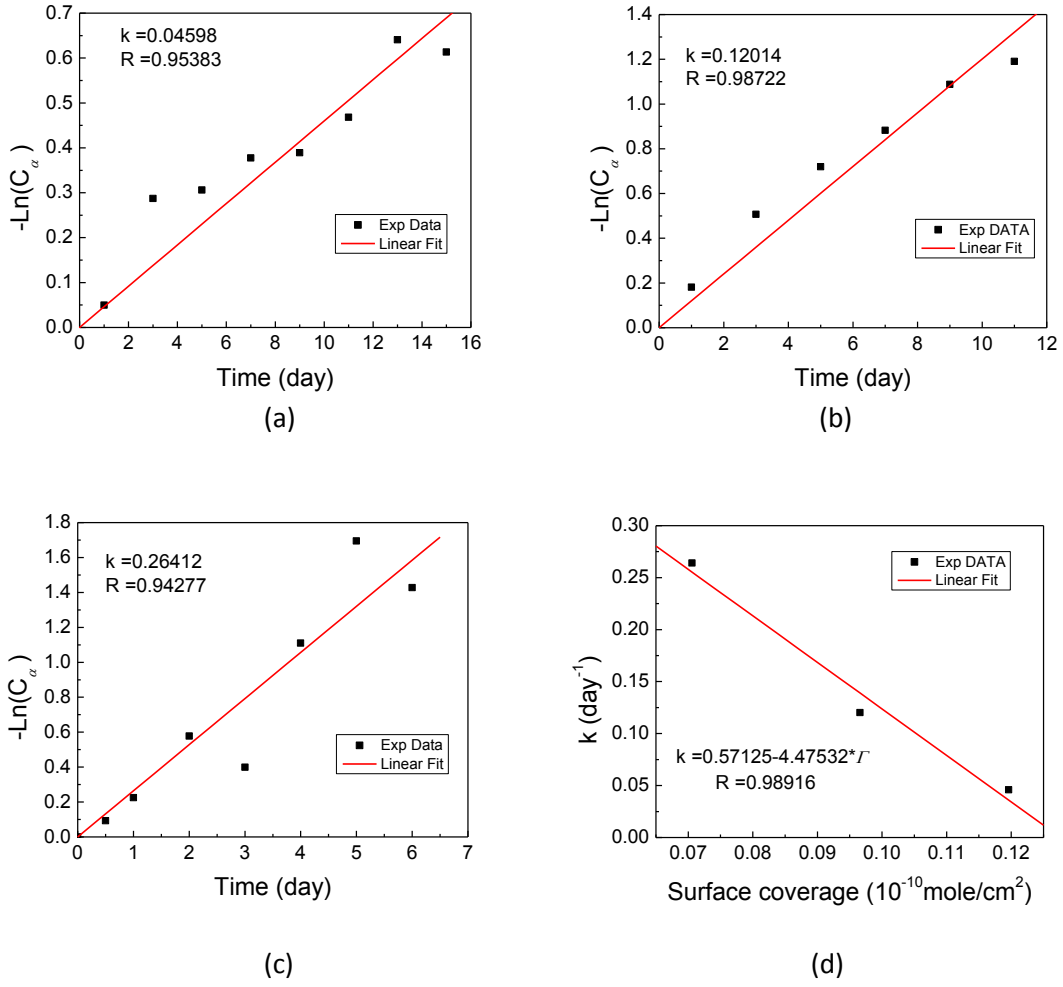

Figure 2.4. Linear regression of α-form crystal mass content versus time for the (a) premix sample, (b) 1st pass sample, and (c) 5th pass sample to estimate values for the polymorphic transformation rate *k*. (d) Linear regression of the polymorphic transformation rate versus surface coverage to estimate the polymorphic transformation rate constant k_0 and the critical surface coverage Γ_c.

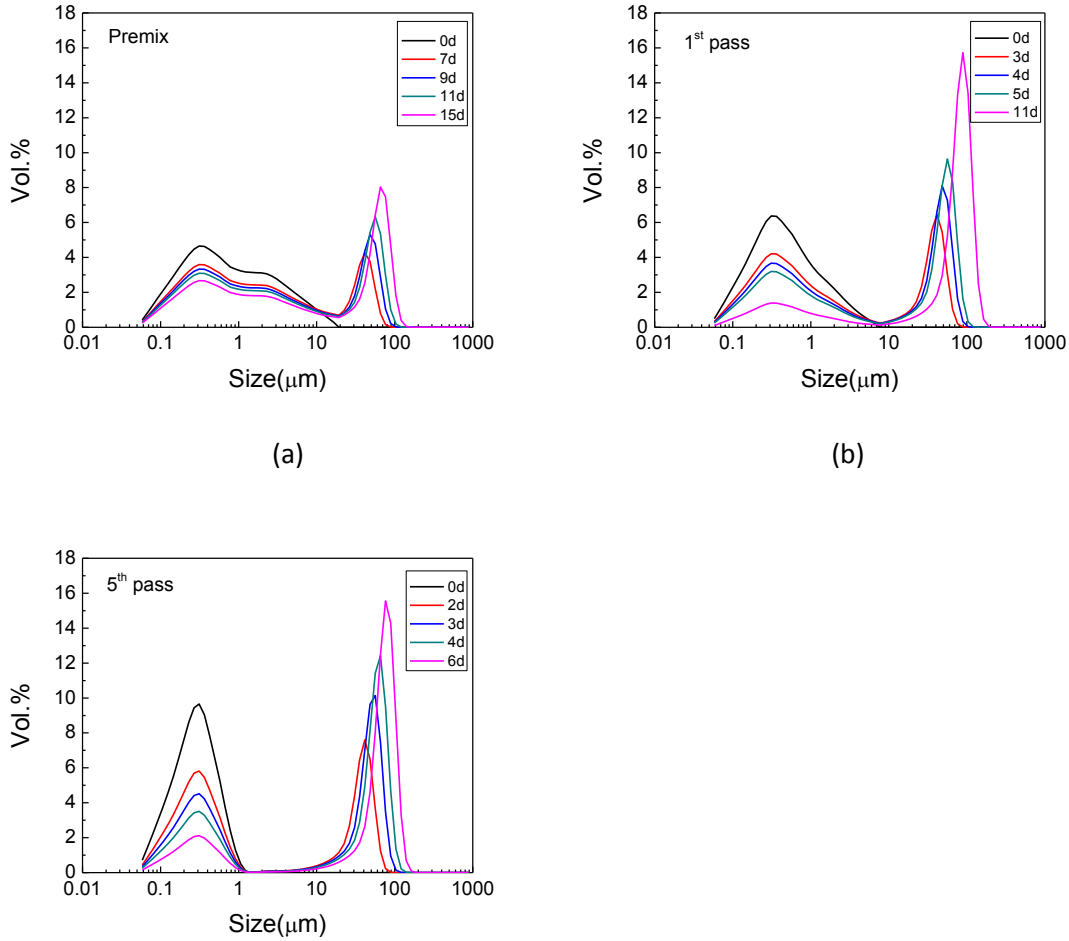

Figure 2.5. Enhanced model simulation results for SLNs prepared with 5 wt% tristearin and 1 wt% surfactant. Evolution of the particle size distribution for the (a) premix sample, (b) 1st pass sample and (c) 5th pass sample on different days.

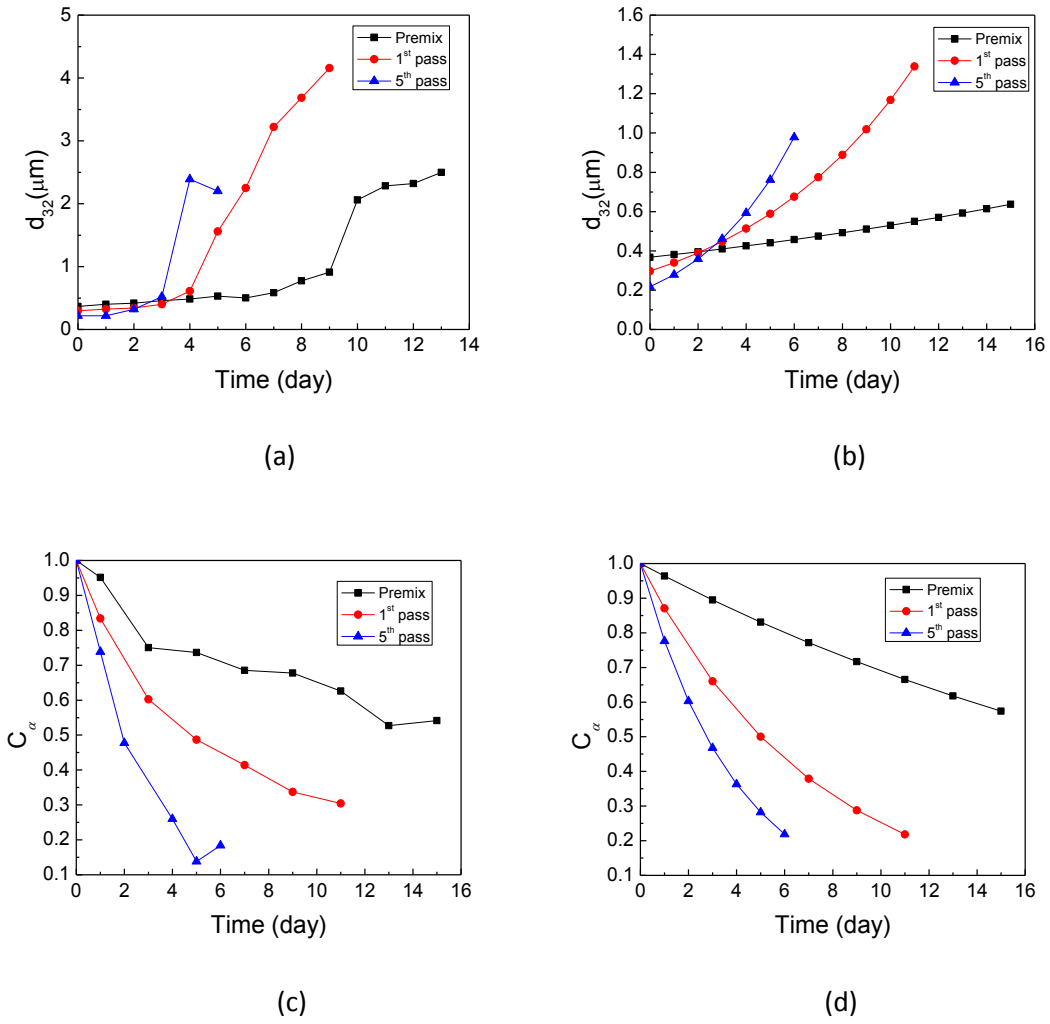

Figure 2.6. Comparison of experimental and enhanced model simulation results for SLNs prepared with 5 wt% tristearin and 1 wt% surfactant. (a) Measured and (b) predicted d_{32} values. (c) Measured and (d) predicted C_α values.

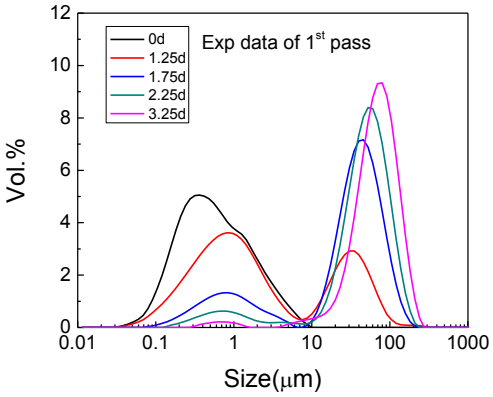
Exp data of 1st pass
0d
1.25d
1.75d
2.25d
3.25d
Vol.%
Size(μm)

(a)

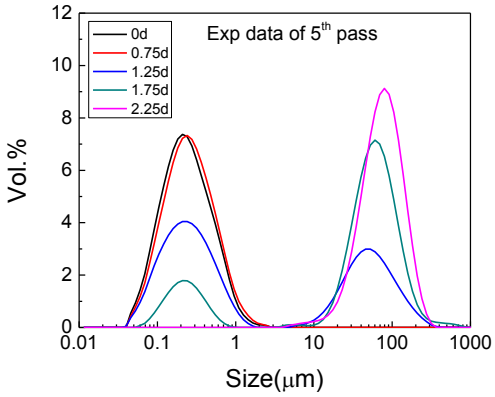
Exp data of 5th pass
0d
0.75d
1.25d
1.75d
2.25d
Vol.%
Size(μm)

(b)

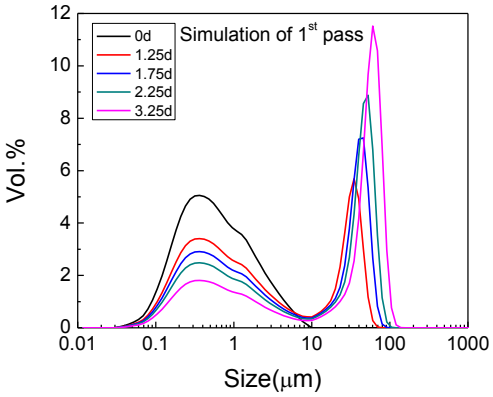
Simulation of 1st pass
0d
1.25d
1.75d
2.25d
3.25d
Vol.%
Size(μm)

(c)

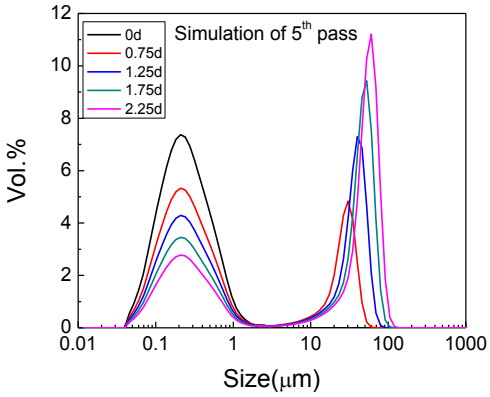
Simulation of 5th pass
0d
0.75d
1.25d
1.75d
2.25d
Vol.%
Size(μm)

(d)

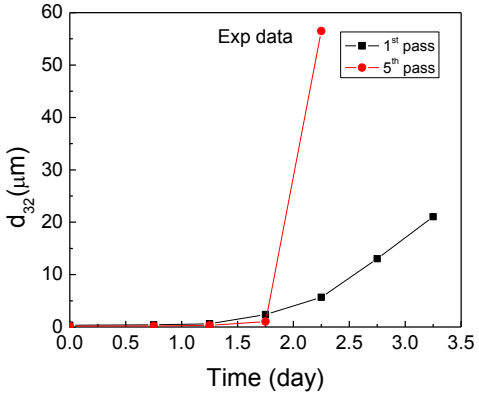
Exp data
1st pass
5th pass
d32 (μm)
Time (day)

(e)

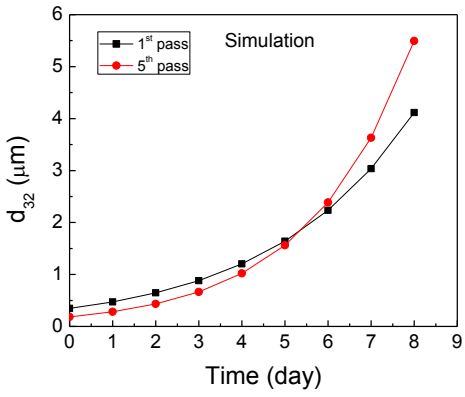
Simulation
1st pass
5th pass
d32 (μm)
Time (day)

(f)

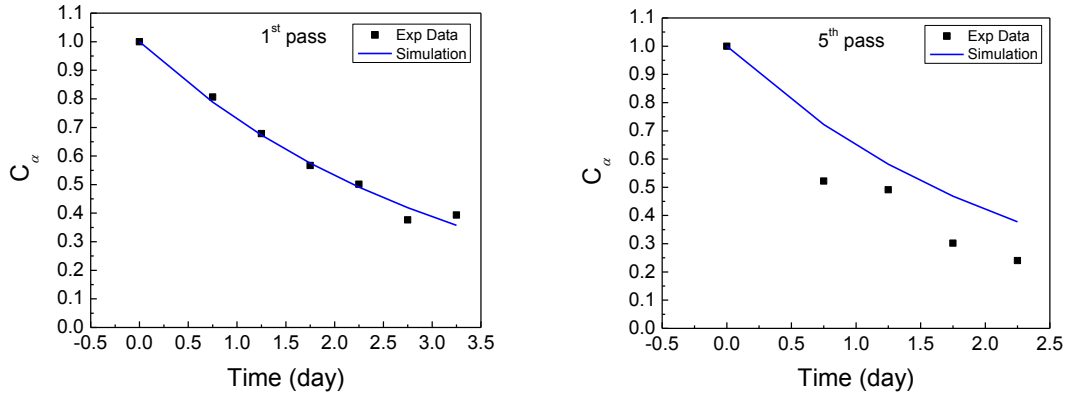

(g) (h)

Figure 2.7. Comparison of experimental and enhanced model simulation results for SLNs prepared with 5 wt% tristearin and 0.5 wt% surfactant. Measured particle size distributions for the (a) 1st pass sample and (b) 5th pass sample. Predicted particle size distributions for the (c) 1st pass sample and (d) 5th pass sample. (e) Measured and (f) predicted average particle diameter d_{32} values. (g) Measured and (h) predicted average α content values.

CHAPTER 3

THE EFFECT OF OIL TYPE ON THE AGGREGATION STABILITY OF NANOSTRUCTURED LIPID CARRIERS

3.1 Introduction

In this chapter, I investigate the effect of carrier oil type and concentration on the polymorphic behavior and aggregation stability of NLCs prepared with the model lipid tristearin. Four pure oils with different structures and two naturally occurring oil mixtures were tested to understand the factors that govern the melting and crystallization temperatures, polymorphic form, particle shape and size distribution of the NLC dispersions. The surfactant concentration was varied for one tristearin/oil system to further examine NLC dispersion stability. To better understand the effect of particle shape change, I modified my previously developed population balance equation model of SLN aggregation dynamics to account for the presence of the carrier oil. I believe that this study represents the first comprehensive investigation of the effect of carrier oil on NLC dispersion stability and represents a first step towards developing rational NLC design strategies.

3.2 Materials and Methods

3.2.1 Materials

Tristearin, triolein and tricaprylin were purchased from TCI America (Portland, OR). Oleic acid, pentadecane and palm oil were purchased from Fisher Scientific (Pittsburgh, PA). Colavita olive oil was purchased from a local grocery store. As shown in Table 3.1, the four pure oils provided a wide range of different melting points and molecular structures. Typical carbon chain distributions of the two common oils listed in Table 3.2 shows the heterogeneous nature of these

materials [92]. The surfactant Tween 60 was supplied by Procter and Gamble. All materials were used as received.

3.2.2 SLN and NLC Preparation

SLNs and NLCs were prepared by using the hot homogenization method. The lipid phase for NLCs was prepared by mixing tristearin and a particular oil at a temperature of 85°C, approximately 10°C above the melting point of tristearin. The lipid phase for SLNs consisted of tristearin without additional oil. The aqueous phase was prepared by mixing deionized nanopure water with Tween 60 surfactant followed by heating to 85°C. Coarse oil-in-water emulsions with 10 weight percent total lipid (tristearin and oil) and 2 weight percent surfactant were prepared by mixing the lipid and aqueous phases at 85°C using a high speed blender (Ultra-Turrax Model T18, IKA-Works Inc.) for 5 minutes at 13,000 rpm. For tristearin/triolein NLCs, the triolein content of the lipid phase was varied from 2.5wt% to 50wt%. For the other oils, the oil content was varied from 2.5wt% to 20wt%. Fine emulsions were prepared by passing the coarse emulsion through a high pressure homogenizer (Emulsiflex C-3, Avestin Inc.) 5 times at 500 bar. The temperature was maintained at 85°C throughout the homogenization process. The coarse and fine emulsions were cooled in a refrigerator (5°C) for 12 hours to obtain SLN and NLC dispersions, which were subsequently stored at room temperature.

3.2.3 SLN and NLC Characterization

3.2.3.1 Particle Size Distribution

Particle size distributions of SLN and NLC dispersions were measured by static light scattering (Mastersizer 2000, Malvern Instruments). Refractive indices of 1.54 for the particles and 1.33 for water were used to calculate particle size distributions [27]. The Mastersizer analyzer

calculates the size of non-spherical particles as the diameter of a volume equivalent sphere. I assumed that aggregate breakage within the Mastersizer was negligible.

3.2.3.2 Differential Scanning Calorimetry (DSC)

A differential scanning calorimeter (Q100-0416, TA Instruments) was used to determine melting and crystallization temperatures and the polymorph content of SLN and NLC dispersions. A 7-10 mg sample drawn from the dispersion was placed in a hermetic aluminum pan and sealed. An empty pan was used as a reference. The dispersions were scanned in the temperature range of 40°C to 90°C with constant heating and cooling rates (10°C/min). The melting and crystallization temperatures were identified from the peak heat flow of the melting and crystallization cycles. To better understand the rate of polymorphic transformation, a so-called quick DSC scan was performed for each sample. The sample was fully melted by holding the temperature at 90°C for 1 minute and then cooled to 0°C at rate of 10°C/min to reform solid particles. After an isothermal hold at 0°C for 1 min, the sample was heated up to 90°C at 10°C/min. This procedure allowed the polymorph content to be determined about 6 minutes after crystallization.

3.2.3.3 Cryo-Transmission Electron Microscopy (cryo-TEM)

SLN and NLC samples were shipped to Procter and Gamble for morphological analysis by cyro-TEM. Samples were prepared for analysis by placing ~2 µl of the dispersion onto a lacey carbon grid, blotting away the excess and plunging the specimen rapidly into liquid ethane using a Controlled Environment Vitrification System (CEVS) device. Once frozen, the samples were stored under liquid nitrogen until being loaded into a single tilt cryotransfer system *(*Gatan Model 626 Cryo-stage, Pleasanton, CA). The samples were then loaded into a transmission *electron microscope* (FEI Tecnai G2 20, Hillsboro, OR) and imaged at 120 KV in low dose mode. The sample was maintained below -175°C during transfer into the microscope and during analysis. Cryo-TEM

analysis was performed approximately 4 weeks following preparation of the samples. This delay was deemed acceptable because the goal of the analysis was to observe the shape of α and β form particles rather than to study the rate of the polymorphic transformation process.

3.2.4 Mathematical Model

I previously developed a population balance equation (PBE) model for SLN aggregation dynamics by incorporating the hypothesized effects of the polymorphic transformation and surfactant surface coverage on particle aggregation [93]. The model was formulated under the simplifying assumptions that primary particles comprised entirely of α crystals are transformed into primary particles comprised entirely of β crystals, particles collide due to Brownian motion and only β-form particles could aggregate. The polymorphic transformation was assumed to occur entirely in solid state and was modeled with nucleation-controlled kinetics, which were first order in the concentration of α particles [88]. The PBE was written as:

$$\frac{dN_{\alpha,i}(t)}{dt} = -kN_{\alpha,i} \tag{3.1}$$

$$\frac{dN_{\beta,i}(t)}{dt} = kN_{\alpha,i} + \frac{1}{2}\sum_{k=1}^{i-1}\beta_{i-k,k}N_{\beta,i-k}(t)N_{\beta,k}(t) - N_{\beta,i}(t)\sum_{k=1}^{M}\beta_{i,k}N_{\beta,k}(t) \tag{3.2}$$

where $N_{\alpha,i}$ is the number concentration of α-form particles with volume x_i, $N_{\beta,i}$ is the number concentration of β-form particles with volume x_i, $\beta_{j,k}$ is the aggregation rate between particles of volume x_j and x_k, and k is the polymorphic transformation rate.

As discussed below, I modified the aggregation rate $\beta_{j,k}$ from my previous study to account for the presence of carrier oil in the NLCs. To account for the effect of surfactant surface coverage on aggregation, the following aggregation rate function was used in this study:

$$\beta(x_j, x_k) = \begin{cases} 0 & \text{if} \quad \Gamma \geq \Gamma_\infty \\ \dfrac{2k_B T}{3\mu W}\left(1-\dfrac{\Gamma}{\Gamma_\infty}\right)^2 \left(x_j^{1/3}+x_k^{1/3}\right)\left(\dfrac{1}{x_j^{1/3}}+\dfrac{1}{x_k^{1/3}}\right) & \text{if} \quad \Gamma < \Gamma_\infty \end{cases} \tag{3.5}$$

where Γ is the surface coverage of the primary β-form particles (mole/cm^2), Γ_∞ is the maximum surface coverage above which collisions do not produce aggregation, T is the absolute temperature, μ is the dynamic viscosity of the dispersion, k_B is the Boltzmann constant and W is the stability ratio which was used as an adjustable parameter to match the experimentally observed time scale of aggregation. In my previous study, the β-form particles were assumed to have constant surface coverage throughout the aggregation process [93]. In this study, the surface coverage Γ was calculated at every time step by dividing the total amount of supplied surfactant by the total surface area of particles assuming that all surfactant was equally adsorbed on particle surfaces. The surface area increase S due to polymorphic transformation was calculated by assuming β-form particles have a cylindrical shape:

$$S = \frac{1+p}{2(0.75p)^{2/3}} \tag{3.4}$$

where p is the aspect ratio, which was calculated as the height divided by the diameter of the cylinder. The PBE model was solved numerically in Matlab using the fixed pivot technique [91] as described in my previous publication [93].

3.3 Results

3.3.1 Pure Oils

Four pure oils (triolein, tricaprylin, oleic acid and pentadecane) with different molecular structures were investigated to better understand the relationship between oil type and NLC dispersion stability.

3.3.1.1 Triolein

Triolein is C18:1 triglyceride that has the same number of carbons as tristearin but contains one degree of unsaturation on each carbon chain. I hypothesized that the three bent carbon chains of triolein could disrupt the packing of tristearin crystals. NLCs with different triolein-trstearin compositions were prepared and stored at ambient temperature to examine dispersion stability. Particle size distributions (PSDs) from samples collected at different times during storage are shown in Fig. 3.1(a)-(e). Aggregation had already started in the pure tristearin SLN dispersion when the sample was removed from the refrigerator, as exemplified by the bimodal distribution at day zero. No small particles were detected after one day, which suggested all that the primary particles had become aggregated. For the NLC dispersion prepared with 2.5wt% triolein, a small second peak at large particle size emerged after 1 day as particles began to aggregate. The second peak became substantially larger after 3 days but did not change significantly during almost 200 additional days of storage, indicating that the dispersion was partially stable to aggregation. When 5wt% triolein was used for NLC preparation, the dispersion was very stable as only a very small amount of large aggregates were detected during long term storage. Similar results were obtained when NLCs prepared with 7.5wt% and 10wt% triolein were stored for more than 200 days. No aggregation was observed in a sample prepared with 20wt% triolein (not shown). Average diameter d_{32} values for eight NLC dispersions prepared with 2.5-50wt% triolein are shown in Fig. 3.1(f). The 2.5wt% triolein sample exhibited significant aggregation, while the samples prepared with more triolein were very stable. These results demonstrated that the addition of a relatively small amount of triolein can dramatically enhance the stability of tristearin NLCs against aggregation, which was consistent with results reported in the literature for other lipid/oil systems [37].

The melting and crystallization behavior and polymorphic transformation kinetics of tristearin-triolein NLCs were examined by differential scanning calorimetry (DSC). Fig. 3.2(a) shows DSC scans at day zero for SLN dispersions with different triolein-trstearin compositions. The melting points of the two crystal forms correspond to peaks in the heating curve at approximately 54.0°C for the α polymorph and 72.5°C for the β polymorph [94]. Roughly equal amounts of α and β crystals were observed for the pure tristearin SLN sample. This suggested that the polymorphic transformation started during 12 hours of cooling in the refrigerator. A small amount of α crystals was detected in the 2.5wt% triolein NLC sample, while no α crystals were observed in samples with more than 5wt% triolein. These results suggested that oil addition accelerated the polymorphic transformation rate. To gain a clearer understanding of the effect of triolein on the polymorphic transformation kinetics, quick DSC scans (see Materials and Methods) were performed for all the samples. This procedure allowed the polymorph content to be determined just 6 minutes after crystallization. As shown in Fig. 3.2(b), a large fraction of α crystals was observed in the tristearin SLN sample. As the triolein content was increased in the NLC samples, increasingly large fractions of β crystals were detected until no α crystals were observed for 20wt% triolein. Moreover, a distinct broadening of the melting peak for β crystals was observed with increasing oil content. The crystallization temperature (T_c), the β crystal melting temperature (T_m) and the β crystal melting enthalpy decreased linearly with increasing oil content (Fig. 3.2 (c)-(d)).

Fig. 3.3 shows the morphology of the tristearin SLNs and the tristearin-triolein NLCs analyzed by cryo-TEM 4 weeks after the samples were prepared. A large number of spherical particles, presumably comprised of α crystals [24], as well as needle-like particles, presumably comprised of β crystals [24], were observed in the pure tristearin sample (Fig. 3.3(a)). The presence of many α-form particles after four weeks of storage can be explained by the high

melting point of the Tween 60 surfactant and the high surfactant concentration, both of which help to retard the polymorphic transformation [32]. The α-form particles were typically between 200 and 400 nm in diameter, while the β-form particles were typically 100 to 200 nm wide and about 0.5 to 1 μm in length. Very few α-form particles were observed when the NLCs were prepared with more than 5wt% triolein. For the 7.5wt% triolein sample, the β-form particles were again 100–200 nm wide but generally less than ~0.5 μm long (Fig. 3.3 (d)). In this sample, a large number of more needle-like crystals that were only ~10–30 nm across were observed. In some views, these crystals were observed to be stacks of very thin sheets. However, these sheets may simply be very small examples of the larger crystals. The images clearly showed that the β-form particles became more spherical as the triolein content was increased from 0wt% to 7.5wt%. Samples with triolein contents from 7.5wt% to 50wt% produced very similar images. These results demonstrate that triolein addition produces morphological changes in the resulting NLCs.

3.3.1.2 Tricaprylin

To investigate if the unsaturation of triolein played a role in the stabilization of tristearin NLC dispersions, the saturated C8 triglyceride tricaprylin was used as the carrier oil. Fig. 3.4(a)-(b) show the evolution of the particle size distribution of NLC samples prepared with 2.5wt% and 10wt% tricaprylin. Qualitatively similar results to those for tristearin-triolein SLNs were obtained. The 2.5wt% tricaprylin sample partially aggregated in 3 days and then remained stable with a bimodal distribution up to 138 days. When the tricaprylin content increased to 5wt%, only a very small amount of aggregation was detected. No aggregation was detected when the tricaprylin content reached 10wt% (not shown). Fig. 3.4(c) shows the average diameter as a function of time for NLCs prepared with 2.5-20wt% tricaprylin. Aggregation was evident only in the 2.5wt% tricaprylin sample. The DSC scans in Fig. 4(d) performed on day 0 show that only a small amount

of α crystals was present in the 2.5wt% tricaprylin sample and the other samples were comprised almost entirely of β crystals. The melting peak broadened and shifted to lower temperature with increasing tricaprylin content. The DSC quick scan in Fig. 3.4(e) shows that α crystals were negligible when the tricaprylin content reached 5wt%. Linear relationships were found for the melting and the crystallization temperatures as a function of tricaprylin content (Fig. 3.4(f)). Unlike tristearin-triolein SLNs, the relationship between the melting enthalpy and oil content was not found to be linear. Taken together these results suggest that tricaprylin stabilized NLC dispersions by accelerating the polymorphic transformation rate and altering the crystal packing structure similarly to triolein.

3.3.1.3 Oleic Acid

The single chain C18:1 fatty acid oleic acid was also studied to better understand the relationship between carrier oil structure and NLC dispersion stabilization. Fig. 3.5(a) shows the particle size distribution measured at day 0 for NLC samples containing 2.5-20wt% oleic oil. The 2.5wt% sample was highly aggregated, the 5wt% sample had gelled and the 10wt% oleic acid sample was partially gelled at day 0 and completely gelled by day 2 (not shown). By contrast, the sample containing 20wt% oleic acid showed minimal aggregation at day 0 and remained stable for 164 days (Fig. 3.5(b)). DSC scans for the tristearin-oleic acid NLCs produced similar results as the triglyceride oils. The polymorphic transformation was dramatically accelerated and the melting curves became broader and shifted to lower temperature as the oleic acid content was increased (Fig. 3.5(c)). While the melting and crystallization temperatures decreased approximately linearly with increasing oleic acid content (Fig. 3.5 (d)), no simple relationship was found between the melting enthalpy and oleic acid content. These results demonstrate that oleic

acid is a less effective stabilizing oil than either triolein and tricaprylin and that oil molecular structure has an effect on NLC dispersion stability.

3.3.1.4 Pentadecane

The C15 hydrocarbon pentadecane was investigated as a carrier oil because of its single chain structure compared to the triglycerides and to better understand the poor stabilization performance of oleic acid. The evolution of the particle size distribution of a NLC dispersion prepared with just 2.5wt% pentadecane shown in Fig. 3.6(a). Over a period of 108 days, very little aggregation was evident and the dispersion was highly stable. Average particle diameters as a function of time for NLC dispersions prepared with 2.5-20wt% pentadecane demonstrate that pentadecane was the most effective stabilizing oil of the four pure oils considered in this study (Fig. 3.6(b)). The small d_{32} decrease observed in the 2.5wt% sample was most likely attributable to experimental error. The polymorphic transformation appeared to be more accelerated compared to the other three pure oils, as no α crystals were observed by DSC quick scan when the oil content was just 5wt% (Fig. 3.6(c)). Similar to the other oils, the melting and crystallization temperatures were found to decrease linearly with increasing pentadecane content (Fig. 3.6(d)).

3.3.2 Common oils

To gain further understanding of the carrier oil stabilization mechanism and to investigate commercially viable oil types, experiments were performed with two common oils: olive oil (melting point -6°C) and palm oil (melting point 35°C), which is a solid at room temperature. The two oils have different fatty acid chain distributions, with olive oil containing more unsaturated carbon chains (Table 3.2).

3.3.2.1 Olive Oil

Fig. 3.7(a)-(b) show the particle size distribution evolution of NLC dispersions prepared with 2.5wt% and 5wt% olive oil. Partial aggregation was observed in the 2.5wt% sample, while the 5wt% sample was stable at room temperature for 129 days. The evolution of average diameter d_{32} of NLC dispersions prepared with 2.5-20wt% olive oil is shown in Fig. 3.7(c). Only the 2.5wt% sample exhibited the particle size increase indicative of significant aggregation. DSC measurements at day 0 (Fig. 3.7(d)) and DSC quick scans (Fig. 3.7(e)) show that the polymorphic transformation rate was accelerated by increasing olive oil concentrations, albeit not as rapidly as observed for the four pure oils. Both the melting and crystallization temperatures decreased linearly with the olive oil content, as observed for the pure oils. Collectively these results suggest that olive oil can serve as an effective carrier oil and that its stabilization mechanism is similar to that of the pure oils.

3.3.2.2 Palm Oil

The evolution of particle size distributions of NLC dispersions prepared with 10wt% and 20wt% palm oil are shown in Fig. 3.8(a)-(b). Significant aggregation was evident in the 10wt% sample, while the 20wt% sample showed very little aggregation that rapidly stabilized to produce a time-invariant size distribution. The d_{32} values calculated for NLC dispersions prepared with 2.5-20wt% palm oil showed that only the 20wt% sample was stable to aggregation over 153 days of storage (Fig. 3.8(c)). As with the other pure and common oils, the melting and crystallization temperatures were found to be linear functions of the palm oil content. These results show that palm oil was a much less effective carrier oil than olive oil and the pure oils except oleic acid.

3.3.3 Modeling Results

My experimental data suggest that the carrier oils accelerated the polymorphic transformation rate but inhibited the large shape change normally associated with the transformation. I attempted to modify my population balance equation model (see Materials and Methods) to account for the oil effect in NLC dispersions by increasing the transformation rate constant to k = 2.0 h^{-1}, which was an order of magnitude larger than the value previously used, and by increasing the aspect ratio of β-form particles from p = 0.2 to p = 0.75 based on my cryo-TEM images. However, the model predicted much faster and more complete aggregation than was observed experimentally (not shown). While my model did not account for increased attractive forces due to the presence of anisometric particles [95], I hypothesized that shape change might not be the only cause of reduced aggregation in my NLC dispersions.

Motivated by this modeling result, I performed another set of experiments to investigate the amount of surfactant required to stabilize the tristearin NLC dispersions. The lipid phase was comprised of 90wt% tristearin and 10wt% triolein, while the Tween 60 surfactant concentration was reduced from 2wt% used in my previous experiments to vary between 0.1wt% and 1wt%. Particle size distributions of these NLC samples after storage at room temperature up to 41 days are presented in Fig. 3.9(a). The dispersions could be stabilized with as little as 0.5wt% surfactant, while a pure tristearin SLN dispersion with 2wt% surfactant gelled within 1 day (Fig. 3.1(a)). NLC dispersions prepared with 0.1wt% and 0.5wt% surfactant both exhibited significant aggregation, but neither sample gelled within the time period of the experiment. These results demonstrate that much less surfactant is needed to stabilize tristearin nanoparticles in the presence of an effective carrier oil such as triolein.

I attempted to model the effect of the carrier oil on surfactant efficiency by adjusting Γ_∞, the parameter that represents the maximum surface coverage above which collisions do not

produce aggregation. Rather than maintain this parameter constant as in my previous study [93], I allowed Γ_∞ to vary under the assumption that the carrier oil may change the lipid-surfactant interfacial properties (e.g. interfacial tension, zeta potential, surfactant coverage on the particle surface, hydrophilic-lipophilic balance) as well as the maximum surface coverage. The model was further altered by modifying the aggregation rate function and the method used to calculate the surface coverage Γ (see Materials and Methods). Simulation results obtained with the modified model for different values of Γ_∞ are presented in Fig. 3.9(b)-(d). For sufficiently small Γ_∞, the model was able to capture negligible aggregation as observed experimentally for sufficiently high surfactant concentrations (Fig. 3.9(a)). An intermediate value of Γ_∞ produced partial aggregation consistent with my experiment that used an intermediate surfactant concentration. Finally, a relatively large value of Γ_∞ produced complete aggregation similar to that observed for the lowest surfactant concentration. When combined with my experimental findings, these simulation results suggest that the carrier oil enhanced the effectiveness of the surfactant to stabilize the dispersion against aggregation.

3.4 Discussion

My experimental results demonstrated that tristearin nanoparticle dispersions can be stabilized by mixing the lipid with different types of carrier oils prior to emulsification and crystallization to form nanostructured lipid carriers (NLCs). Dispersion stability was strongly dependent on the type and concentration of the carrier oil. The C18:1 triglyceride triolein and the C8:0 triglyceride tricaprylin proved very effective at retarding aggregation. Both these oils can be viewed as being spatially incompatible with tristearin, as triolein has unsaturated carbon chains and tricaprylin has shorter carbon chains. I hypothesize that these oils may create crystal packing heterogeneities that result in a less ordered matrix structure within the NLCs. Because both

unsaturated and shorter carbon chains result in lower melting points, the melting point of triglyceride oils could be an important factor affecting the stability of NLC dispersions. This trend was followed in experiments with olive oil (melting point -6°C) and palm oil (melting point 35°C) which showed that olive oil produced much more stable dispersions. According to my hypothesis, the enhanced stabilizing effect of olive oil was attributed to it having more unsaturated carbon chains than palm oil. Experiments in which the hydrocarbon pentadecane was used as the carrier oil produced highly stable dispersions and demonstrated that a glycerol backbone in the oil is not a requirement for NLC stabilization. When the fatty acid oleic acid was used as the carrier oil, NLC dispersions exhibited significant aggregation until a relatively high oil concentration was used. A possible explanation of this poor performance is that oleic acid has an acid functional group, which may change the oil-surfactant interfacial properties in an undesirable way. This hypothesis requires further experimental investigation beyond the scope of this study.

For all the carrier oils studied, DSC results showed that a large increase in the polymorphic transformation rate was induced by the addition of a relatively small amount of carrier oil into the lipid phase. This behavior has been attributed to the presence of oil increasing the mobility of the saturated tristearin molecules, thereby enabling them to reorganize their crystal structure more rapidly [37]. Furthermore, melting and crystallization temperatures were shown to decrease linearly with increasing oil content and the melting peak became broader as the oil content increased. A broadening in melting range is correlated with the presence of impurities or a less ordered crystal structure [11]. These results strongly suggest a less ordered packing of β-form tristearin crystals in the presence of the carrier oils considered in this study.

For the four pure oils studied, I found a reasonable correlation between the slope of the melting temperature decrease and the minimum amount of oil needed to stop NLC aggregation (Table 3.3). Pentadecane produced the largest decrease in the melting point slope and required

the lowest concentration for dispersion stabilization. By contrast, oleic acid produced the smallest slope decrease and required the highest concentration for stabilization. This trend follows the hypothesis postulated above that oils which produce less ordered NLC matrix structures will be more stabilizing. However, this trend does not appear to be followed by more complex common oils. Olive oil and palm oil produced similar melting temperature decreases but olive oil was much more effective for dispersion stabilization (Table 3.3). I found no clear relationship between the slope of the crystallization temperature decrease and the minimum amount of oil needed to stop NLC aggregation. I hypothesize that olive oil produced more stable NLC dispersions than palm oil because the fluid olive oil likely promoted a more mobile interface compared with the solid palm oil. Increased mobility of surfactant at the particle surface could allow the surfactant molecules to move around the interface during the polymorphic transformation to stabilize uncovered hydrophobic surfaces.

Cyro-TEM images collected for tristearin-triolein NLCs showed that β crystals became more spherical as the triolein content was increased. These images suggest that the presence of triolein resulted in less particle shape change due to the polymorphic transformation, a result consistent with tripalmitin-fish oil NLCs studied by dynamic light scattering [37]. Because the effect on shape change was not clear at low triolein concentrations at which aggregation occurred, I hypothesize that the oil-induced retardation of shape change is an important factor in the NLC stabilization mechanism. My TEM images did not indicate triolein phase separation within the particles or triolein located on particle surfaces, which suggests that tristearin and triolein formed a homogeneous phase within the particles. By contrast, NLCs prepared with Compritol as the lipid and Miglyol as the oil have been interpreted as solid lipid platelets with oil present between the platelet surface and the surfactant layer [54-56]. I suspect that these differences are

attributable to the particular lipid-oil systems studied, although this issue warrants further investigation.

I modified my previously developed population balance equation model of SLN aggregation [93] to account for the effects of the carrier oil. Increasing the rate of polymorphic transformation and decreasing the amount of particle shape change did not reproduce the stabilizing effects of the carrier oil observed experimentally. Additional experiments performed with the tristearin-triolein system demonstrated that much less Tween 60 surfactant was able to stabilize NLC dispersions than was required to stabilize SLN dispersions in the absence of triolein. I hypothesized that the carrier oil may change the lipid-surfactant interfacial properties and alter the maximum surfactant surface coverage needed to stop aggregation. Simulations performed with different values of the model parameter Γ_∞, which represents the maximum surface coverage above which particle collisions do not produce aggregation, reproduced experimentally observed behaviors of negligible aggregation, partial aggregation and complete aggregation. Based on these experimental and simulation results, I concluded that the carrier oil enhanced the ability of the surfactant to create repulsive interparticle forces needed for dispersion stabilization. While this issue requires further investigation, I hypothesize that the presence of oil molecules within the homogeneous lipid phase could change lipid-surfactant interfacial properties, increase the mobility of surfactant molecules at the particle surface and allow surfactant molecules that are redistributed during the polymorphic transformation to stabilize uncovered hydrophobic surfaces.

3.5 Conclusions

Nanostructured lipid carriers (NLCs) are second generation delivery systems that are prepared by mixing a liquid carrier oil with the solid lipid. NLCs offer several advantages over first

generation solid lipid nanoparticles (SLNs), including superior bioactive compound encapsulation, protection and release properties. Considerably less studied is the role of the carrier oil in the superior resistance of NLC suspensions to aggregation stability. I believe that my study represents the first systematic investigation of different carrier oils on the crystallization and aggregation behavior of NLCs prepared with the model lipid tristearin.

My major conclusions are that:

1. NLC suspension stability was strongly affected by the type and amount of the carrier oil.
2. When triolein was used as the carrier oil, the crystallization and melting temperatures decreased, the polymorphic transformation rate increased, the particles became more spherical, and suspension stability was enhanced as the oil concentration was increased. Similar trends were observed for the other pure and common oils studied.
3. Triglyceride oils with lower melting temperatures and pure oils with larger slopes between oil content and NLC melting temperature favored the formation of stable suspensions.

When triolein was used as the carrier oil, considerably less Tween 60 surfactant was necessary to produce stable NLC suspensions than was required to stabilize SLN suspensions. The results could be reproduced by a suitably formulated population balance equation model of NLC aggregation dynamics.

My results led to the following hypotheses:

1. Carrier oil trapped within the growing crystal matrix accelerated the polymorphic transformation but retarded the large shape change normally associated with the transformation.
2. Enhanced NLC suspension stability was attributable to both reduced particle shape change, which created less new surface area to be covered by surfactant, and increased

mobility of surfactant molecules on the particle surface, which resulted in available surfactant being more efficient at covering newly created interfaces.

I believe that this study represents a first step towards mechanistic and quantitative understanding of carrier oil effects on NLC suspension stability and ultimately could lead to rational strategies for designing stable NLC systems for various bioactive compound delivery applications.

Table 3.1 Physicochemical property data for the pure oils

Material	Melting point (°C)	Structure
Tristearin	73	C18:0 triglycerides
Triolein	5	C18:1 triglycerides
Tricaprylin	10	C8:0 triglycerides
Oleic acid	13	C18:1 fatty acid
Pentadecane	12	C15 hydrocarbon

Table 3.2 Physicochemical property data for the common oils

Material	Melting point (°C)	Unsat./Sat. ratio	Saturated			Mono unsaturated	Poly unsaturated	
			Myristic Acid C14:0	Palmitic Acid C16:0	Stearic Acid C18:0	Oleic Acid C18:1	Linoleic Acid (ω6) C18:2	Alpha Linolenic Acid (ω3) C18:3
Olive oil	-6	4.6	-	13	3	71	10	1
Palm oil	35	1.0	1	45	4	40	10	-

Table 3.3 Pure material melting temperature (T_m), minimum oil concentration needed to stop NLC aggregation (C_{min}) and the regressed slopes of the melting (T_m slope) and crystallization (T_c slope) temperatures versus oil concentration.

Material	T_m (°C)	C_{min} (wt%)	T_m slope (°C)	T_c slope (°C)
Pentadecane	12	2.5	-30.54	-19.82
Tricaprylin	10	5	-12.17	-20.15
Triolein	5	7.5	-8.51	-13.16
Oleic acid	13	20	-5.46	-29.31
Olive oil	-6	5	-7.67	-9.75
Palm oil	35	20	-7.02	-8.98

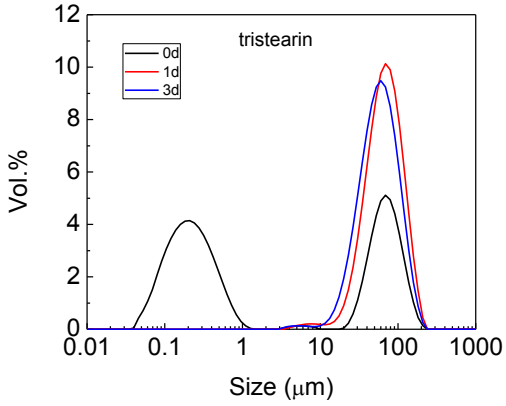
tristearin
0d
1d
3d
Vol.%
Size (μm)

(a)

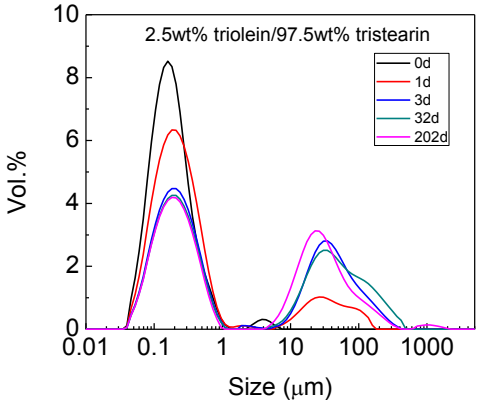
2.5wt% triolein/97.5wt% tristearin
0d
1d
3d
32d
202d
Vol.%
Size (μm)

(b)

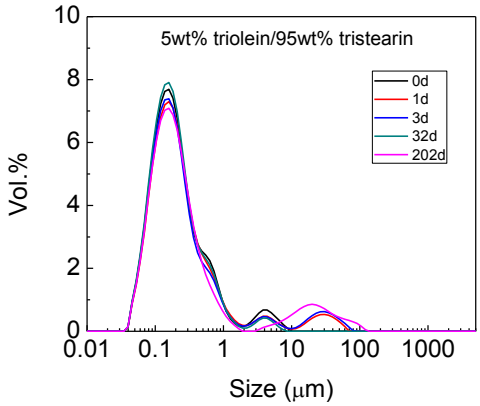
5wt% triolein/95wt% tristearin
0d
1d
3d
32d
202d
Vol.%
Size (μm)

(c)

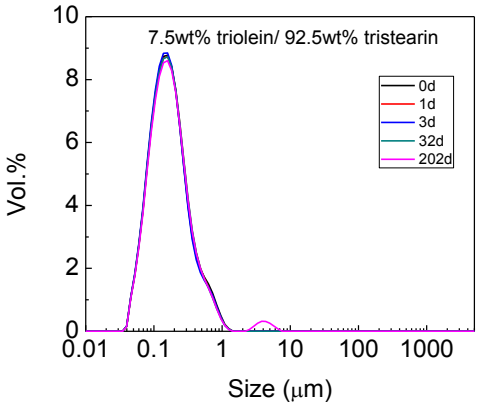
7.5wt% triolein/ 92.5wt% tristearin
0d
1d
3d
32d
202d
Vol.%
Size (μm)

(d)

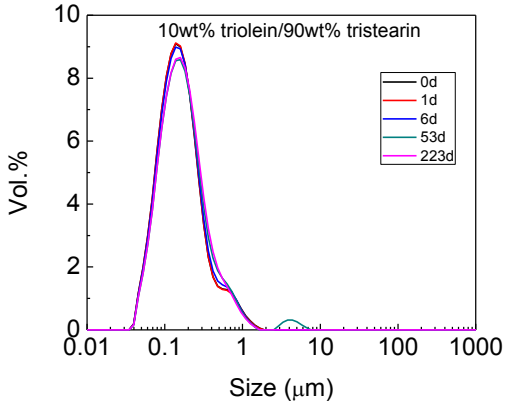
10wt% triolein/90wt% tristearin
0d
1d
6d
53d
223d
Vol.%
Size (μm)

(e)

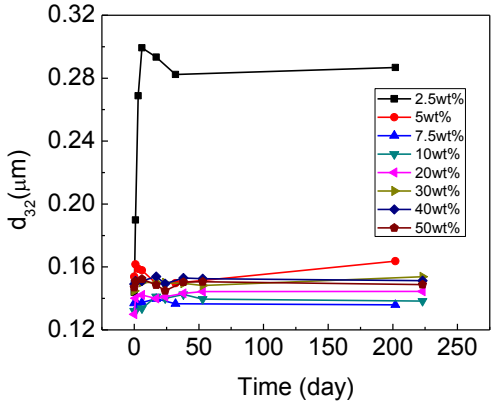
2.5wt%
5wt%
7.5wt%
10wt%
20wt%
30wt%
40wt%
50wt%
d32(μm)
Time (day)

(f)

Figure 3.1. Tristearin-triolein system. Evolution of the particle size distribution for (a) tristearin SLNs; (b) 2.5wt% triolein NLCs; (c) 5wt% triolein NLCs; (d) 7.5wt% triolein NLCs; and (e) 10wt% triolein NLCs. (f) Evolution of average particle size d_{32} for samples with different triolein compositions.

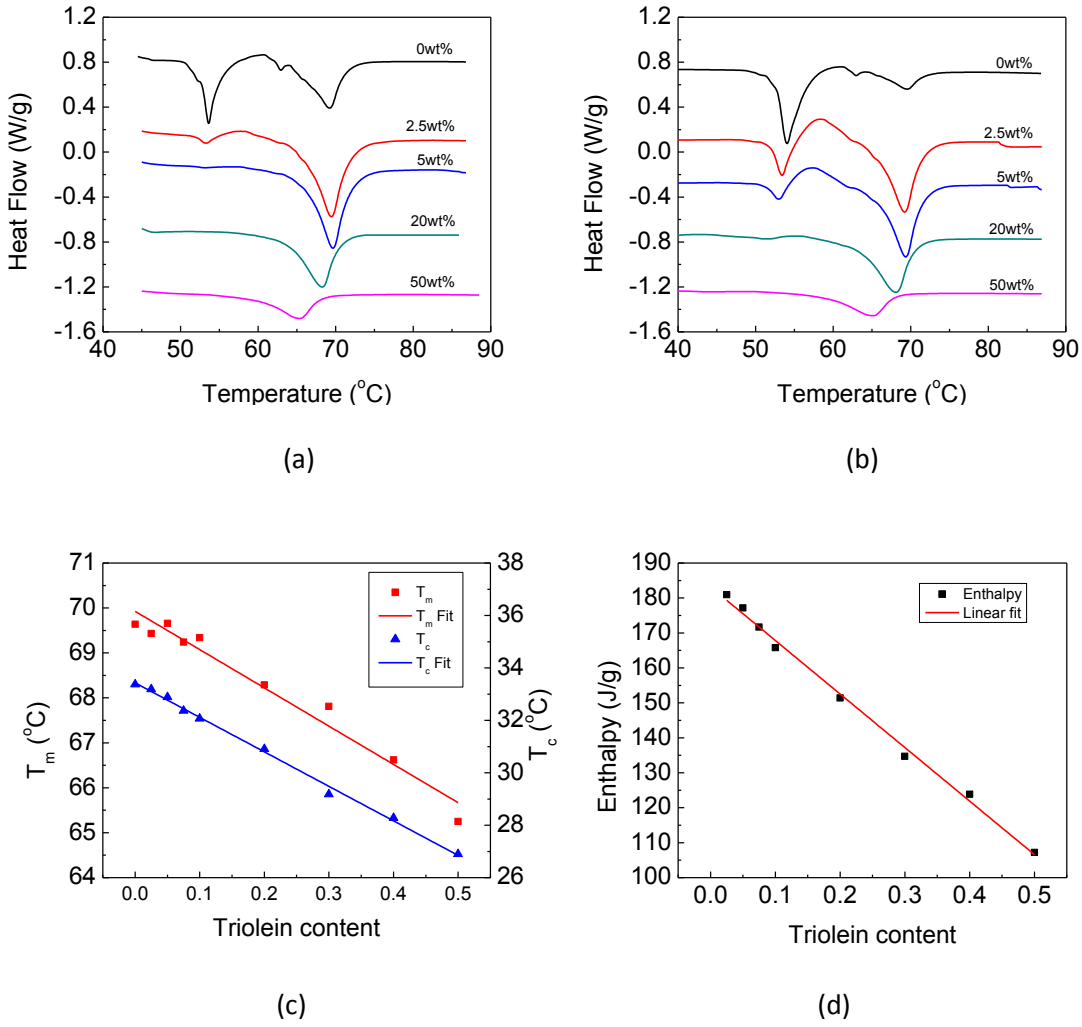

Figure 3.2. DSC results for tristearin SLNs and tristearin-triolein NLCs. (a) DSC scans at day zero for different triolein compositions; (b) DSC quick scans for different triolein compositions; (c) the dependence of the melting and crystallization temperatures on triolein content; and (d) the dependence of the melting enthalpy on triolein content. The correlation coefficients (R^2) were 0.996, 0.962 and 0.995 and the slopes were -13.2°C, -8.5°C and -153.2J/g for the T_c, T_m and melting enthalpy linear regressions, respectively.

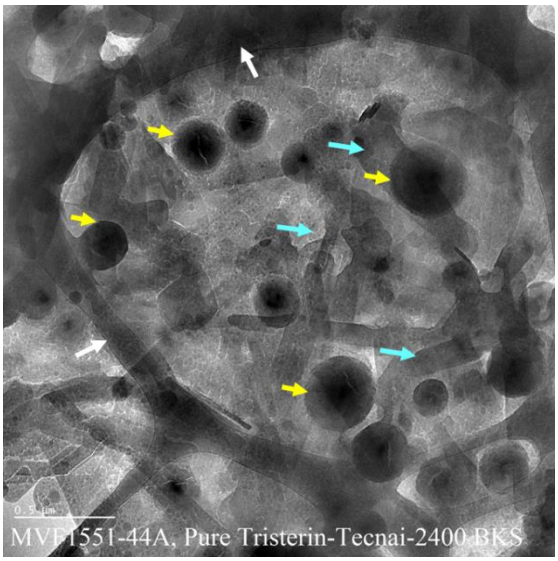
MVF1551-44A, Pure Tristerin-Tecnai-2400 BKS

(a)

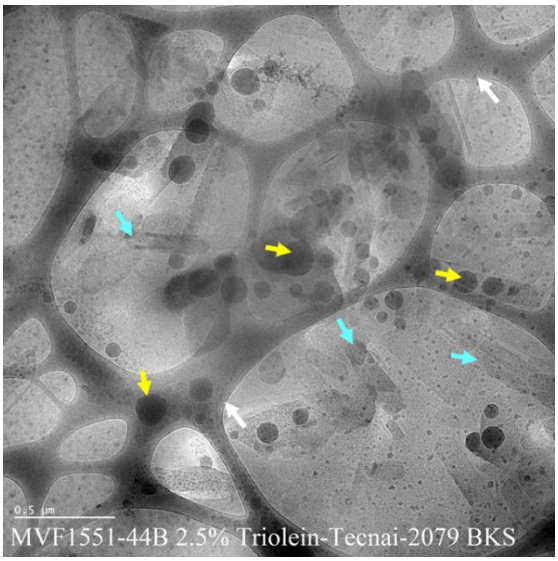
MVF1551-44B 2.5% Triolein-Tecnai-2079 BKS

(b)

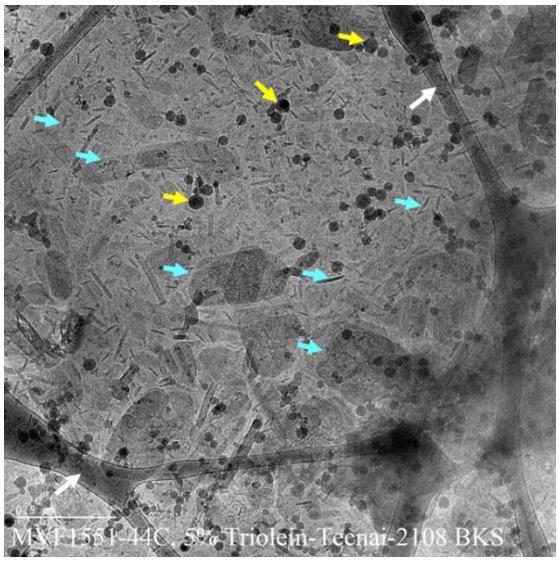
MVF1551-44C, 5% Triolein-Tecnai-2108 BKS

(c)

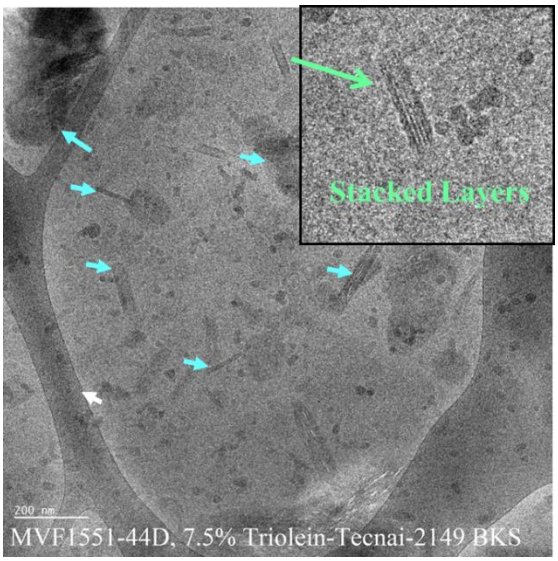
Stacked Layers
MVF1551-44D, 7.5% Triolein-Tecnai-2149 BKS

(d)

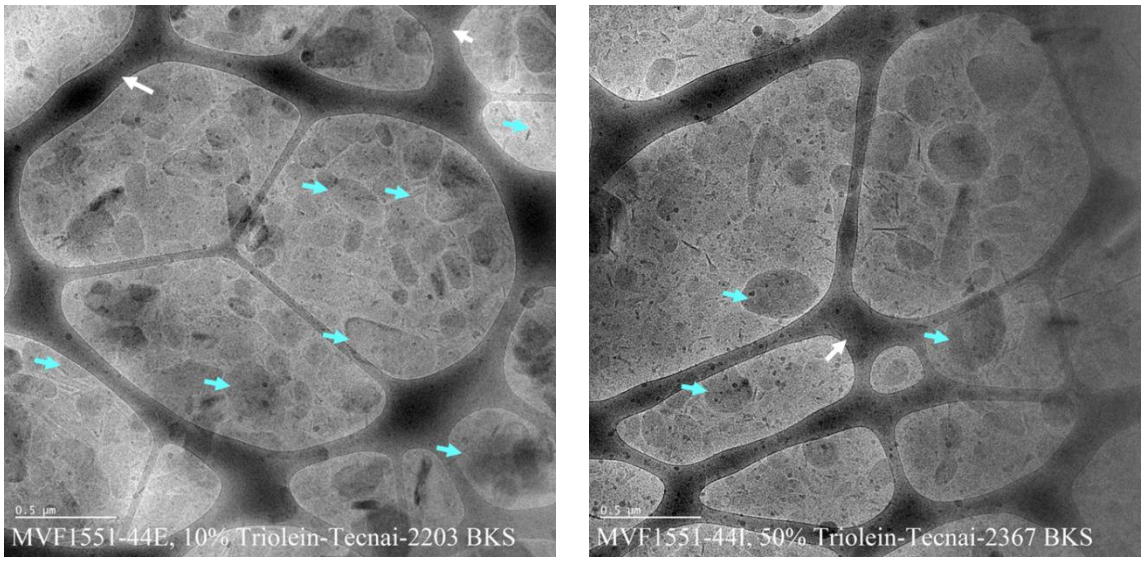

(e) (f)

Figure 3.3. Cyro-TEM images of tristearin SLNs and triolein-tristearin NLCs. (a) tristearin SLNs; (b) 2.5wt% triolein NLCs; (c) 5wt% triolein NLCs; (d) 7.5wt% triolein NLCs at a reduced scale; (e) 10wt% triolein NLCs; and (f) 50wt% triolein NLCs. Yellow arrows: α-form particles; blue arrows: β-form particles; white arrows: support grid.

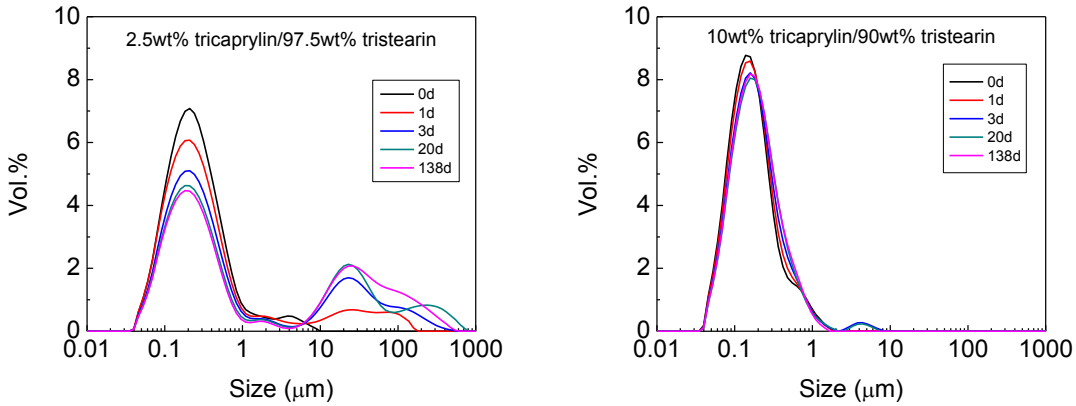

(a) (b)

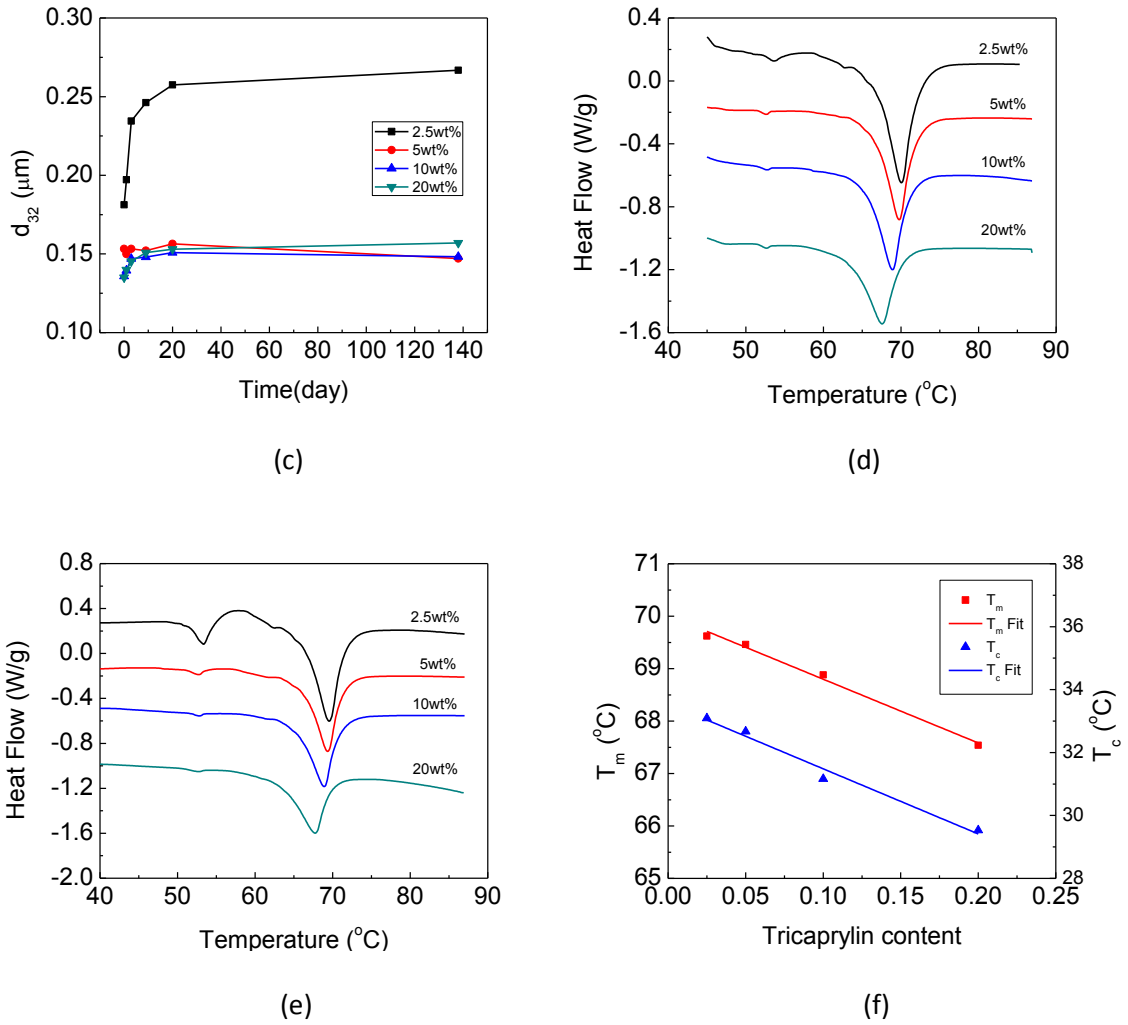

Figure 3.4. Tristearin-tricaprylin system. Evolution of the particle size distribution for (a) 2.5wt% tricaprylin NLCs and (b) 10wt% tricaprylin NLCs. (c) Evolution of average particle size d_{32} for samples with different tricaprylin compositions. (d) DSC scans at day zero for different tricaprylin compositions; (e) DSC quick scans for different tricaprylin compositions; (f) the dependence of the melting and crystallization temperatures on tricaprylin content. The correlation coefficients (R^2) were 0.972 and 0.989 and the slopes were -20.7°C and -12.2°C for T_c and T_m, respectively.

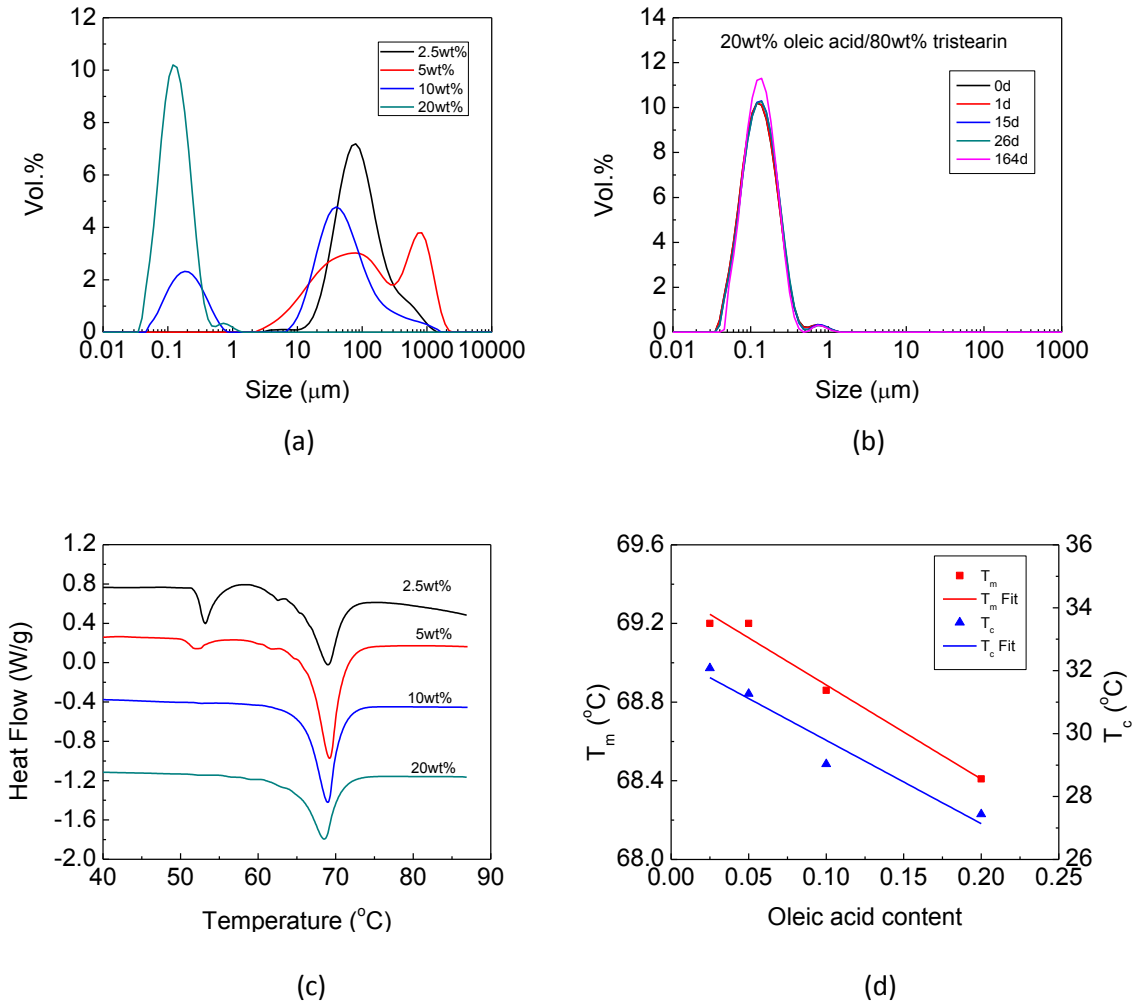

Figure 3.5. Tristearin-oleic acid system. (a) Particle size distributions for different oleic acid compositions at day 0. (b) Evolution of the particle size distribution for 20wt% oleic acid NLCs. (c) DSC quick scans for different oleic acid compositions; (d) Dependence of the melting and crystallization temperatures on oleic acid content. The correlation coefficients (R^2) were 0.913 and 0.971 and the slopes were -26.5°C and -4.8°C for T_c and T_m, respectively.

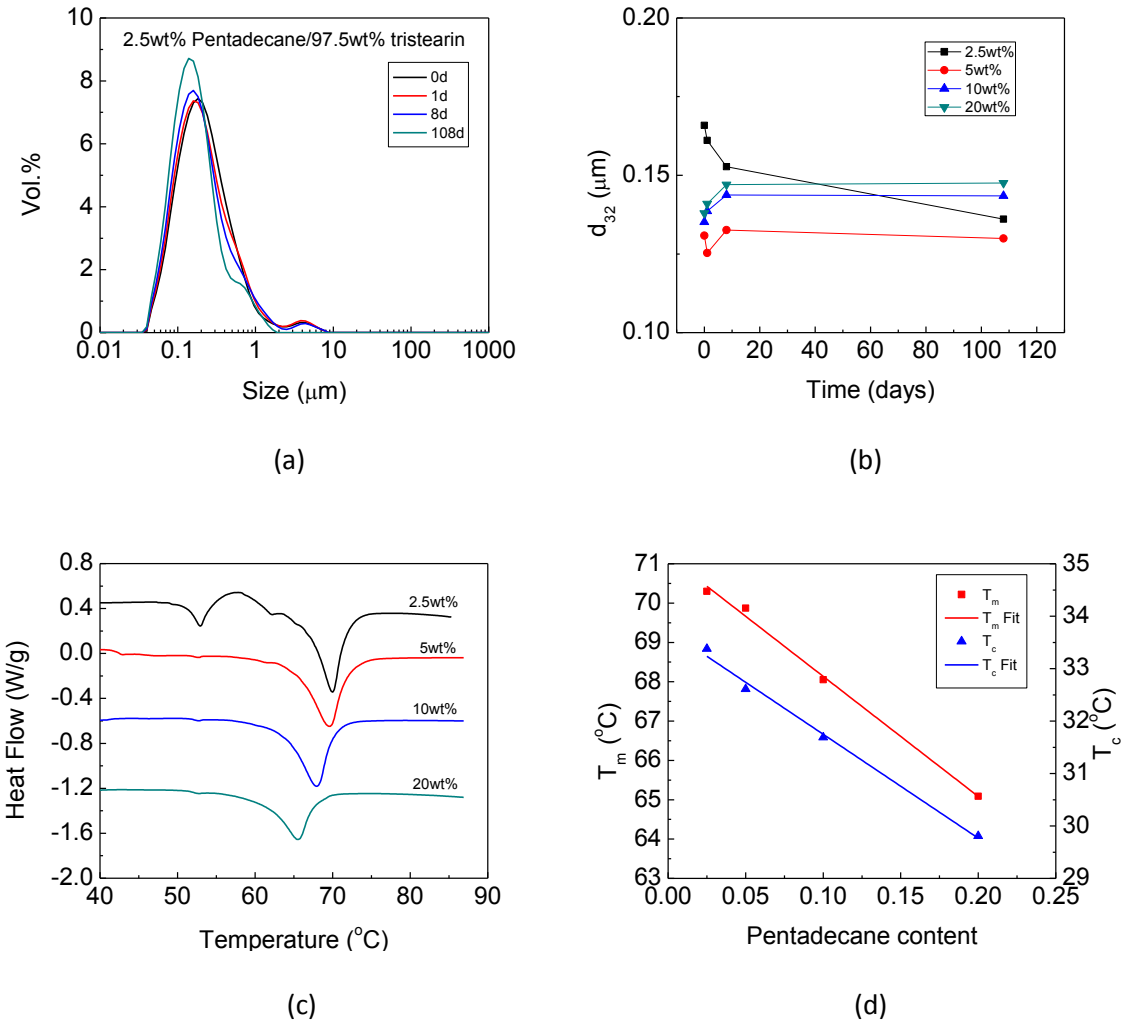

Figure 3.6. Tristearin-pentadecane system. (a) Evolution of the particle size distribution for 2.5wt% pentadecane NLCs. (b) Evolution of average particle size d_{32} for samples with different pentadecane compositions; (c) DSC quick scans for different pentadecane compositions; (d) Dependence of the melting and crystallization temperatures on pentadecane content. The correlation coefficients (R^2) were 0.991 and 0.994 and the slopes were -19.8°C and -30.5°C for T_c and T_m, respectively.

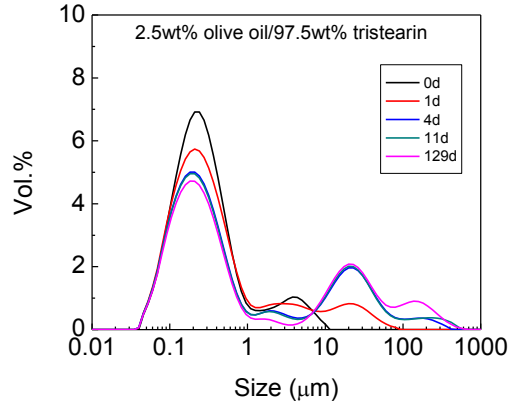
2.5wt% olive oil/97.5wt% tristearin
0d
1d
4d
11d
129d
Vol.%
Size (μm)

(a)

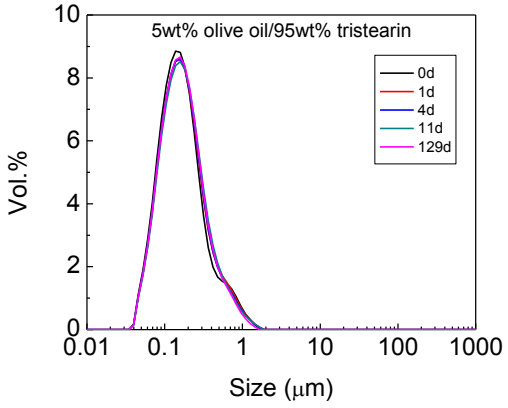
5wt% olive oil/95wt% tristearin
0d
1d
4d
11d
129d
Vol.%
Size (μm)

(b)

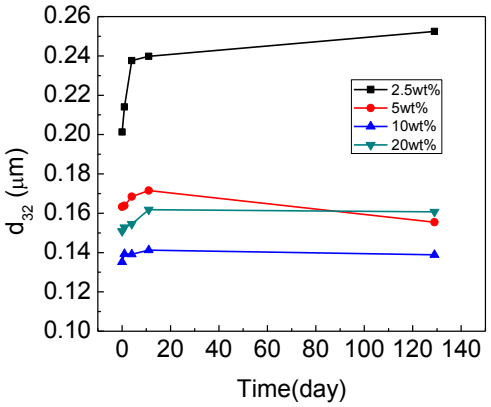
2.5wt%
5wt%
10wt%
20wt%
d32 (μm)
Time(day)

(c)

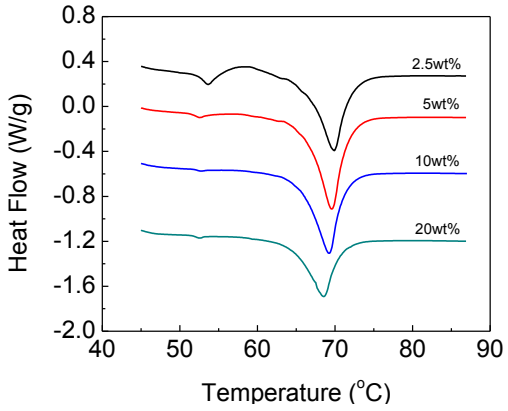
2.5wt%
5wt%
10wt%
20wt%
Heat Flow (W/g)
Temperature (°C)

(d)

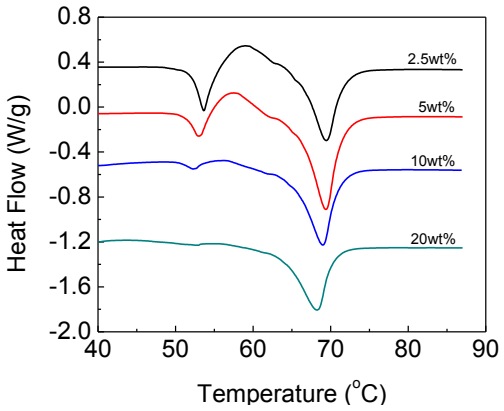
2.5wt%
5wt%
10wt%
20wt%
Heat Flow (W/g)
Temperature (°C)

(e)

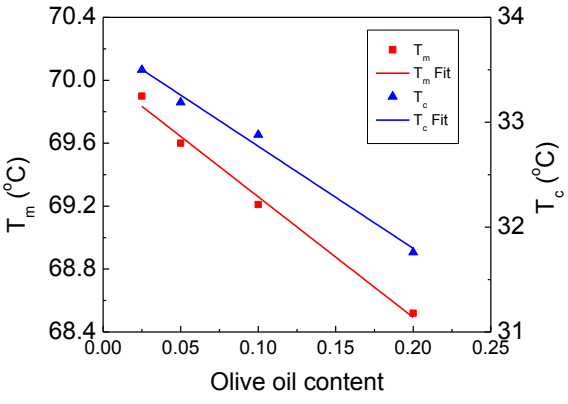
Tm
Tm Fit
Tc
Tc Fit
Tm (°C)
Tc (°C)
Olive oil content

(f)

Figure 3.7. Tristearin-olive oil system. Evolution of the particle size distribution for (a) 2.5wt% olive oil NLCs and (b) 5wt% olive oil NLCs. (c) Evolution of average particle size d_{32} for samples with different olive oil compositions. (d) DSC scans at day zero for different olive oil compositions; (e) DSC quick scans for different olive oil compositions; (f) the dependence of the melting and crystallization temperatures on olive oil content. The correlation coefficients (R^2) were 0.985 and 0.987 and the slopes were -9.8°C and -7.7°C for T_c and T_m, respectively.

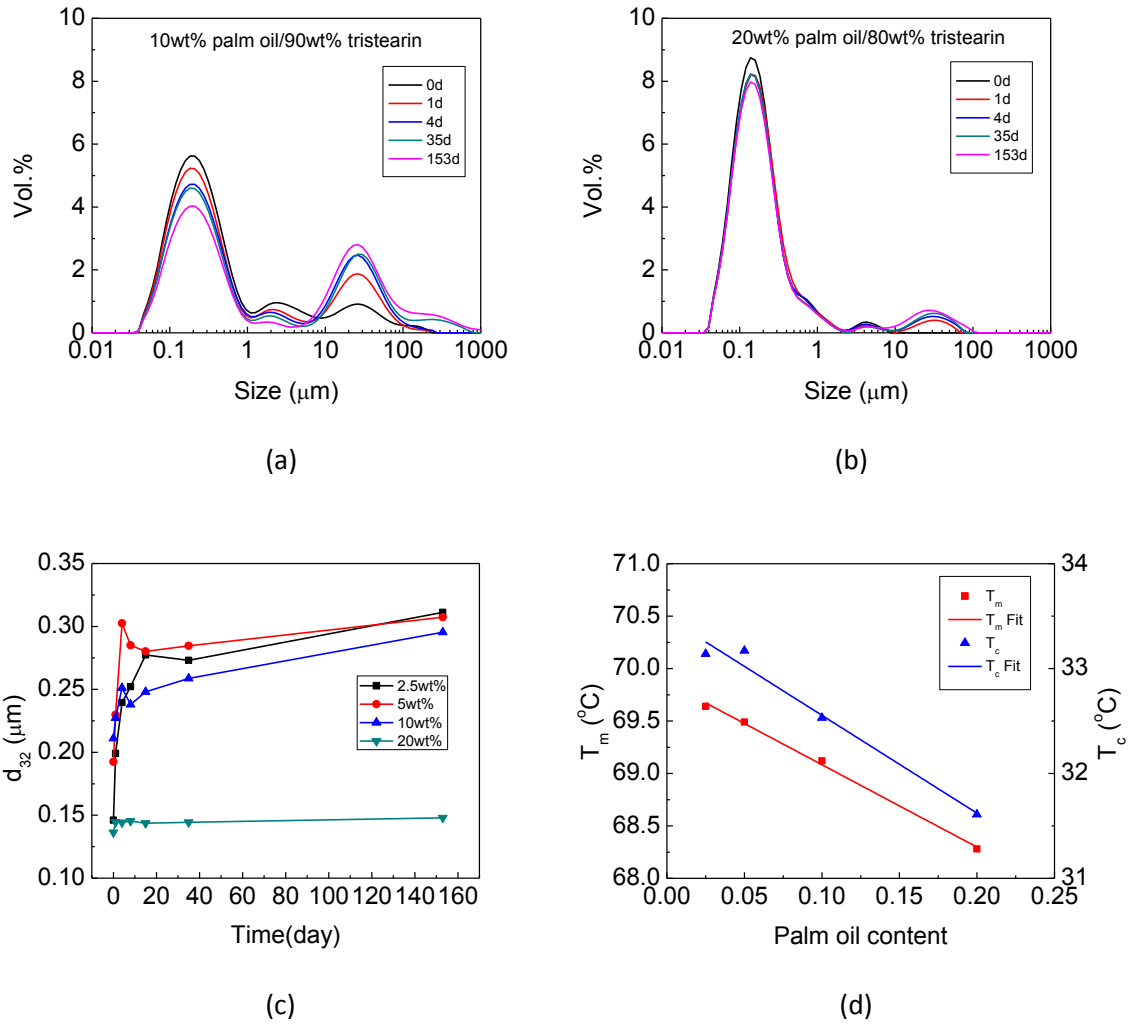

Figure 3.8. Tristearin-palm oil system. Evolution of the particle size distribution for (a) 10wt% palm oil NLCs and (b) 20wt% palm oil NLCs. (c) Evolution of average particle size d_{32} for samples with different palm oil compositions. (d) Dependence of the melting and crystallization temperatures on palm oil content. The correlation coefficients (R^2) were 0.966 and 0.996 and the slopes were -9.3°C and -7.9°C for T_c and T_m, respectively

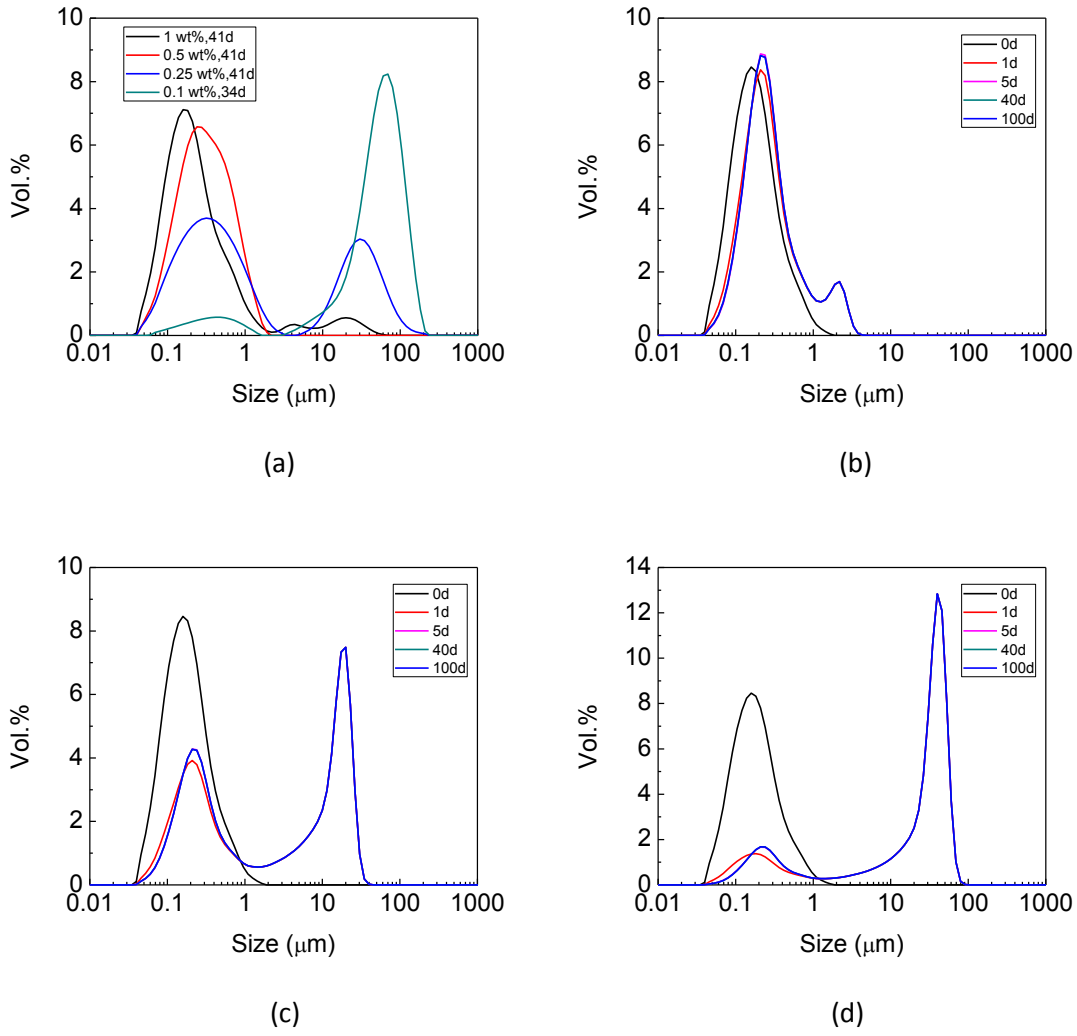

Figure 3.9. (a) Evolution of the particle size distribution for 10wt% tristearin-triolein NLCs with 10wt% triolein and different surfactant contents. Simulation results for (b) $\Gamma_\infty = 0.4\times10^{-13}$ mole/cm^2; (c) $\Gamma_\infty = 0.8\times10^{-13}$ mole/cm^2, and (d) $\Gamma_\infty = 2.0\times10^{-13}$ mole/cm^2.

CHAPTER 4

THE CONTROLLED AGGREGATION AND TUNABLE VISCOSITY OF NANOSTRUCTURED LIPID CARRIER DISPERSIONS

4.1 Introduction

In this chapter, I investigated the effect of formulation variables (dispersed phase, carrier oil and surfactant concentrations) on particle aggregation and rheological properties of NLC dispersions. Tristearin and triolein were selected as the solid lipid and carrier oil, respectively, since I have used this model system in my previous work on NLC dispersion stability in Chapter 2 [96]. A previously developed model for weakly aggregated dispersions [69, 70] was fit to my experimental data to provide insights into the aggregation effect. I believe that my study represents the first comprehensive investigation focused on controlling aggregation to tune the rheological properties of NLC dispersions and therefore represents an important step towards developing rational NLC design strategies for bioactive compound delivery and rheology modification.

4.2 Materials and methods

4.2.1 Materials

Tristearin and triolein were purchased from TCI America (Portland, OR). The surfactant Tween 60 was supplied by Procter and Gamble. All materials were used as received.

4.2.2 NLC Preparation

NLC dispersions were prepared by using the hot homogenization method [12]. The dispersed phase was prepared by mixing tristearin and triolein at a temperature of 85°C,

approximately 10°C above the melting point of tristearin. The aqueous phase was prepared by mixing deionized nanopure water with Tween 60 surfactant followed by heating to 85°C. Different NLC formulations consisting of 5-30wt% total lipid phase were prepared. The triolein content in the lipid phase varied from 5wt% to 50wt%. The mass ratio of surfactant to dispersed phase varied from 1% to 20%. Coarse oil-in-water emulsions were prepared by mixing the lipid and aqueous phases together at 85°C using a high speed blender (Ultra-Turrax Model T18, IKA-Works Inc.) for 5 minutes at 16,000 rpm. Fine emulsions were prepared by passing the coarse emulsion through a high pressure homogenizer (Emulsiflex C-3, Avestin Inc.) 4 times at 800 bar with the temperature was maintained at 85°C. The coarse and fine emulsions were cooled in a refrigerator for 12 hours to obtain NLC dispersions, which were subsequently stored at room temperature.

4.2.3 NLC Characterization

4.2.3.1 Particle Size Distribution

Particle size distributions of NLC dispersions were measured by static light scattering (Mastersizer 2000, Malvern Instruments). Refractive indices of 1.54 for the particles and 1.33 for water were used to calculate particle size distributions [27].

4.2.3.2 Rheology

The rheological measurements were performed with a stress-controlled rheometer (TA Instruments AR 2000) using an aluminum cone and plate geometry with a 20 mm diameter, 4° cone. All measurements were carried out at a temperature of 20°C. Continuous flow measurements were performed by increasing the shear rate from 0.001 s^{-1} to 100 s^{-1} and measuring the resulting viscosity. For some dilute samples, data at the lowest shear rates were below the limit of sensitivity of the rheometer's torque transducer; these data points are not

shown. Additionally, a few more concentrated samples were observed to display some type of phase separation at the highest shear rates, with one phase exhibiting opacity, a cream-like consistency, and a sudden increase in the viscosity. These data are also not shown. Oscillation stress sweep tests were performed at a frequency of 1 Hz in a stress range of 0.01-100 Pa. Oscillation frequency sweep tests were carried out over a range from 0.1 Hz to 10 Hz at stresses of 0.02 Pa and 4 Pa.

4.2.4 Mathematical Model

A mathematical model developed to predict the steady shear viscosity of weakly aggregated dispersions [69, 70] was selected to fit my experimental data.

$$\eta = \mu\left(1 - \frac{\phi_a}{\phi_m}\right)^{-2.5\phi_m} + \frac{\sigma^*(\phi_p,\phi_a)}{\gamma} \tag{4.1}$$

$$\sigma^*(\phi_p, \phi_a) \approx \alpha \frac{F_c h_c}{a^3} \phi_a^2 \left(\frac{\phi_p}{\phi_a}\right)^{(5-2d_f-d_l)/(3-d_f)} \tag{4.2}$$

The steady shear viscosity of the dispersion is described by Eq. (4.1), where η is the viscosity of the dispersion, μ is the viscosity of the continuous phase, ϕ_a is the volume fraction of aggregates, ϕ_p is the volume fraction of particles, ϕ_m is maximum packing fraction, γ is the shear rate and σ^* can be interpreted as the yield stress of the system at fixed ϕ_a. The first term on the right hand side of Eq. (4.1) is the hydrodynamic contribution to the viscosity, while the second term is the structural contribution. The yield stress σ^* is approximated using Eq. (4.2), where α is the capture efficiency or the fraction of particle collisions resulting in rigid interaggregate chains, F_c is the bonding force between particles, h_c is the equilibrium value of the gap width between particles, a is the particle radius (I used the surface-averaged radius in my simulations), d_f is the fractal dimension of aggregates and d_l is the chemical dimension of chains [70]. In my study, experimentally determined values of η, μ, ϕ_p and a were inputs to the model and ϕ_a was calculated

from other parameters. The parameters F_c, h_c, d_f, d_l, ϕ_p and α were used to fit my experimental data by minimizing the following objective function using the MATLAB code lsqnonlin:

$$\Psi = \sum_{i=1}^{n} \left(\frac{\eta_{model,i} - \eta_{exp,i}}{\eta_{exp,i}} \right)^2 \quad (4.3)$$

where n is the number of data points, η_{model} is the calculated viscosity value and η_{exp} is the measured viscosity value. The dataset for each formulation was fit individually to obtain a new set of parameters such that parameter trends could be analyzed.

4.3 Results

4.3.1 Effect of Formulation Variables on NLC Dispersion Aggregation and Viscosity

The effect of dispersed phase concentration on the viscosity of stable (non-aggregating) NLC dispersions was studied at a constant ratio of solid lipid (tristearin)/carrier oil (triolein)/surfactant (Tween 60). Each sample was labeled with three different numbers: dispersed phase concentration, oil content in the dispersed phase and total surfactant content. For example, the sample labeled "5%L-10%O-1%S" contained 5wt% total dispersed phase (lipid phase) and 1wt% surfactant with the 5wt% dispersed phase prepared by mixing 90wt% tristeain and 10wt% triolein. The particle size distributions (PSDs) from samples collected at different times are shown in Fig. 4.1 (a-c). In each plot, the black line is the PSD of the emulsion before cooling, while the red and blue lines are the PSDs when the dispersion was first removed from the refrigerator and right before the viscosity measurement, respectively. The PSDs of these three samples with dispersed phase concentrations of 5wt%, 10wt% and 20wt% were similar. No significant PSD change was observed during storage, which indicated negligible particle aggregation. The viscosity of each sample as a function of shear rate is presented in Fig. 4.1 (d). The results showed a shear thinning behavior for all three samples, as the viscosity decreased with increasing shear rate and reached an approximately constant value at high shear rates. As

expected [58], the dispersion viscosity increased significantly as the dispersed phase concentration increased from 5wt% to 20wt%.

Next the effect of surfactant concentration on particle aggregation and dispersion viscosity was investigated. Three samples were prepared using 10wt% total dispersed phase, 10wt% oil in the dispersed phase, and 0.25wt%, 1wt% and 2wt% surfactant. The PSD behaviors of the three NLC dispersions are shown in Fig. 4.2 (a-c). After 3 days significant aggregation was evident in the sample with 0.25wt% surfactant. By contrast, the sample with 1wt% surfactant showed little aggregation after 5 days and negligible aggregation was observed after 2 days when the surfactant content was increased to 2wt%. my previous study on the aggregation stability of NLC dispersions showed that such samples remained stable and the PSD was unchanged beyond the first two days of storage at room temperature [96]. Therefore, these results demonstrate that controlled aggregation of NLC dispersions can be achieved by varying the amount of surfactant. The steady shear viscosities of these three dispersions are shown in Fig. 4.2 (d). Despite having the same dispersed phase volume fraction, the three samples produced substantially different viscosity profiles with the 0.25wt% surfactant sample exhibiting low shear viscosities that were more than two orders of magnitude larger than those at 2wt% surfactant. The 1wt% surfactant sample produced viscosities between the other two samples, suggesting that viscosity was directly affected by the degree of aggregation. These results indicated that the surfactant concentration can be adjusted to obtain controlled aggregation and tunable viscosity behavior.

Samples with the same dispersed phase and surfactant concentrations but different oil contents in the lipid phase were prepared to investigate the effect of oil content on dispersion aggregation and viscosity. Three samples were prepared using 10wt% dispersed phase concentration, 1wt% surfactant concentration and oil contents in the lipid phase of 5wt%, 10wt% and 30wt%. PSDs collected for sample are presented in Fig. 4.3 (a-c). Paralleling the results for

surfactant concentration (Fig. 4.2), substantial aggregation was observed in the 5wt% oil sample, little aggregation was observed in the 10wt% oil sample and negligible aggregation was observed in the 30wt% oil sample. The steady shear viscosities of the three dispersions are shown in Fig. 4.3 (d). Qualitatively similar results to those observed by changing the surfactant concentration were obtained. More specifically, low shear viscosities were increased by more than an order of magnitude by reducing the oil content from 30wt% to 5wt%. Collectively these results suggested that the surfactant concentration and/or the oil content could be reduced to obtain controlled aggregation and tunable viscosity behavior at a constant dispersed phase concentration.

For substantially aggregated samples (e.g. Fig. 4.2 (a) and 4.3 (a)), the effect of the dispersed phase concentration on viscosity was also studied. For samples with 5wt% and 10wt% dispersed phase concentrations, the mass ratio of lipid/oil/surfactant was held constant. However, the sample prepared with 20wt% dispersed phase concentration using the same mass ratio was visually observed to form a gel during storage. In an attempt to achieve roughly the same degree of aggregation as the other two samples, the amount of surfactant used in the 20wt% dispersed phase concentration sample was doubled. All three samples exhibited a substantial but controlled amount of aggregation as shown in Fig. 4.4 (a-c). The steady shear viscosities of the three dispersions are shown in Fig. 4.4 (d). Similar to non-aggregated samples (Fig. 4.1), the dispersed phase concentration appeared to be an important parameter that affected the viscosity of aggregated dispersions. However the interpretation of the aggregated results was more difficult because the samples exhibited different degrees of aggregation, which perhaps resulted in the 10wt% and 20wt% dispersed phase concentration samples producing similar viscosities below 1 s^{-1}. Although not shown here, I found that controlled aggregation was difficult to achieve at dispersed phase concentrations greater than 30wt%.

4.3.2 Oscillatory Sweep Experiments

To gain a better understanding of the microstructure of my NLC dispersions, oscillation stress and oscillation frequency sweep experiments were performed on non-aggregated and aggregated NLC dispersions with 5wt% and 10wt% dispersed phase concentration. An oscillation stress sweep test at a constant frequency of 1 Hz was performed for each sample to determine the linear viscoelastic region over which the aggregated network structure was intact. These tests yielded the complex modulus (*G**) as a function of stress at a constant frequency. The complex modulus is a measure of the total resistance of the sample to strain. The linear viscoelastic region is the range of stress over which *G** and the phase angle δ are independent of the applied stress [60]. The stability of the system is also reflected in the change of phase angle δ from the elastic region ($\delta < 45°$) to the viscous region ($\delta > 45°$).

A representative oscillation stress sweep is shown in Fig. 4.5 (a) for an aggregated sample with 10wt% dispersed phase. The linear viscoelastic region extended to a stress of 0.06 Pa, at which point the complex modulus decreased dramatically with increasing stress. As the stress was increased, the phase angle increased from a value less than 10° (elastic region) to a value around 80° (viscous region). The results indicated the destruction of the internal network structure of the aggregated dispersion. A sample with more stable structure would be expected to have a wider linear viscoelastic region than a sample with a weaker structure [60]. The oscillation stress sweep data for four representative NLC dispersions are shown in Fig. 4.5 (b). All four samples had the same oil content of 10wt% and either 5wt% or 10wt% dispersed phase concentration. The two samples prepared with a 40:1 dispersed phase/surfactant ratio (labeled 5-10-0.125 and 10-10-0.25) exhibited a substantial degree of aggregation, while the two samples prepared with a 5:1 dispersed phase/surfactant ratio (labeled 5-10-1 and 10-10-2) exhibited a negligible amount of aggregation. The stress sweep data showed that both aggregated samples have much larger *G**

than the non-aggregated samples. For the non-aggregated samples, there was no significant change of G^* over the range of measurement and the fluctuations at low stress were due to limitations of the equipment. For the aggregated samples, the size of the linear viscoelastic region increased as the dispersed phase concentration was increased from 5wt% to 10wt%. For both types of dispersions, the 10wt% samples produced larger G^* values than the 5wt% samples. The stress values of 0.02 Pa and 4 Pa were selected in the linear viscoelastic regions of the aggregated and non-aggregated samples, respectively, for the oscillation frequency sweep tests presented below.

Oscillation frequency sweeps were conducted to study the viscoelastic behavior of aggregated and non-aggregated dispersions and the network structure formed by particle interactions. An oscillation frequency sweep measures the response of the dispersion as a function of frequency at a constant stress. From these experiments, I obtained the storage modulus G' (elastic response), which indicated the energy stored in the system after an applied stress, and the loss modulus G'' (viscous response), which reflected the energy loss after an applied stress. If performed within the linear viscoelastic region, oscillatory frequency sweeps provide information about the system structure under non-destructive conditions [60]. The dispersions were measured without significantly disrupting their structure, as may occur in a continuous shear flow experiment [97].

Fig. 4.6 (a) presents the oscillation frequency sweep data for two non-aggregated samples with 5wt% and 10wt% dispersed phase (again labeled 5-10-1 and 10-10-2). These two samples produced similar data including an increase of G' and G'' with increasing frequency. The fluctuations of G' at low frequencies were due to the low torque limit of the equipment. At low frequencies G'' was larger than G', while at higher frequencies G' was larger than G''. For two aggregated dispersions (again labeled 5-10-0.125 and 10-10-0.25), very different rheological

behavior was observed as shown in Fig. 4.6 (b). More specifically, the aggregated samples produced much larger values of both moduli than the non-aggregated samples and both *G'* and *G"* of the aggregated samples exhibited only weak dependency on frequency. Because the aggregated samples produced *G'* values approximately one order of magnitude larger than the corresponding *G"* values over the whole frequency range, these samples strictly satisfy the rheological definition of a gel. However, aggregation produced very weak gels with *G'* = 20-30 Pa and these samples visually still flowed upon sample inversion [98].

To better visualize the effect of formulation variables on the degree of particle aggregation, the state diagram shown in Fig. 4.7 was generated. The diagram only includes samples with 10wt% oil content, as all samples prepared with 30wt% and 50wt% oil content were stable against particle aggregation (not shown). Additionally, the states shown in Fig. 4.7 represent samples at rest; this diagram does not account for samples that may gel or phase separate at high shear rates. I referred to samples with no PSD change during storage or with an area of the second peak at large size less than 3% of the total volume as non-aggregated samples. Samples that exhibited aggregation but with an area of the second peak less than 15% were classified as marginally aggregated samples. If the area of the second peak was larger than 15vol% but the sample did not visually form a gel, I used term controlled aggregation. As I mentioned above, even some of the controlled aggregated samples satisfy the rheological definition of a gel, albeit a weak gel as the samples visually still appear to be fluids. Here, I use the term strong gel to refer to samples that visually appear to be gels; that is, those samples that do not visually flow and support their own weight when inverted. However, I also expect these samples to behave rheologically as gels, with the storage modulus *G'* mainly independent of frequency and larger than the loss modulus *G"* for all frequencies measured.

The black data points in Fig. 4.7 represent non-aggregated samples. The area under the black line is the region where non-aggregated samples definitely would be formed, since decreasing dispersed phase concentration and/or increasing surfactant concentration will result in less aggregation. The green data points represent samples that formed strong gels. The area above the green line is the region where strong gelled samples definitely would be formed, since higher dispersed phase concentration and/or less surfactant will facilitate gelation. No gelation was visually observed for samples with 5wt% and 10wt% dispersed phase concentrations, although again as I showed above, some of these samples rheologically displayed significant elasticity. If dispersion occupied the area between the two lines, the sample could be in the non-aggregation regime, the marginally aggregated regime (red points), the controlled aggregation regime (blue points) of the strong gel regime depending on the formulation.

4.3.3 Modeling Results

The mathematical model described in Section 4.1.4 for prediction of the steady shear viscosity of weakly aggregated dispersions [69, 70] was fit to my shear rate versus viscosity data. The model fitting parameters were F_c, h_c, d_f, d_l, ϕ_p and α. Each formulation was fit individually to obtain a new set of parameters such that parameter trends could be analyzed. A representative set of model fitting results for NLC dispersions prepared with 10wt% oil concentration, 10wt% oil content and 0.25-2.0% surfactant concentration are shown in Fig. 4.8. The fitted models provided satisfactory viscosity predictions over the wide range of shear rates studied.

Two fitting parameters (d_l, ϕ_p) showed no obvious trends with respect to the NLC formulation (not shown). By contrast, clear trends were observed for the remaining three parameters: the bonding force F_c, the fractal dimension d_f and the aggregation efficiency α. These trends are shown in Fig. 4.9 for samples prepared with 10wt% dispersed phase concentration. The

fitting parameters obtained for samples prepared with 10% oil content and different surfactant concentrations are shown in Fig. 4.9 (a). Both F_c and α decreased as the surfactant concentration was increased, suggesting diminished bonding forces between particles and a reduced aggregation efficiency. The fractal dimension d_f increased from about 1.7 for low surfactant samples to about 2.2 for samples with high surfactant. Similar trends were observed for samples prepared with 1% surfactant concentration as the oil content was increased from 5wt% to 50wt% (Fig. 4.9 (b)).

I hypothesized that increasing surfactant concentration resulted in increased surfactant coverage on particle surfaces, reduced hydrophobic attractive forces between particles and weaker bonding forces. Similarly, increased surface coverage could lead to improved particle stabilization and reduced aggregation efficiency. I further hypothesized that increasing oil content increased the mobility of surfactant molecules on particle surfaces and inhibited particle shape change, both of which will resulted in weaker hydrophobic attractive forces and reduced aggregation. The observed variations in the fractal dimension parameter indicated an internal structure change of the aggregated dispersions. More specifically, the fractal dimension increase suggested the internal structure changed from porous network to more compact structure [99, 100] as the surfactant concentration and/or oil content was increased.

4.4 Discussion

My experimental results demonstrated that the rheological properties of NLC dispersions can be substantially modified through controlled aggregation of the lipid nanoparticles. While the viscosity can be increased through the usual approach of simply increasing the dispersed phase concentration (Fig. 4.1), controlled aggregation represents a potentially more cost effective approach for producing large dispersion volumes with tunable viscosity. I showed that the

viscosity could be increased by a least of magnitude at moderate shear rates (<10 s^{-1}) by decreasing the surfactant concentration (Fig. 4.2) and/or the amount of carrier oil mixed with the lipid prior to solid particle formation (Fig. 4.3) through controlled aggregation without changing the dispersed phase concentration. I attributed the increased viscosity of the aggregated dispersions to increased hydrophobic attraction between particles mediated by low surfactant concentrations and/or low oil contents. Both factors resulted in increased particle aggregation and the formation of an internal network structure within the dispersion. While additional increases in NLC dispersion viscosity could be obtained by increasing the dispersed phase concentration (Fig. 4.4), I found that controlled aggregation was difficult to achieve at total lipid concentrations exceeding 30wt%.

Oscillation stress sweep tests on aggregated samples indicated a linear viscoelastic region where the dispersions behaved like an elastic solid (Fig. 4.5). When the stress was increased beyond the viscoelastic region, the complex modulus decreased sharply with increasing stress indicating the breakdown of the internal network structure. The viscoelastic region became wider as the dispersed phase concentration was increased from 5wt% to 10wt%, suggesting a more rigid structure due to increased particle interactions [60]. Oscillation frequency sweep tests performed in the linear viscoelastic region indicated that non-aggregated dispersions behaved like a viscoelastic liquid with a more viscous response at low frequencies (<2 Hz) and a more elastic response above this crossover frequency (Fig. 4.6). As expected, aggregated dispersions produced more complex oscillation frequency sweep results. Both the storage modulus *G'* and the loss modulus *G"* were much larger than the corresponding values for non-aggregated dispersions, and both moduli showed only a weak dependency on the applied frequency which is typical for a viscoelastic solid [60]. The storage modulus was approximately one order of magnitude larger than the loss modulus over the entire range of applied frequencies, which indicated the presence

of a gel-like structure. However, these aggregated dispersions are actually weak gels and most likely have very weak network structures. My experimental results were collectively used to produce a state diagram that showed the effect of the surfactant concentration and the oil content on the degree of particle aggregation for NLC dispersions with 10wt% dispersed phase concentration (Fig. 4.7).

A previously developed viscosity model for weakly aggregated dispersions fit to the viscosity versus shear rate data for different NLC formulations (Fig. 4.8) produced clear trends in three fitting parameters (Fig. 4.9). The bonding force parameter F_c decreased as the surfactant concentration or oil content was increased, suggesting that attractive hydrophobic forces between particles were decreased. A similar trend was observed for the aggregation efficiency parameter α as increased amounts of surfactant or oil stabilized the particles and reduced the efficiency of particle collisions. When the surfactant concentration or oil content was increased, the fractal dimension parameter d_f increased from about 1.7 for aggregated samples to roughly 2.3 for non-aggregated samples. The d_f value of 1.7 obtained for aggregated samples indicated the formation of a porous, interconnected network structure in the aqueous liquid [99], which was consistent with my results from oscillatory sweep experiments. Conversely the d_f value of roughly 2.3 obtained for non-aggregated samples suggested a more compact structure [100] and should represent the fractal dimension of individual particles.

Collectively my results have demonstrated that the viscosity of NLC dispersions can be tuned by controlling the degree of particle aggregation through appropriate selection of the surfactant concentration and/or oil content of the formulation. The controlled aggregation mechanism provides a means to dramatically increase the dispersion viscosity without altering the dispersed phase concentration. As a result, partially aggregated NLC dispersions hold promise

as low cost viscosity enhancers for applications in the food, pharmaceutical and consumer product industries.

4.5 Conclusions

I investigated the effect of dispersed phase concentration, oil content and surfactant concentration on the aggregation and viscosity of NLC dispersions. Higher dispersed phase concentrations produced dispersions with higher viscosity. For a constant dispersed phase concentration, the viscosity of the dispersion could be modified by controlling the amount particle aggregation using different oil content and surfactant concentrations. The viscosity of the dispersion could be tuned by at least an order of magnitude by controlling the particle aggregation. Oscillation sweep tests showed typical behaviors of a viscoelastic liquid and a viscoelastic solid for non-aggregated and aggregated dispersions, respectively. Oscillation frequency sweep tests further indicated a weak gel structure in the aggregated dispersions. Modeling results suggested an increase of the bonding force between particles and the aggregation efficiency as the oil content and surfactant concentration were decreased. The fractal dimension obtained by model fitting of aggregated systems indicated the formation of a porous, interconnected network structure in the dispersion.

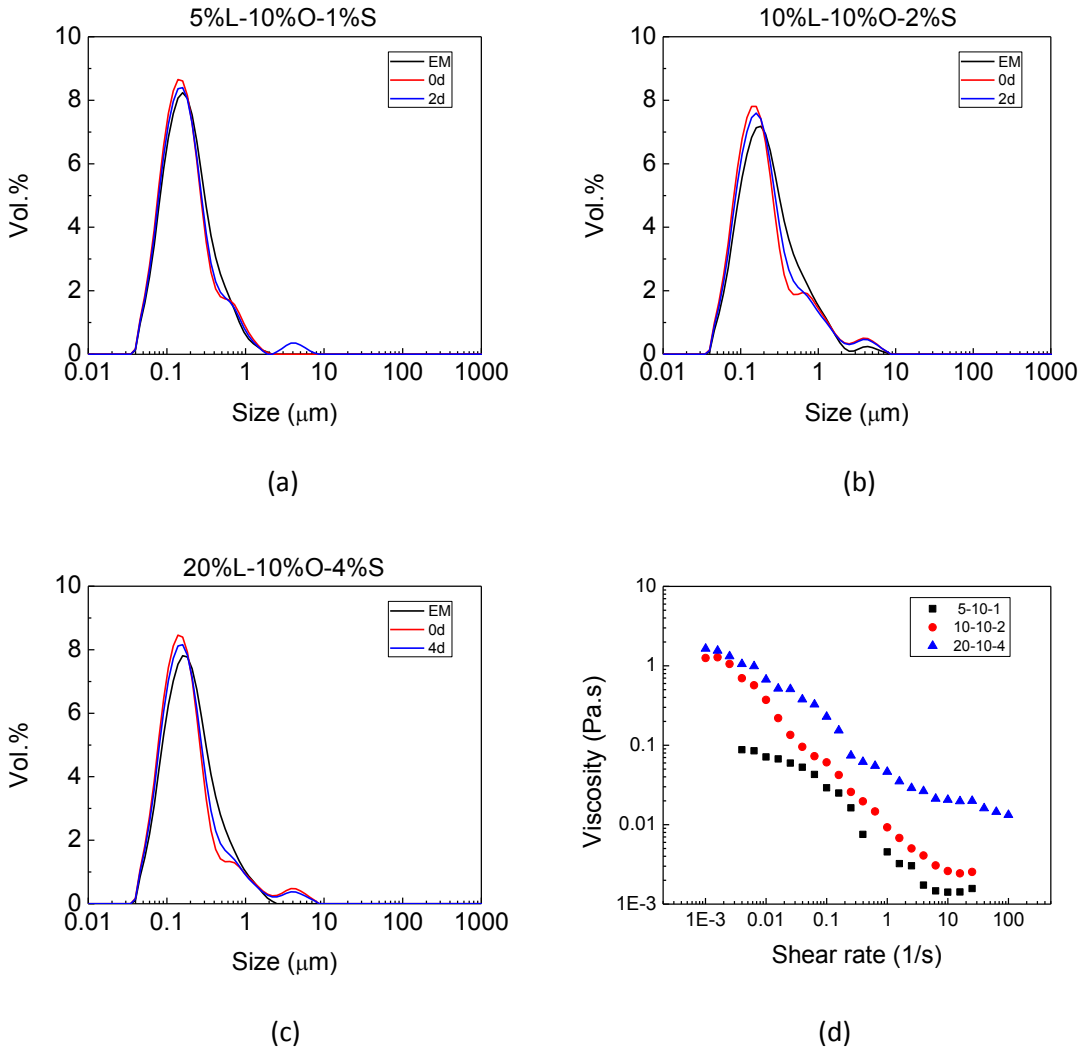

Figure 4.1. Effect of dispersed phase concentration on the viscosity of non-aggregating NLC dispersions: (a)-(c) particle size distributions (PSD) of samples prepared with 5wt%, 10wt% and 20wt% dispersed phase concentrations; (d) steady shear viscosities of the three samples.

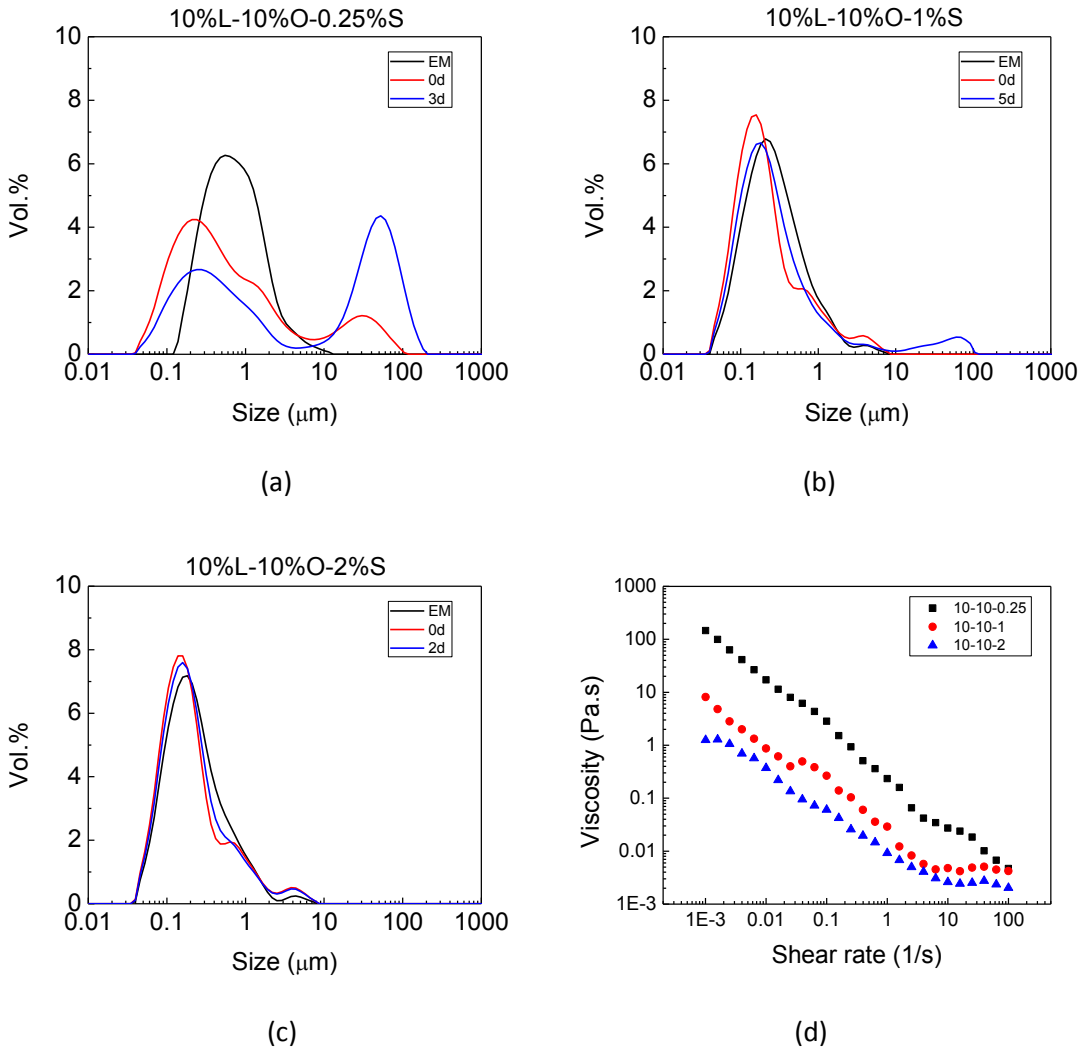

Figure 4.2. Effect of surfactant concentration on the aggregation and viscosity of NLC dispersions: (a)-(c) PSDs of samples prepared with 10wt% dispersed phase concentration and 10wt% oil containing 0.5, 1 and 2wt% surfactant; (d) steady shear viscosities of the three samples.

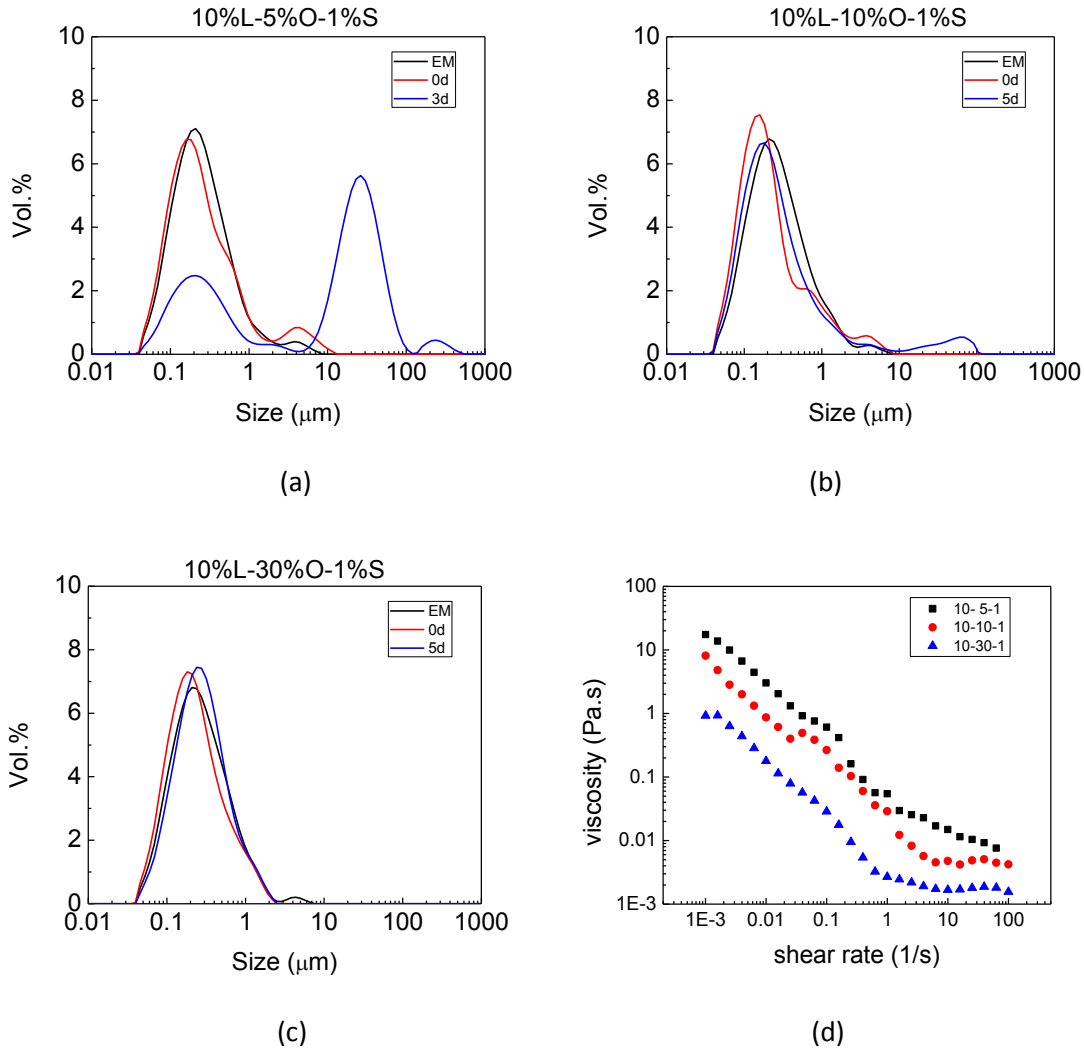

Figure 4.3. Effect of oil content on the aggregation and viscosity of NLC dispersions: (a)-(c) PSDs of samples prepared with 10wt% lipid concentration and 1wt% surfactant containing 5, 10 and 30wt% oil; (d) steady shear viscosities of the three samples.

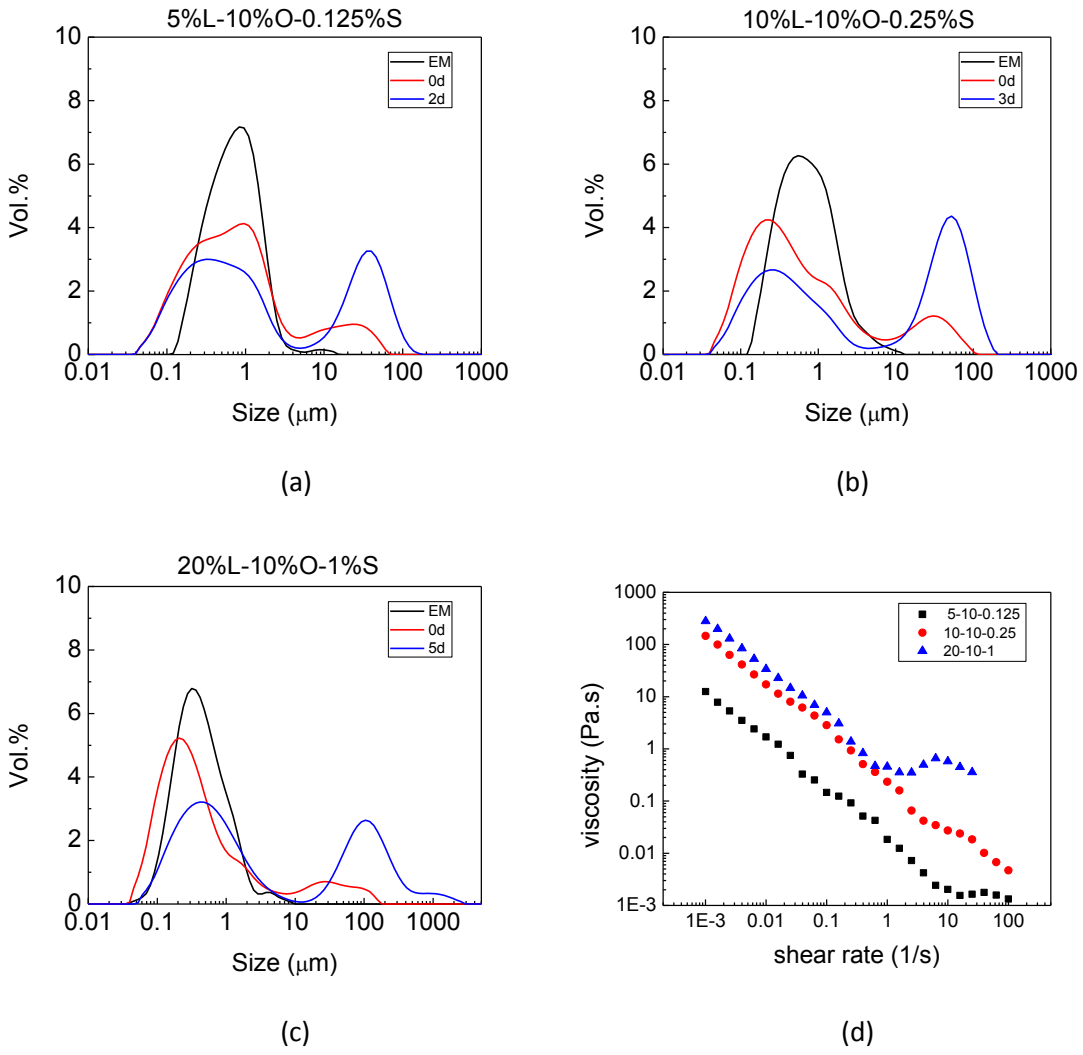

Figure 4.4. Effect of dispersed phase concentration on the viscosity of aggregated NLC dispersions: (a)-(c) PSDs of samples prepared with 5wt%, 10wt% and 20wt% dispersed phase concentrations and the amounts of oil and surfactant indicated; (d) steady shear viscosities of the three samples.

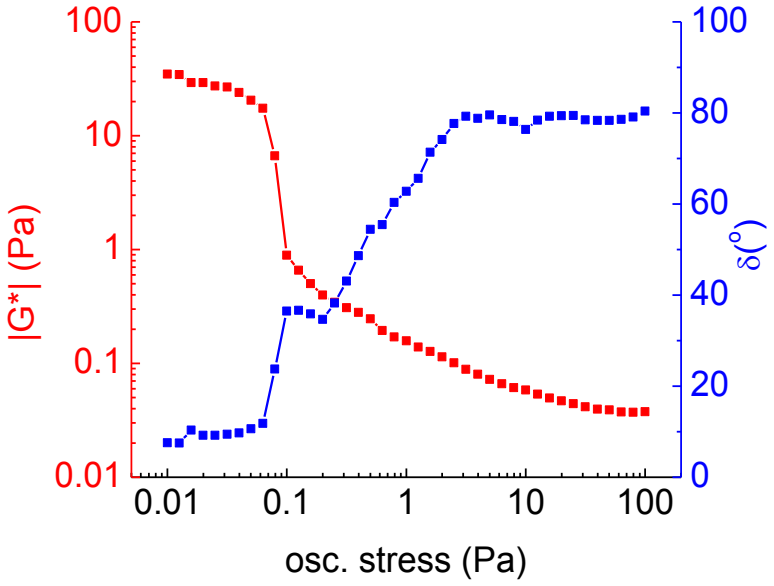

(a)

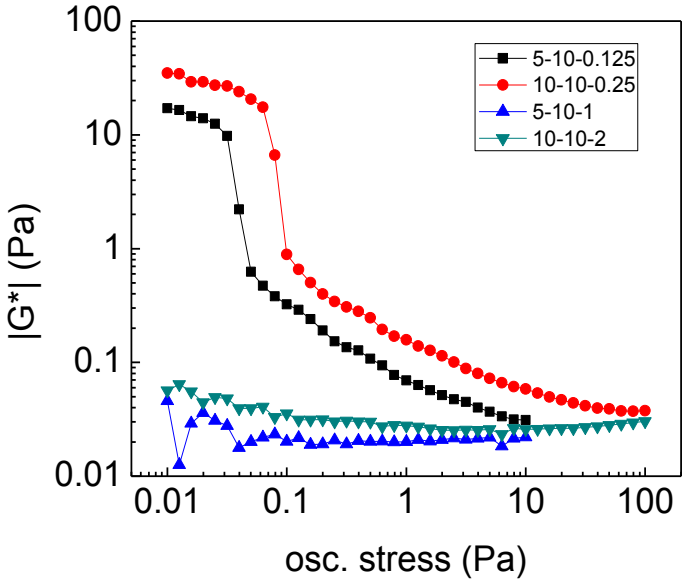

(b)

Figure 4.5. Oscillation stress sweep tests: (a) aggregated dispersion with 10wt% dispersed phase, 10wt% oil and 0.25wt% surfactant. (b) aggregated (5-10-0.125 and 10-10-0.25) and non-aggregated samples (5-10-1 and 10-10-2).

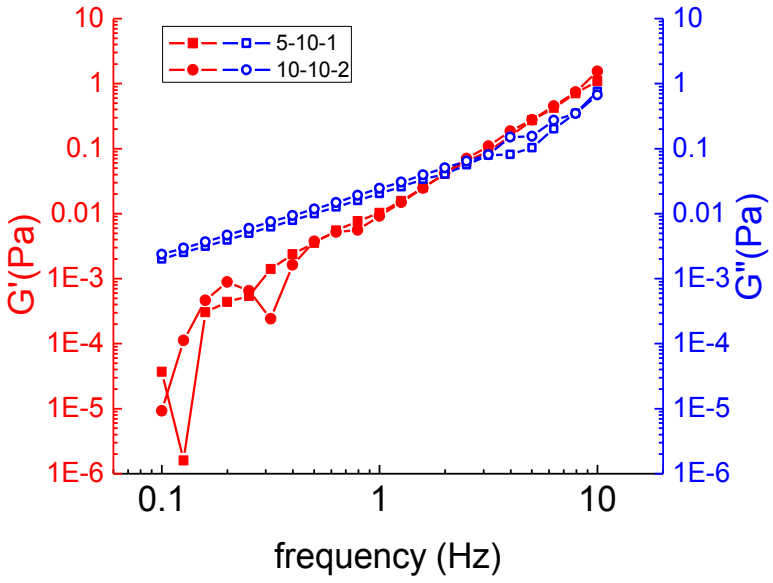

(a)

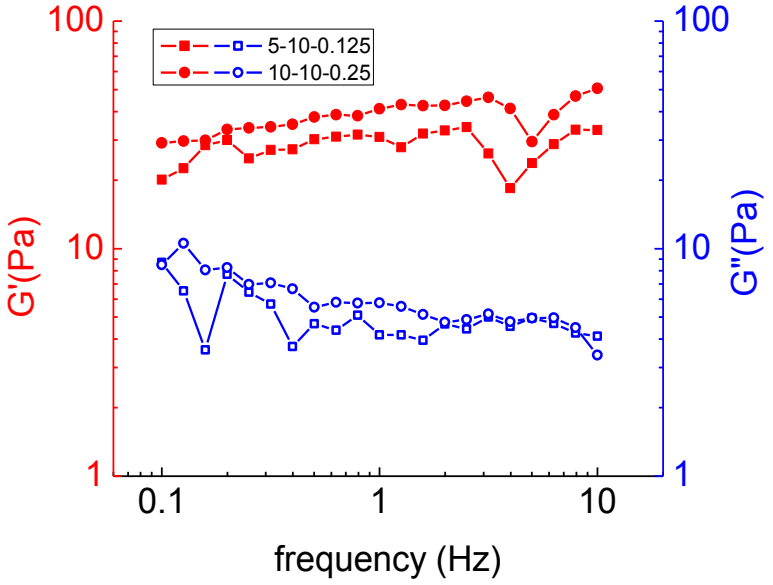

(b)

Figure 4.6. Oscillation frequency sweep tests: (a) non-aggregated samples (5-10-1 and 10-10-2); (b) aggregated samples (5-10-0.125 and 10-10-0.25).

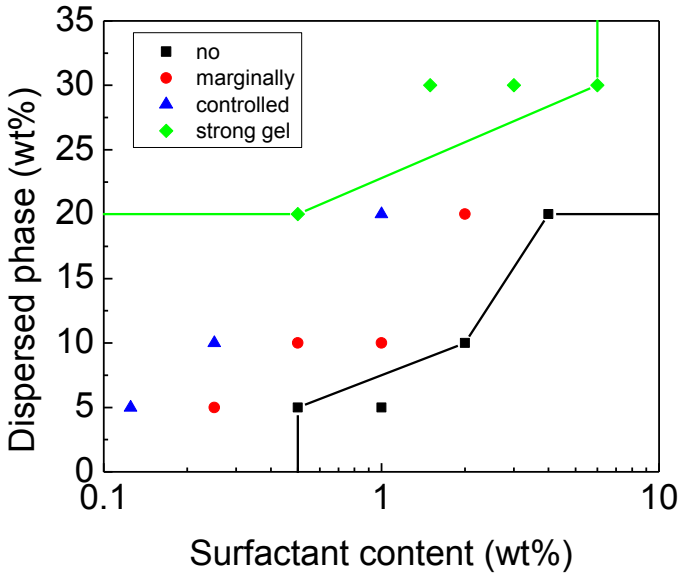

Figure 4.7. State diagram with 10wt% oil content for NLC dispersions at rest. Black squares: no aggregation; red circles: marginally aggregation; blue triangles: controlled aggregation; green diamonds: strong gel formation.

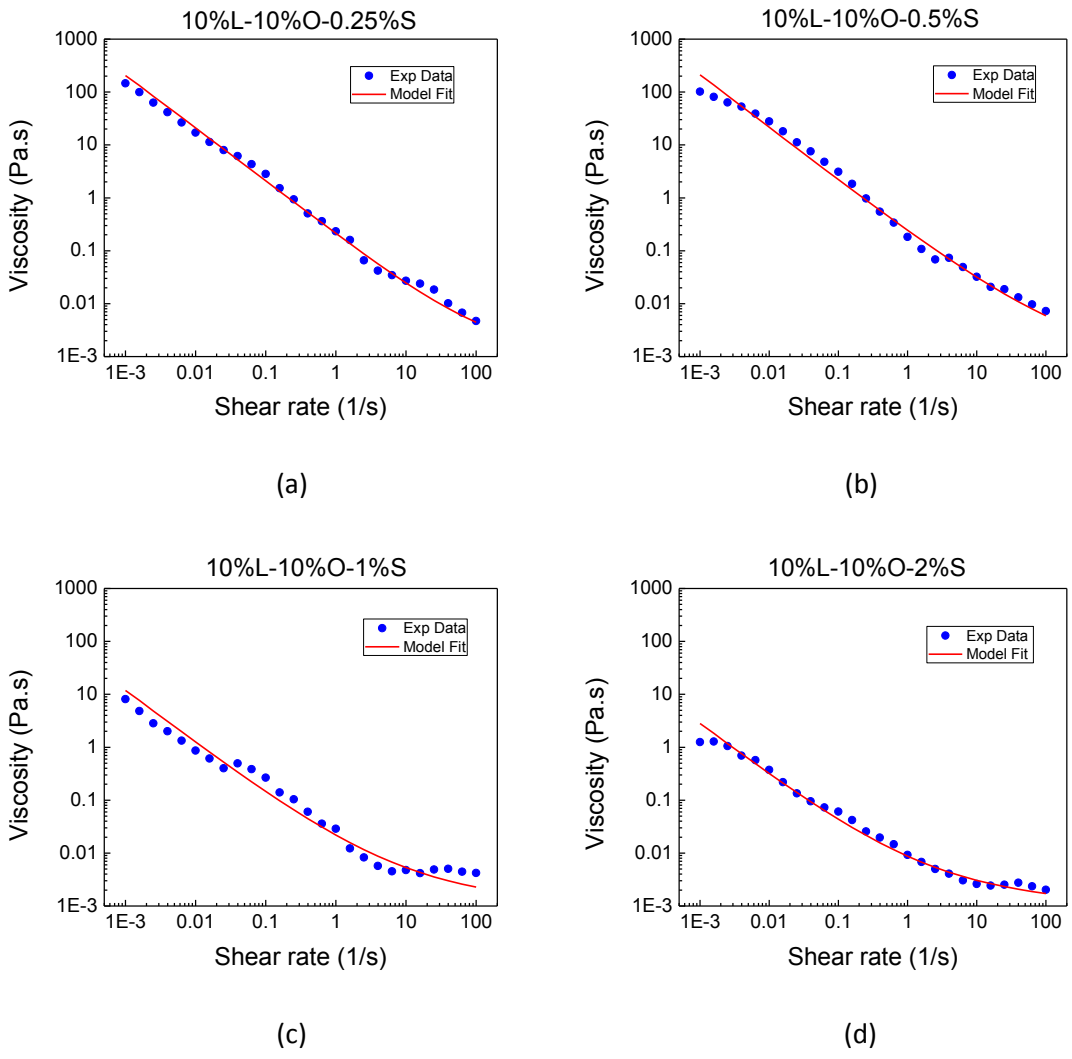

Figure 4.8. Viscosity model fitting for NLC dispersions prepared with 10% dispersed phase concentration, 10% oil content and 0.25-2% surfactant concentration.

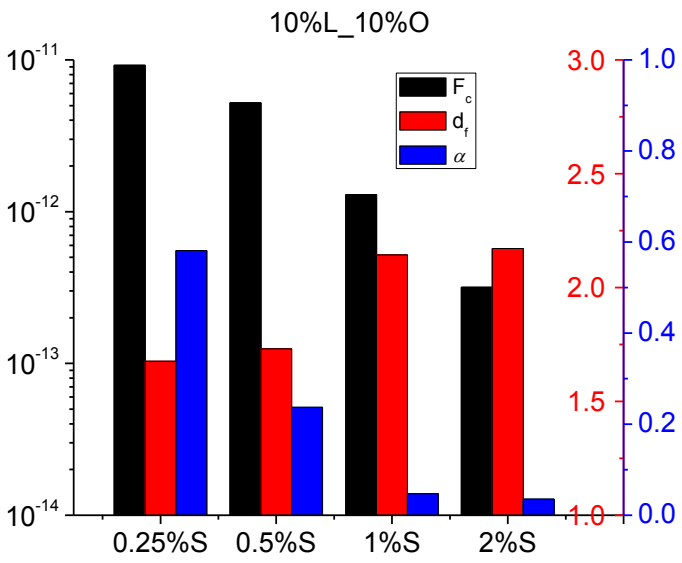

(a)

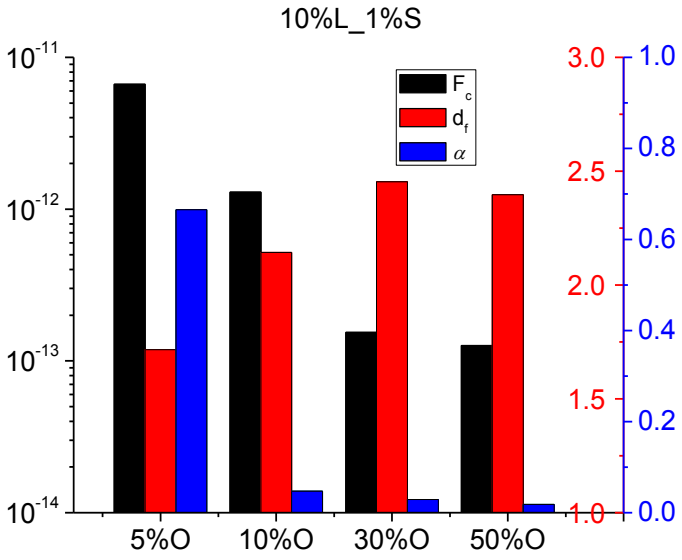

(b)

Figure 4.9. Viscosity model fitting parameters for NLC dispersions with: (a) 10% dispersed phase concentration, 10% oil content and 0.25-2% surfactant concentration; (b) 10% dispersed phase concentration, 1% surfactant and 5-50% oil content.

CHAPTER 5

CONCLUSIONS AND FUTURE WORK

5.1 Conclusions

I developed a population balance equation (PBE) model to describe aggregation dynamics in stored dispersions of solid lipid nanoparticles (SLNs). The model was based on the hypothesis that particle aggregation was driven by lipid crystals undergoing a polymorphic transformation from the thermodynamically unstable α form the stable β form, which created an increase in particle surface area, a decrease in surfactant surface coverage, and an increase hydrophobic attraction between particles. Experiments showed that the polymorphic transformation was the rate determining step in the aggregation process, SLNs with smaller initial size distributions underwent polymorphic transformation and aggregation more rapidly, and aggregates contained particles with both α and β crystals. The PBE model generated predictions of the average polymorph content and the aggregate size distribution under the simplifying assumptions that primary particles comprised entirely of α crystals were transformed into primary particles comprised entirely of β crystals, the polymorphic transformation rate was first order in the α-form particle concentration and surfactant coverage, only β-form particles could aggregate, and particles collided due to Brownian motion. I found that the model was able to capture the bimodal nature of aggregate size distributions, the α-to-β polymorph ratio, and the faster aggregation dynamics of SLNs with smaller initial size distributions. Without re-estimation of parameters, the model was able to capture the faster aggregation dynamics of SLNs prepared with 5 weight percent lipid and 0.5 weight percent surfactant. Collectively these results provide support for the hypothesis that aggregation was driven by the creation of new particle surface area and reduced surfactant coverage due to the polymorphic transformation.

Next I studied the effects of different carrier oils on the aggregation stability of tristearin SLNs. I found that the carrier oil type and concentration strongly affected SLN aggregation behavior. In the absence of carrier oil, SLNs quickly aggregated and formed a gel. When mixed with oil, the stability of SLN suspensions was highly increased. However, the minimum amount of oil needed to stop the aggregation varied for different types of oils. The melting temperature was shown to be an important determinant of effectiveness for triglyceride carrier oils. However, this may not be applicable for other structured oils. For a given carrier oil, oil concentration was a key factor affecting the polymorphic transformation rate and SLN dispersion stability. As the carrier oil concentration was increased, both the melting and crystallization temperatures decreased linearly and the melting peak became broaden, which suggest a less ordered matrix. For all these different types of oils, no relationship was found between the stability of SLN suspensions and the slopes of linear regressions for melting and crystallization temperatures. The polymorphic transformation rate increased such that negligible α-particle content was observed at oil concentrations that yielded stable dispersions. Cryogenic TEM images showed that increasing carrier oil concentrations produced more spherical particles. Taken together, these results suggest that carrier oil trapped within the growing crystal matrix accelerated the polymorphic transformation but retarded the large shape change normally associated with the transformation. The aggregation process was also studied with my model for SLN aggregation. Along with the series of experiments for SLNs prepared from same triolein-trisearin mixture and different amount of surfactant, the model suggested that much less surfactant was needed to stabilize the system when oil was incorporated to the lipid matrix. These results suggest that, other than inhibiting shape change, carrier oil in the SLNs might also increase the efficiency of surfactant.

Finally I investigated the effect of dispersed phase concentration, oil content and surfactant concentration on the aggregation and viscosity of NLC dispersions. Higher dispersed

phase concentrations produced dispersions with higher viscosity. For a constant dispersed phase concentration, the viscosity of the dispersion could be modified by controlling the amount particle aggregation using different oil content and surfactant concentrations. The viscosity of the dispersion could be tuned by at least an order of magnitude by controlling the particle aggregation. Oscillation sweep tests showed typical behaviors of a viscoelastic liquid and a viscoelastic solid for non-aggregated and aggregated dispersions, respectively. Oscillation frequency sweep tests further indicated a weak gel structure in the aggregated dispersions. Modeling results suggested an increase of the bonding force between particles and the aggregation efficiency as the oil content and surfactant concentration were decreased. The fractal dimension obtained by model fitting of aggregated systems indicated the formation of a porous, interconnected network structure in the dispersion.

5.2 Future Work

I showed that particle aggregation and gelation occurred when SLN suspensions were held under conditions where polymorphic transitions from the α-to-β form occurred. I hypothesized that aggregation was due to hydrophobic attraction between exposed patches on the surfaces of lipid nanoparticles when they changed from spherical to ellipsoid, since this increased their surface area. If this hypothesis is true, then the tendency for particle aggregation to occur should depend on the rate at which the polymorphic transition occurs, the nature of the shape change (kinetics, morphology, exposed surface area), the rate at which the emulsifier molecules adsorb to the newly formed oil-water interface, and the ability of emulsifiers to increase the repulsive interactions between particles. A systematic study on the influence of these parameters on the tendency for shape change, aggregation and gelation to occur in SLNs would be desirable.

My model of aggregation dynamics was able to quantitatively predict the α-to-β polymorph ratio and qualitatively predict the particle size distribution of SLN dispersions stored at room temperature. This model was based on several simplifying assumptions concerning the polymorphic transformation and particle interactions. The polymorphic transformation was assumed to follow first-order kinetics such that all particles underwent the transformation at the same rate and only β-form particles could aggregate. These assumptions were in contradiction to my data, which showed significant α content in highly aggregated samples. β-form particles were assumed to have a disc shape with constant aspect ratio despite my data showing highly variable shapes across the population. Furthermore, even large aggregates were assumed to collide due to Brownian motion and the stability ratio was simply assumed to be a constant that yielded an appropriate aggregation timescale rather than being computed from interparticle forces. It would be useful to test the validity of these assumptions and incorporate the necessary physicochemical detail to make the PBE model sufficiently accurate for computational product design.

My group has developed PBE models that can generate quantitatively accurate predictions of oil-in-water emulsion drop size distributions generated from high pressure homogenization [101]. To allow prediction of concentrated dispersions with different emulsifier types and concentrations, these models were extended to account for surfactant adsorption and drop surface coverage. Developing a more sophisticated PBE model to predict the drop size distribution and surfactant surface coverage of lipid nanoemulsions needs to be considered. These predictions will serve as essential inputs to the SLN aggregation model.

In my study of the effect of oil type on the aggregation stability of NLCs, when the fatty acid oleic acid was used as the carrier oil, NLC dispersions exhibited significant aggregation until a relatively high oil concentration was used. A possible explanation of this poor performance is that oleic acid has an acid functional group, which may change the oil-surfactant interfacial

properties in an undesirable way. Further experimental investigation should be considered to test this hypothesis. I also hypothesized that the presence of oil molecules within the homogeneous lipid phase could change lipid-surfactant interfacial properties, increase the mobility of surfactant molecules at the particle surface and allow surfactant molecules that are redistributed during the polymorphic transformation to stabilize uncovered hydrophobic surfaces, which requires further investigation.

BIBLIOGRAPHY

[1] F. Kesisoglou, S. Panmai, Y. Wu, Application of Nanoparticles in Oral Delivery of Immediate Release Formulations, Curr. Nanosci., 3 (2007) 183-190.

[2] L. Sagalowicz, M.E. Leser, H.J. Watzke, M. Michel, Monoglyceride self-assembly structures as delivery vehicles, Trends Food Sci. Tech., 17 (2006) 204-214.

[3] C.J. Porter, N.L. Trevaskis, W.N. Charman, Lipids and lipid-based formulations: optimizing the oral delivery of lipophilic drugs, Nat. Rev. Drug Discov., 6 (2007) 231-248.

[4] C.J. Porter, K.M. Wasan, P. Constantinides, Lipid-based systems for the enhanced delivery of poorly water soluble drugs, Adv Drug Deliv Rev, 60 (2008) 615-616.

[5] R.H. Muller, C.M. Keck, Challenges and solutions for the delivery of biotech drugs--a review of drug nanocrystal technology and lipid nanoparticles, J. Biotechnol., 113 (2004) 151-170.

[6] D.J. McClements, Y. Li, Structured emulsion-based delivery systems: Controlling the digestion and release of lipophilic food components, Adv. Colloid Interface Sci., 159 (2010) 213-228.

[7] S.A. Wissing, O. Kayser, R.H. Müller, Solid lipid nanoparticles for parenteral drug delivery, Adv. Drug Delivery Rev., 56 (2004) 1257-1272.

[8] J. Weiss, E. Decker, D.J. McClements, K. Kristbergsson, T. Helgason, T. Awad, Solid Lipid Nanoparticles as Delivery Systems for Bioactive Food Components, Food Biophys., 3 (2008) 146-154.

[9] D.J. McClements, E.A. Decker, Y. Park, J. Weiss, Structural design principles for delivery of bioactive components in nutraceuticals and functional foods, Crit. Rev. Food Sci. Nutr., 49 (2009) 577-606.

[10] M.D. Joshi, R.H. Muller, Lipid nanoparticles for parenteral delivery of actives, Eur. J. Pharm. Biopharm., 71 (2009) 161-172.

[11] V. Jenning, M. Schäfer-Korting, S. Gohla, Vitamin A-loaded solid lipid nanoparticles for topical use: drug release properties, J. Controlled Release, 66 (2000) 115-126.

[12] W. Mehnert, K. Mäder, Solid lipid nanoparticles: Production, characterization and applications, Adv. Drug Delivery Rev., 47 (2001) 165-196.

[13] R. Lander, W. Manger, M. Scouloudis, A. Ku, C. Davis, A. Lee, Gaulin homogenization: a mechanistic study, Biotechnol. Prog., 16 (2000) 80-85.

[14] H. Bunjes, B. Siekmann, K. Westesen, Emulsions of super-cooled melts - a novel drug delivery system, in: S. Benita (Ed.) Submicron Emulsions in Drug Targeting and Delivery, Harwood Academic Publishers, Amsterdam, 1998, pp. 175-204.

[15] A.z. Muhlen, Feste Lipid-Nanopartikel mit prolongierter Wirkstoffliberation: Herstellung, Langzeitstabilitat, Charak terisierung, Freisetzungsverhalten und mechanismen, Free University of Berlin, 1996.

[16] B. Siekmann, K. Westesen, Melt-homogenized solid lipid nanoparticles stabilized by the nonionic surfactant tyloxapol. I. Preparation and particle size determination, Pharm. Pharmacol. Lett., 3 (1994) 194-197.

[17] R.H. Muller, W. Mehnert, J.-S. Lucks, C. Schwarz, A. Zur Muhlen, H. Meyhers, C. Freitas, D. Ruhl, Solid lipid nanoparticles(SLN) - An alternative colloidal carrier system for controlled drug delivery, Eur. J. Pharm. Biopharm., 41 (1995) 62-69.

[18] C. Schwarz, Feste Lipidnanopartikel: Herstellung, Charakterisierung, Arzneistoffinkorporation und freisetzung, Sterilisation und Lyophilisation, Free University of Berlin, 1995.

[19] S. Jahnke, The theory of high pressure homogenization, in: R.H. Muller, S. Benita, B. Bohm (Eds.) Emulsions and nanosuspensions for the formulation of poorly soluble drugs, Medpharm Scientific Publishers, Stuttgart, 1998.

[20] B. Sjöström, B. Bergenståhl, Preparation of submicron drug particles in lecithin-stabilized o/w emulsions I. Model studies of the precipitation of cholesteryl acetate, Int. J. Pharm., 88 (1992) 53-62.
[21] M.R. Gasco, Method for producing solid lipid microspheres having a narrow size distribution, 1993, USS 188837.
[22] K. Sato, N. Garti, Crystallization and polymorphism of fats and fatty acids, Marcel Dekker, New York, 1988.
[23] T. Helgason, T.S. Awad, K. Kristbergsson, D.J. McClements, J. Weiss, Influence of Polymorphic Transformations on Gelation of Tripalmitin Solid Lipid Nanoparticle Suspensions, J. Am. Oil. Chem. Soc., 85 (2008) 501-511.
[24] H. Bunjes, F. Steiniger, W. Richter, Visualizing the Structure of Triglyceride Nanoparticles in Different Crystal Modifications, Langmuir, 23 (2007) 4005-4011.
[25] B. Siekmann, K. Westesen, Thermoanalysis of the recrystallization process of melt-homogenized glyceride nanoparticles, Colloids Surf. B, 3 (1994) 159-175.
[26] K.M. Rosenblatt, H. Bunjes, Poly(vinyl alcohol) as emulsifier stabilizes solid triglyceride drug carrier nanoparticles in the alpha-modification, Mol. Pharm., 6 (2009) 105-120.
[27] H. Bunjes, M.H.J. Koch, Saturated phospholipids promote crystallization but slow down polymorphic transitions in triglyceride nanoparticles, J. Controlled Release, 107 (2005) 229-243.
[28] C. Freitas, Stability determination of solid lipid nanoparticles (SLN TM) in aqueous dispersion after addition of electrolyte, J. Microencapsulation, 16 (1999) 59-71.
[29] R.H. Müller, S. Heinemann, Fat emulsions for parenteral nutrition. III: Lipofundin MCT/LCT regimens for total parenteral nutrition (TPN) with low electrolyte load, Int. J. Pharm., 101 (1994) 175-189.
[30] K. Westesen, B. Siekmann, Investigation of the gel formation of phospholipid-stabilized solid lipid nanoparticles, Int. J. Pharm., 151 (1997) 35-45.
[31] H. Bunjes, M.H. Koch, K. Westesen, Influence of emulsifiers on the crystallization of solid lipid nanoparticles, J Pharm Sci, 92 (2003) 1509-1520.
[32] T. Helgason, T.S. Awad, K. Kristbergsson, E.A. Decker, D.J. McClements, J. Weiss, Impact of Surfactant Properties on Oxidative Stability of β-Carotene Encapsulated within Solid Lipid Nanoparticles, J. Agric. Food Chem., 57 (2009) 8033-8040.
[33] T. Helgason, T.S. Awad, K. Kristbergsson, D.J. McClements, J. Weiss, Effect of surfactant surface coverage on formation of solid lipid nanoparticles (SLN), J Colloid Interface Sci, 334 (2009) 75-81.
[34] T. Awad, T. Helgason, K. Kristbergsson, E. Decker, J. Weiss, D.J. McClements, Effect of Cooling and Heating Rates on Polymorphic Transformations and Gelation of Tripalmitin Solid Lipid Nanoparticle (SLN) Suspensions, Food Biophys., 3 (2008) 155-162.
[35] C. Freitas, R.H. Müller, Effect of light and temperature on zeta potential and physical stability in solid lipid nanoparticle (SLN™) dispersions, Int. J. Pharm., 168 (1998) 221-229.
[36] R.H. Müller, M. Radtke, S.A. Wissing, Nanostructured lipid matrices for improved microencapsulation of drugs, Int. J. Pharm., 242 (2002) 121-128.
[37] T.S. Awad, T. Helgason, J. Weiss, E.A. Decker, D.J. McClements, Effect of Omega-3 Fatty Acids on Crystallization, Polymorphic Transformation and Stability of Tripalmitin Solid Lipid Nanoparticle Suspensions, Cryst. Growth Des., 9 (2009) 3405-3411.
[38] R.H. Müller, M. Radtke, S.A. Wissing, Solid lipid nanoparticles (SLN) and nanostructured lipid carriers (NLC) in cosmetic and dermatological preparations, Adv. Drug Delivery Rev., 54, Supplement (2002) S131-S155.

[39] A. Dingler, R.P. Blum, H. Niehus, R.H. Müller, S. Gohla, Solid lipid nanoparticles (SLNTM/LipopearlsTM) a pharmaceutical and cosmetic carrier for the application of vitamin E in dermal products, J. Microencapsulation, 16 (1999) 751-767.
[40] A. Saupe, S.A. Wissing, A. Lenk, C. Schmidt, R.H. Muller, Solid lipid nanoparticles (SLN) and nanostructured lipid carriers (NLC) -- structural investigations on two different carrier systems, Bio-med. Mater. Eng., 15 (2005) 393-402.
[41] R. H. Muller, R. Shegokar, C. M. Keck, 20 Years of Lipid Nanoparticles (SLN & NLC): Present State of Development & Industrial Applications, Curr. Drug Discovery Technol., 8 (2011) 207-227.
[42] R.H. Müller, R.D. Petersen, A. Hommoss, J. Pardeike, Nanostructured lipid carriers (NLC) in cosmetic dermal products, Adv. Drug Delivery Rev., 59 (2007) 522-530.
[43] J. Pardeike, A. Hommoss, R.H. Muller, Lipid nanoparticles (SLN, NLC) in cosmetic and pharmaceutical dermal products, Int. J. Pharm., 366 (2009) 170-184.
[44] K.K. Sawant, S.S. Dodiya, Recent advances and patents on solid lipid nanoparticles, Recent. Pat. Drug Deliv. Formul., 2 (2008) 120-135.
[45] S. Das, A. Chaudhury, Recent advances in lipid nanoparticle formulations with solid matrix for oral drug delivery, AAPS PharmSciTech, 12 (2011) 62-76.
[46] M.A. Iqbal, S. Md, J.K. Sahni, S. Baboota, S. Dang, J. Ali, Nanostructured lipid carriers system: recent advances in drug delivery, J. Drug Target, 20 (2012) 813-830.
[47] C. Puglia, F. Bonina, Lipid nanoparticles as novel delivery systems for cosmetics and dermal pharmaceuticals, Expert Opin. Drug Deliv., 9 (2012) 429-441.
[48] J. Araujo, S. Nikolic, M.A. Egea, E.B. Souto, M.L. Garcia, Nanostructured lipid carriers for triamcinolone acetonide delivery to the posterior segment of the eye, Colloids Surf. B, 88 (2011) 150-157.
[49] J. Pardeike, C. Schmidt, I. Volz, R.H. Muller, Nanostructured lipid carriers as delivery system for the phopholipase A2 inhibitors PX-18 and PX-13 for dermal application, Die Pharmazie, 66 (2011) 357-361.
[50] A. Hommoss, Preservative system development for argan oil-loaded nanostructured lipid carriers, Die Pharmazie, 66 (2011) 187-191.
[51] D.B. Vieira, A.M. Carmona-Ribeiro, Cationic nanoparticles for delivery of amphotericin B: preparation, characterization and activity in vitro, J. Nanobiotechnology, 6 (2008) 6.
[52] E.B. Souto, R.H. Muller, Investigation of the factors influencing the incorporation of clotrimazole in SLN and NLC prepared by hot high-pressure homogenization, J Microencapsul, 23 (2006) 377-388.
[53] X. Li, S.-f. Nie, J. Kong, N. Li, C.-y. Ju, W.-s. Pan, A controlled-release ocular delivery system for ibuprofen based on nanostructured lipid carriers, Int. J. Pharm., 363 (2008) 177-182.
[54] K. Jores, W. Mehnert, M. Drechsler, H. Bunjes, C. Johann, K. Mader, Investigations on the structure of solid lipid nanoparticles (SLN) and oil-loaded solid lipid nanoparticles by photon correlation spectroscopy, field-flow fractionation and transmission electron microscopy, J. Control Release, 95 (2004) 217-227.
[55] K. Jores, A. Haberland, S. Wartewig, K. Mader, W. Mehnert, Solid lipid nanoparticles (SLN) and oil-loaded SLN studied by spectrofluorometry and Raman spectroscopy, Pharm. Res., 22 (2005) 1887-1897.
[56] K. Jores, W. Mehnert, K. Mader, Physicochemical investigations on solid lipid nanoparticles and on oil-loaded solid lipid nanoparticles: a nuclear magnetic resonance and electron spin resonance study, Pharm. Res., 20 (2003) 1274-1283.

[57] J.C. Schwarz, A. Weixelbaum, E. Pagitsch, M. Löw, G.P. Resch, C. Valenta, Nanocarriers for dermal drug delivery: Influence of preparation method, carrier type and rheological properties, Int. J. Pharm., 437 (2012) 83-88.
[58] A. Lippacher, R.H. Müller, K. Mäder, Investigation on the viscoelastic properties of lipid based colloidal drug carriers, Int. J. Pharm., 196 (2000) 227-230.
[59] A. Lippacher, R.H. Müller, K. Mäder, Semisolid SLN™ dispersions for topical application: influence of formulation and production parameters on viscoelastic properties, Eur. J. Pharm. Biopharm., 53 (2002) 155-160.
[60] A. Lippacher, R.H. Müller, K. Mäder, Liquid and semisolid SLN™ dispersions for topical application: rheological characterization, Eur. J. Pharm. Biopharm., 58 (2004) 561-567.
[61] A.C. Silva, D. Santos, D.C. Ferreira, E.B. Souto, Minoxidil-loaded nanostructured lipid carriers (NLC): characterization and rheological behaviour of topical formulations, Die Pharmazie, 64 (2009) 177-182.
[62] E.B. Souto, S.H. Gohla, R.H. Müller, R.H. Müller, Rheology of nanostructured lipid carriers (NLC®) suspended in a viscoelastic medium, Die Pharmazie, 60 (2005) 671-673.
[63] E.B. Souto, S.A. Wissing, C.M. Barbosa, R.H. Muller, Comparative study between the viscoelastic behaviors of different lipid nanoparticle formulations, Int. J. Cosmetic Sci., 27 (2005) 36-36.
[64] E.B. Souto, S.A. Wissing, C.M. Barbosa, R.H. Müller, Evaluation of the physical stability of SLN and NLC before and after incorporation into hydrogel formulations, Eur. J. Pharm. Biopharm., 58 (2004) 83-90.
[65] M. Joshi, V. Patravale, Formulation and Evaluation of Nanostructured Lipid Carrier (NLC)–based Gel of Valdecoxib, Drug Dev. Ind. Pharm., 32 (2006) 911-918.
[66] M. Joshi, V. Patravale, Nanostructured lipid carrier (NLC) based gel of celecoxib, Int. J. Pharm., 346 (2008) 124-132.
[67] S. Doktorovova, E.B. Souto, Nanostructured lipid carrier-based hydrogel formulations for drug delivery: A comprehensive review, Expert Opin. Drug Deliv., 6 (2009) 165-176.
[68] V.B. Junyaprasert, V. Teeranachaideekul, E.B. Souto, P. Boonme, R.H. Müller, Q10-loaded NLC versus nanoemulsions: Stability, rheology and in vitro skin permeation, Int. J. Pharm., 377 (2009) 207-214.
[69] R. de Rooij, A.A. Potanin, D. van den Ende, J. Mellema, Steady shear viscosity of weakly aggregating polystyrene latex dispersions, J. Chem. Phys, 99 (1993) 9213-9223.
[70] A.A. Potanin, R. De Rooij, D. Van den Ende, J. Mellema, Microrheological modeling of weakly aggregated dispersions, J. Chem. Phys, 102 (1995) 5845-5853.
[71] M.v. Smoluchowski, Mathematical theory of the kinetics of the coagulation of colloidal solutions, Zeitschrift für Physikalische Chemie, 92 (1917) 129-168.
[72] G.H. Bogush, C.F. Zukoski Iv, Uniform silica particle precipitation: An aggregative growth model, J. Colloid Interface Sci., 142 (1991) 19-34.
[73] W. Peukert, H.-C. Schwarzer, F. Stenger, Control of aggregation in production and handling of nanoparticles, Chem. Eng. Process., 44 (2005) 245-252.
[74] P. Taboada-Serrano, C.-J. Chin, S. Yiacoumi, C. Tsouris, Modeling aggregation of colloidal particles, Curr. Opin. Colloid Interface Sci., 10 (2005) 123-132.
[75] H.-C. Schwarzer, W. Peukert, Prediction of aggregation kinetics based on surface properties of nanoparticles, Chem. Eng. Sci., 60 (2005) 11-25.
[76] M. Tourbin, C. Frances, Experimental characterization and population balance modelling of the dense silica suspensions aggregation process, Chem. Eng. Sci., 63 (2008) 5239-5251.
[77] S. Melis, M. Kemmere, J. Meuldijk, G. Storti, M. Morbidelli, A model for the coagulation of polyvinyl acetate particles in emulsion, Chem. Eng. Sci., 55 (2000) 3101-3111.

[78] D. Ramkrishna, A.W. Mahoney, Population balance modeling. Promise for the future, Chem. Eng. Sci., 57 (2002) 595-606.
[79] J. Gregory, Interaction of unequal double layers at constant charge, J. Colloid Interface Sci., 51 (1975) 44-51.
[80] H.C. Hamaker, The London-van der Waals attraction between spherical particles, Physica, 4 (1937) 1058-1072.
[81] B. Derjaguin, L. Landau, Theory of the stability of strongly charged lyophobic sols and of the adhesion of strongly charged particles in solutions of electrolytes, Prog. Surf. Sci., 43 (1993) 30-59.
[82] G. Madras, B.J. McCoy, A. Navrotsky, Kinetic Model for TiO2 Polymorphic Transformation from Anatase to Rutile, J. Am. Ceram. Soc, 90 (2007) 250-255.
[83] M. Avrami, Granulation, Phase Change, and Microstructure Kinetics of Phase Change. III, J. Chem. Phys, 9 (1941) 177-184.
[84] M. Avrami, Kinetics of Phase Change. II Transformation-Time Relations for Random Distribution of Nuclei, J. Chem. Phys, 8 (1940) 212-224.
[85] M. Avrami, Kinetics of Phase Change. I General Theory, J. Chem. Phys, 7 (1939) 1103-1112.
[86] B.V. Erofeyev, A generalized equation of chemical kinetics and its application in reactions involving solids, C.R. (Dokl.) Acad. Sci. URSS, 52 (1946) 511-514.
[87] A.K. Sheridan, J. Anwar, Kinetics of the Solid-State Phase Transformation of Form β to γ of Sulfanilamide Using Time-Resolved Energy-Dispersive X-ray Diffraction, Chem. Mater., 8 (1996) 1042-1051.
[88] P.T. Cardew, R.J. Davey, A.J. Ruddick, Kinetics of polymorphic solid-state transformations, J. Chem. Soc., Faraday Trans. 2, 80 (1984) 659-668.
[89] G.H. Charbonnet, W.S. Singleton, Thermal properties of fats and oils. VI. Heat capacity, heats of fusion, J. Am. Oil Chem. Soc., 24 (1947) 140.
[90] T. Unruh, H. Bunjes, K. Westesen, M.H.J. Koch, Observation of Size-Dependent Melting in Lipid Nanoparticles, J. Phys. Chem. B, 103 (1999) 10373-10377.
[91] S. Kumar, D. Ramkrishna, On the solution of population balance equations by discretization—I. A fixed pivot technique, Chem. Eng. Sci., 51 (1996) 1311-1332.
[92] Handbook of Chemistry and Physics, 74th ed.1993-1994.
[93] Y. Yang, A. Corona, 3rd, M.A. Henson, Experimental investigation and population balance equation modeling of solid lipid nanoparticle aggregation dynamics, J. Colloid Interface Sci., 374 (2012) 297-307.
[94] G. Charbonnet, W.S. Singleton, Thermal properties of fats and oils, Journal of the American Oil Chemists Society, 24 (1947) 140-142.
[95] M.J. Vold, Van der Waals' attraction between anisometric particles, J. Colloid Sci., 9 (1954) 451-459.
[96] Y. Yang, A. Corona Iii, B. Schubert, R. Reeder, M.A. Henson, The effect of oil type on the aggregation stability of nanostructured lipid carriers, J. Colloid Interface Sci., 418 (2014) 261-272.
[97] G.M. Eccleston, B.W. Barry, S.S. Davis, Correlation of viscoelastic functions for pharmaceutical semisolids: Comparison of creep and oscillatory tests for oil-in-water creams stabilized by mixed emulsifiers, J. Pharm. Sci., 62 (1973) 1954-1961.
[98] D.R. Picout, S.B. Ross-Murphy, Rheology of Biopolymer Solutions and Gels, ScientificWorldJournal, 3 (2003).
[99] W.J. Tseng, K.-C. Lin, Rheology and colloidal structure of aqueous TiO2 nanoparticle suspensions, Mat. Sci. Eng. A, 355 (2003) 186-192.

[100] M. Soos, J. Sefcik, M. Morbidelli, Investigation of aggregation, breakage and restructuring kinetics of colloidal dispersions in turbulent flows by population balance modeling and static light scattering, Chem. Eng. Sci., 61 (2006) 2349-2363.
[101] S.N. Maindarkar, P. Bongers, M.A. Henson, Predicting the effects of surfactant coverage on drop size distributions of homogenized emulsions, Chem. Eng. Sci., 89 (2013) 102-114.